



Michigan Technological University
Create the Future Digital Commons @ Michigan Tech

Dissertations, Master's Theses and Master's Reports - Open

Dissertations, Master's Theses and Master's Reports

2011

Structural characterization of water-soluble atmospheric organic matter by ultrahigh-resolution mass spectrometry

Jeffrey P. LeClair
Michigan Technological University

Follow this and additional works at: <https://digitalcommons.mtu.edu/etds>


 Part of the [Chemistry Commons](#)

Copyright 2011 Jeffrey P. LeClair

Recommended Citation

LeClair, Jeffrey P., "Structural characterization of water-soluble atmospheric organic matter by ultrahigh-resolution mass spectrometry", Master's Thesis, Michigan Technological University, 2011.
<https://digitalcommons.mtu.edu/etds/35>

Follow this and additional works at: <https://digitalcommons.mtu.edu/etds>

 Part of the [Chemistry Commons](#)

STRUCTURAL CHARACTERIZATION OF WATER-SOLUBLE ATMOSPHERIC
ORGANIC MATTER BY ULTRAHIGH-RESOLUTION MASS SPECTROMETRY

By

Jeffrey P. LeClair

A THESIS

Submitted in partial fulfillment of the requirements for the degree of

MASTER OF SCIENCE

(Chemistry)

MICHIGAN TECHNOLOGICAL UNIVERSITY

2011

© 2011 Jeffrey LeClair

This thesis, "Structural Characterization of Water-Soluble Atmospheric Organic Matter by Ultrahigh-resolution Mass Spectrometry," is hereby approved in partial fulfillment of the requirements for the Degree of MASTER OF SCIENCE IN CHEMISTRY.

Department of Chemistry

Signatures:

Thesis Advisor _____
Dr. Lynn R. Mazzoleni

Committee Member _____
Dr. Sarah A. Green

Committee Member _____
Dr. Paul Doskey

Committee Member _____
Dr. Judith Perlinger

Department Chair _____
Dr. Sarah A. Green

Date _____

Table of Contents

List of Figures	5
List of Tables	8
Acknowledgements.....	9
Abstract	10
1 Introduction.....	11
2 Fragmentation Analysis of Water-Soluble Atmospheric Organic Matter using Ultrahigh-Resolution Mass Spectrometry.....	21
2.1 Abstract	22
2.2 Introduction	23
2.3 Experimental Methods	27
2.3.1 Sample Collection and Preparation.....	27
2.3.2 Instrumental Parameters.....	28
2.3.3 Data Processing and Assignment of Molecular Compositions.....	29
2.4 Results and Discussion.....	29
2.4.1 AOM Fragmentation & Functional Groups.....	31
2.4.2 Fragmentation of Selected SOA Components	39
2.4.3 Atmospheric Implications and Oxidation State	46

2.5	Acknowledgements	48
2.6	Supplemental Information.....	48
2.7	Additional Fragmentation Studies.....	56
3	Analysis of Nitrophenols and Other Selected Compounds.....	73
3.1	LC/MS Methodology	73
3.1.1	Nitrophenol Quantitation	73
3.1.2	Exploration of Higher Molecular Weight Compounds.....	76
3.2	FT-ICR-MS Analysis of Nitrophenols Found Between 100-200 u	77
3.2.1	Nitrophenol Analysis	77
3.2.2	NO Loss Mechanism.....	88
3.2.3	Other High Abundance Low Mass Range Compounds (100-200 u).....	90
3.3	Fragmentation Analysis of Nitrophenol Standards by LC/MS	91
3.4	Quantification of Nitrophenols in Fog Water by LC/MS	92
3.5	Linear Alkylbenzene sulfonate (LAS) Analysis	93
4	References.....	97
5	Appendix.....	106

List of Figures

- Figure 2.1: An excerpt of the mass spectra from $342.02 < m/z > 343.24$ is shown (top). A #C vs. m/z plot of the same mass range $342.02 < m/z > 343$ (bottom). ... 31
- Figure 2.2: van Krevelen diagrams with colored symbols to represent aromaticity index (AI) categories: aliphatic, olefinic, aromatic, and condensed aromatic as described in Table 2.1. The plots A-F represent precursor losses: A) all compounds with a carboxyl loss; B) all compounds without carboxyl losses; C) CHNO and CHNOS compounds with a nitrate loss; D) CHNO and CHNOS compounds without a nitrate loss; E) CHOS and CHNOS compounds with a sulfate loss; and F) CHOS and CHNOS compounds without a sulfate loss..... 36
- Figure 2.3: van Krevelen diagrams comparing all identified precursor compounds (top) and fragment ions (bottom) using aromaticity index (AI). 50
- Figure 2.4: van Krevelen diagrams using aromaticity index (AI) are shown comparing precursor compounds from each of the compound classes..... 51
- Figure 2.5: The frequency of neutral losses separated by chemical group. These compounds are all “aliphatic” species (AI = 0). 52
- Figure 2.6: The frequency of neutral losses separated by chemical group. These compounds are all “olefinic” species ($0 < AI < 0.50$). 53
- Figure 2.7: The frequency of neutral losses separated by chemical group. These compounds are all “aromatic” species ($0.50 < AI < 0.67$)..... 54
- Figure 2.8: frequency of neutral losses separated by chemical group. These compounds are all “condensed aromatic” species (AI > 0.67)..... 55
- Figure 2.9: Priority Losses for CHO Compounds. The frequency of neutral losses for CHO separated by aromaticity index (AI). 57
- Figure 2.10: Additional Losses for CHO Compounds. The frequency of neutral losses for CHO separated by aromaticity index (AI). 58
- Figure 2.11: Priority Losses for CHNO Compounds. The frequency of neutral losses for CHNO separated by aromaticity index (AI). 60

Figure 2.12: Additional Losses for CHNO Compounds. The frequency of neutral losses for CHNO separated by aromaticity index (AI).	60
Figure 2.13: Priority Losses for CHOS Compounds. The frequency of neutral losses for CHOS separated by aromaticity index (AI).	61
Figure 2.14: Additional Losses for CHOS Compounds. The frequency of neutral losses for CHOS separated by aromaticity index (AI).	62
Figure 2.15: Losses for CHNOS Compounds. The frequency of neutral losses for CHNOS separated by aromaticity index (AI).	63
Figure 2.16: Additional Losses for CHNOS Compounds. The frequency of neutral losses for CHNOS separated by aromaticity index (AI).	64
Figure 2.17: Frequency of priority losses for previously reported CHO monoterpene derivatives.	66
Figure 2.18: Frequency of additional losses for previously reported CHO monoterpene derivatives.	67
Figure 2.19: Left Side: CH ₂ O (Top) vs. C ₂ H ₆ (Bottom); Middle: CO ₂ (Top) vs. C ₃ H ₈ (Bottom); and Right Side: C ₃ H ₄ O ₂ (Top) vs. C ₅ H ₁₂ (Bottom). The squares indicate the precursors that show both losses.	70
Figure 3.1: Possible nitrophenol structure of m/z 138.	78
Figure 3.2: CID spectra of the nitrophenol at m/z 152.	79
Figure 3.3: Possible structure of 3-methyl-4-nitrophenol.	80
Figure 3.4: CID spectra containing the nitrophenol at m/z 166.	81
Figure 3.5: Possible structure of the nitrophenol at m/z 166.	82
Figure 3.6: CID spectra of the nitrophenol at m/z 183.	83
Figure 3.7: Close up of the precursors present in the scan at m/z 183.	84
Figure 3.8: Possible structure of the dinitrophenol at m/z 183.0047.	85

Figure 3.9: CID spectra of the scan containing the nitrophenol at m/z 197.	86
Figure 3.10: Close up of the precursors present in the scan at m/z 197	87
Figure 3.11: Possible structure of the dinitrophenol at m/z 197	88
Figure 3.12: Proposed NO radical loss mechanism	88
Figure 3.13: Proposed LAS Structures	95
Figure 3.14: Neutral structures of key LAS fragment ions.....	96

List of Tables

Table 2.1: Statistics of fragmentation losses per compound group and separated into the four aromaticity index (AI) classifications: aliphatic, olefinic, aromatic and condensed aromatic.....	33
Table 2.2: Comparison of Additional Neutral Losses.	68
Table 2.3: Table of compounds that lost multiple alkyl groups, categorized by aromaticity index (AI).....	72
Table 3.1: Nitrophenol standard calibration level concentrations	73
Table 3.2: LCQ Solvent Gradient Program	74
Table 3.3: MS method parameters	75
Table 3.4: Higher molecular weight compounds.....	77
Table 3.5: Average Concentration of Nitrophenols in Fog Water.....	92
Table 3.6: Fragmentation behavior of LAS compounds.....	94
Table 5.1: A complete list of mass spectrometry scan parameters is listed. Also, recalibration and composition parameters used in Composer for formula assignments is listed.....	106
Table 5.2: A complete list of all formula assigned precursor ions along with corresponding priority losses.....	106
Table 5.3: A complete list of all formula assigned precursor ions along with corresponding additional losses.....	107
Table 5.4: A complete list of all formula assigned fragment ions produced during fragmentation analysis by collision induced dissociation.....	108

Acknowledgements

I would like to thank my advisor Dr. Lynn Mazzoleni for her generous support and guidance over the course of this project, Drs. Melissa Soule and Elizabeth Kujawinski for their assistance in data collection at Woods Hole Oceanographic Institute, Sandy Orłowski and Nick Maynard for laying the ground work of the LC/MS chromatographic separation methods, and the rest of the research group for their support and assistance during the project. Also, I want to thank my wife, Kat, and the rest of my family for their support, as without them, this would not have been possible. I would like to thank the MTU Research for Excellence Fund and the WHOI Student Travel Grant for financial assistance.

Abstract

Isolated water-soluble analytes extracted from fog water collected during a radiation fog event near Fresno, CA were analyzed using collision induced dissociation and ultrahigh-resolution mass spectrometry. Tandem mass analysis was performed on scan ranges between 100-400 u to characterize the structures of nitrogen and/or sulfur containing species. CHNO, CHOS, and CHNOS compounds were targeted specifically because of the high number of oxygen atoms contained in their molecular formulas. The presence of 22 neutral losses corresponding to fragment ions was evaluated for each of the 1308 precursors. Priority neutral losses represent specific polar functional groups (H₂O, CO₂, CH₃OH, HNO₃, SO₃, etc., and several combinations of these). Additional neutral losses represent non-specific functional groups (CO, CH₂O, C₃H₈, etc.) Five distinct monoterpene derived organonitrates, organosulfates, and nitroxy-organosulfates were observed in this study, including C₁₀H₁₆O₇S, C₁₀H₁₇NO₇S, C₁₀H₁₇NO₈S, C₁₀H₁₇NO₉S, and C₁₀H₁₇NO₁₀S. Nitrophenols and linear alkyl benzene sulfonates were present in high abundance. Liquid chromatography/mass spectrometry methodology was developed to isolate and quantify nitrophenols based on their fragmentation behavior.

1 Introduction

Both the chemical and physical properties of atmospheric aerosol govern its ability to interact directly and indirectly with incoming radiation, thus affecting the Earth's climate (Ramanathan et al. 2001). Direct radiative effects involve the scattering or absorption of solar radiation, which correspond to climate cooling and heating, respectively. Indirect radiative effects mean that an increase in aerosols corresponds to an increase in the number of cloud droplets with longer lifetimes. The increase in the number of droplets in a cloud means that the droplet sizes decrease which leads to a decrease in precipitation and an increase in cloudiness (increases albedo). Aerosols have the ability to absorb and/or reflect solar radiation that would otherwise be absorbed by the Earth's surface (Ramanathan et al. 2001). The absorption of solar radiation would result in the atmosphere heating and the reflection or scattering of solar radiation would prevent solar radiation from reaching the Earth's surface. This reduces the potential global warming caused by greenhouse gases, which can absorb infrared radiation that is leaving the Earth's surface. In other words, aerosols play an important role in determining the amount of incoming solar radiation that reaches the surface of the Earth, as well as the amount of the outgoing radiation since outgoing radiation is a function of incoming radiation. If the future comprises of a cleaner atmosphere, aerosol cooling would decline in relation to warming caused by greenhouse gases, due to the shorter atmospheric lifetime of aerosols (Andreae et al. 2005). Although the physical properties of aerosol have been studied in detail, there remain large uncertainties on the climate forcing estimation of aerosol (IPCC 2007) as well as effects on human health (Poschl 2005). In

fact, the magnitude of the impact of aerosols on the Earth's climate was stated as a key uncertainty in the IPCC 2007 report on climate change (IPCC 2007). This large uncertainty greatly limits the ability of current climate models to predict future climate changes. The uncertainty may be reduced by an improved understanding of the chemical composition of aerosols at the molecular level. The chemical composition of atmospheric organic matter (AOM), more specifically the individual molecules and their functional groups, may have the ability to significantly influence the physical properties of aerosols and their effect on the environment (Rudich et al. 2007).

Atmospheric aerosols originate from both biogenic and anthropogenic emission sources. Fine particles and semi-volatile compounds which partition to aerosols are emitted directly to the atmosphere and are often referred to as primary organic aerosols. Emission sources of primary organic compounds include: biomass burning, combustion of fossil fuels, and biogenic sources such as sea spray, soil, and vegetation. Due to atmospheric processes, up to 70% of the aerosol organic mass is secondary in nature (Gelencser et al. 2007). Secondary organic aerosols (SOA) are the molecules produced in the atmosphere from the oxidation of primary volatile organic compounds (VOCs) and the heterogeneous reactions of primary components. The secondary reactions create products of lower volatility which partition to or remain in the aerosol phase. Aqueous phase reactions may also occur and are thought to be responsible for the formation of the higher molecular weight SOA products (Altieri et al. 2009b; Perri et al. 2009; Perri et al. 2010; Yasmeen et al. 2010; Tan et al. 2011). Low molecular weight compounds found in the gas and aqueous phases may lead to SOA product formation via oxidation and

accretion reactions (Blando and Turpin 2000; Yasmeen et al. 2010). Even though SOA is widely abundant, it is poorly understood due to the multitude of possible pathways and chemical reactions. The polar organic components of SOA can enhance the hygroscopic properties of the aerosols; this increases the direct and indirect effects of aerosols on the global climate (Ramanathan et al. 2001; Fuzzi et al. 2006). They directly affect climate by enhancing aerosol light scattering. They indirectly affect climate by enhancing the ability of aerosol to act as cloud condensation nuclei. Thus SOA affects cloud properties and ultimately the hydrological cycle (Ramanathan et al. 2001). In addition to the climate effects of atmospheric aerosols, they are important because of the effects they may have on human health. Studies have shown several severe health problems (e.g., enhanced mortality, cardiovascular, respiratory, and allergic diseases) to be associated with aerosols and air pollution (Poschl 2005).

Atmospheric aerosols can act as condensation nucleation sites for droplet formation in both clouds and fogs. Radiation fogs are in essence a ground-level cloud, making them easy to sample for chemical analyses. Formation events are common during the winter in the California Central Valley (Holets and Swanson 1981; Waldman et al. 1987; Suckling and Mitchell 1988; Underwood et al. 2004). The events form during stagnant and humid conditions, where under a clear night sky the moist surface air cools quickly and promotes water vapor condensation onto pre-existing aerosol particles. Because the fogs form during stagnant time periods with little mixing, a variety of emissions from agricultural, industrial, and residential activities in the valley accumulates and undergoes secondary chemical processes. These secondary chemical processes are analogous to

those that take place in clouds, except that they are expected to be more polluted. The compounds observed in fog water are from a variety of emission sources and the secondary reactions that may have occurred before and/or during the sampled fog events. The suspended fog droplets represent an aqueous phase reactor which allows secondary reactions to occur between water-soluble gases, the water-soluble portion of scavenged aerosol particles, and atmospheric oxidants (Waldman and Hoffmann 1987; Fuzzi et al. 1988). It has been shown that aqueous phase reactions can contribute to new particle growth and the production of secondary organic aerosols (Blando and Turpin 2000).

There are many possible aqueous phase SOA reaction products and the mechanisms of their formation are not well known. The gas phase oxidation of low molecular weight VOC results in the production of water-soluble volatile and semi-volatile organic compounds that freely partition to the aqueous phase, whether it is aerosol, cloud, or fog water. In the aqueous phase, compounds undergo further oxidation and subsequent accretion, likely contributing to further SOA production (Blando and Turpin 2000). SOA production by atmospheric oxidation happens for most organic compounds (Kroll et al. 2011). Products are typically the result of functionalization, fragmentation, and accretion reactions (Kroll et al. 2011) which include organic acids and the under characterized higher molecular weight SOA (aka oligomers), multifunctional compounds, organosulfates, and organonitrates (Altieri et al. 2009b; Perri et al. 2009; Perri et al. 2010; Yasmeen et al. 2010; Tan et al. 2011). Secondary aqueous products may form with or without photo-oxidation (Yasmeen et al. 2010). Accretion reactions have also been shown to proceed through two different mechanisms: hydration followed by

acetal/hemiacetal formation or acid-catalyzed aldol condensation (Yasmeen et al. 2010). The aldol condensation mechanism is prevalent at the higher pHs often found in fog water (Yasmeen et al. 2010). The possibilities that exist for reaction products and mechanisms contribute to the complexity of and difficulty of the characterization of AOM associated with aerosols and cloud/fog droplets.

In addition to the effects upon aerosol processes, fog events are of importance because of the effects they can have on environmental health (Waldman and Hoffmann 1987; Waldman et al. 1987; Weathers 1999; Herckes et al. 2007; Collett et al. 2008). Wet deposition of fog droplets can both remove hazardous pollutants from the air and in turn deposit them (Waldman and Hoffmann 1987; Waldman et al. 1987; Weathers 1999; Herckes et al. 2007; Collett et al. 2008) and their oxidized reaction products onto plant life and into bodies of water, causing harm. However, fog is very important as it deposits water and nutrients to ecosystems (Waldman and Hoffmann 1987; Weathers 1999). Fog is high in organic content and there are a wide range of water soluble organic compounds present. In order to understand the effects fog may have on the surrounding area, it is essential to characterize the AOM chemical composition. Thus far, only a small fraction of the organic compounds present have been identified. Nitrophenols are a great example. They have been known to be present in the atmosphere for some time (Nojima 1975), and their presence in the fog water has been well established (Richartz et al. 1990; Herterich 1991; Harrison et al. 2005a). In fact, nitrophenols are present at higher concentrations in fog than in air, due to the more effective scavenging ability of fog and the high water solubility of nitrophenols (Rippen et al. 1987; Richartz et al. 1990;

Harrison et al. 2005a). The occurrence of these compounds in fog means exposure to plant and animal life through wet deposition. Nitrophenols have been shown to be toxic to both humans (Allen and Allen 1997; Harrison et al. 2005a) and plants (Shea et al. 1983; Shafer and Schonherr 1985; Rippen et al. 1987). Studies have shown that nitrophenol deposition contributes to plant damage and forest degradation (Rippen et al. 1987; Leuenberger et al. 1988; Hinkel et al. 1989; Natangelo et al. 1999). Two nitrophenols have also been listed by the Environmental Protection Agency as priority pollutants (2000). Nitrophenols may be emitted directly to or formed in the atmosphere. Primary sources are mainly due to traffic and industrial activities (Leuenberger et al. 1988; Harrison et al. 2005a; Morville et al. 2006). Some nitrophenols are well known herbicides/pesticides used in agriculture and forestry (Rippen et al. 1987), however, it is unlikely to be a major source of nitrophenols in the atmosphere (Richartz et al. 1990; Harrison et al. 2005a). Secondary formation of nitrophenols can take place in both the gas and liquid phases (Harrison et al. 2005b). They are formed by oxidation and/or nitration of other primary emissions such as benzenes and phenols (Rippen et al. 1987; Hinkel et al. 1989; Richartz et al. 1990; Luttke et al. 1997; Bolzacchini et al. 2001; Kohler and Heeb 2003; Harrison et al. 2005a; Harrison et al. 2005b). The nitrophenols most commonly detected are 4-nitrophenol, 2-nitrophenol, and 2,4-dinitrophenol (Harrison et al. 2005a); of which, 4-nitrophenol is typically reported at the highest concentrations (Richartz et al. 1990; Luttke et al. 1997; Harrison et al. 2005a). The presence of dinitrophenols has been attributed to the additional nitration of mono-nitrated phenols (Richartz et al. 1990; Luttke et al. 1997; Harrison et al. 2005a; Vione et al.

2005). Although the presence and amount of nitrophenols in the atmosphere has been thoroughly reported, the majority of the water-soluble AOM in fog is uncharacterized. This is due to the wide variety of secondary processes occurring in the aqueous phase and the need for advanced analytical techniques for identification of the individual components.

A few studies employing ultrahigh-resolution mass spectrometry (MS) have shown that AOM is quite complex (Wozniak et al. 2008; Mazzoleni et al. 2010). Ultrahigh-resolution Fourier transform ion cyclotron resonance (FT-ICR) MS results in very well resolved and accurately measured mass enabling molecular formula assignment of its thousands of organic components (Marshall et al. 1998; Kujawinski 2002; Marshall et al. 2006; Sleighter and Hatcher 2007). Electrospray ionization (ESI) coupled with a FT-ICR-MS is ideally suited for analysis of any type of natural organic matter (NOM) (Fievre et al. 1997; Marshall et al. 1998; Kujawinski 2002; Stenson et al. 2002; Sleighter and Hatcher 2007). Due to its soft ionization, ESI does not fragment the molecules and thus preserves its structure during ionization (Fievre et al. 1997; Stenson et al. 2002), making it possible to obtain molecular formula assignments post MS. ESI FT-ICR MS is a highly sensitive technique thus it requires only small sample volumes, however, ionization efficiency may vary from compound to compound. Overall, FT-ICR-MS is the best mass analyzer for AOM because it has very high resolving power, mass accuracy, and sensitivity (Marshall et al. 1998). Identified molecular formulas of AOM do not provide structural information, only insights from the calculated double bond equivalents and atomic ratios. Thus, further investigations of the structures are needed to understand

the functional groups present and to better evaluate how these molecules affect the physical properties of aerosols. The acquisition of ultrahigh-resolution fragmentation data by tandem mass spectrometric analysis (MS/MS or MSⁿ) can help to provide structural characterization of these compounds. There have been many studies on the characterization of NOM using high-resolution mass spectrometry (Fievre et al. 1997; Kujawinski 2002; Kujawinski et al. 2002; Tolocka et al. 2004; Reemtsma et al. 2006b; Reinhardt et al. 2007; Sleighter and Hatcher 2007; Gomez-Gonzalez et al. 2008; Walser et al. 2008; Wozniak et al. 2008; Altieri et al. 2009b; Altieri et al. 2009a; Bateman et al. 2009; Laskin et al. 2009; Muller et al. 2009; Witt et al. 2009; Mazzoleni et al. 2010; Bones et al. 2010; Gao et al. 2010; Laskin et al. 2010; Nguyen et al. 2010; Roach et al. 2010) , however, far fewer have been done using tandem mass analysis (Tolocka et al. 2004; Reemtsma et al. 2006b; Gomez-Gonzalez et al. 2008; Sadezky et al. 2008; Muller et al. 2009; Witt et al. 2009; Bones et al. 2010; Gao et al. 2010; Laskin et al. 2010).

Previous mass spectrometric analysis of this fog water sample provided exact mass measurements and the molecular formulas of low molecular weight water-soluble AOM components (Mazzoleni et al. 2010). Of the 1300+ organic compounds present, nearly 500 of them contained nitrogen (Mazzoleni et al. 2010). From this data, a set of target compounds was selected for further structural identification. Of particular interest was to use FT-ICR-MS to obtain mass spectra and tandem mass spectra with ultrahigh-resolution and high mass accuracy for isolated organic anions of fog water samples, in order investigate climate relevant CHNO, CHOS, and CHNOS compounds. These compounds are of interest climatically because their polar functional groups (i.e.

hydroxyl, carboxyl, carbonyl, nitrate and sulfate). The functional groups have a significant amount of oxygen which has been shown to be correlated with the hygroscopic properties of the atmospheric aerosols (Zhang et al. 1993; Pang et al. 2006).

The structural characterization of identified water-soluble organic compounds in polluted fog water is presented in Chapter 2. The sample was obtained during a radiation fog event in January 2006 near Fresno, CA in California's Central Valley. Tandem mass analysis by collision induced dissociation (CID) was conducted within various scan ranges between 100 and 400 u to capture the targeted organic components of atmospheric aerosols. Due to the complexity of the water-soluble AOM in the sample, the scan ranges included additional precursor ions as well. Functional group analysis by matching precursors and fragment ions via neutral losses was more feasible than complete structural characterization. This work helps to shed light on the polar functional groups present on the molecules found in the aqueous phase. By analyzing the presence of these polar functional groups it is possible to gain a better understanding of the hygroscopic properties of SOA. Specifically the presence of nitrate, methyl-nitrate, sulfate, carboxyl, and hydroxyl functional groups associated with AOM were analyzed using tandem mass spectrometry by CID. Additionally, the presence of several suspected monoterpene derived molecules and their fragmentation behavior will be presented. Many of these monoterpene derivatives have been previously reported in both SOA chamber experiments and/or ambient samples (Gao et al. 2006; Iinuma et al. 2007; Surratt et al. 2007; Surratt et al. 2008; Altieri et al. 2009b; Altieri et al. 2009a). Evaluation of the whole data allows for a better understanding of the aerosol aging process. This method

was particularly useful in determining the presence of the various polar functional groups found on the molecules in the fog water.

Also presented in Chapter 2 are additional results of the fragmentation analysis. Fragmentation trends are discussed for each of the chemical groups (CHO, CHNO, CHNOS, and CHOS). The frequencies at which each neutral loss was observed are separated by structural classification determined by the Aromaticity Index proposed by Koch and Dittmar (2006). Presented in Chapter 3 is the presence of nitrophenols and linear alkylbenzene sulfonates (LAS) and their fragmentation behavior will also be discussed. Liquid chromatography/mass spectrometry (LC/MS) methodology will be discussed which was developed to isolate nitrophenols (m/z 138 – 197) from the bulk of the AOM present in the sample and to use tandem mass analysis to quantify their presence. Improvement of the structural understanding of atmospheric aerosols will allow for a better understanding of the aerosol aging process as well as the implications to human and environmental health and climate.

2 Fragmentation Analysis of Water-Soluble Atmospheric Organic Matter using Ultrahigh-Resolution Mass Spectrometry

The ultrahigh resolution analysis and data interpretation in the following section was completed by Jeffrey LeClair. Samples were provided by Dr. Jeffrey Collett, Jr. This work represents the draft of material to be submitted to the *Environmental Science and Technology* journal for publication in August 2011.

Approved by co-author/advisor Dr. Lynn R. Mazzoleni

Fragmentation Analysis of Water-Soluble Atmospheric Organic Matter using Ultrahigh- Resolution Mass Spectrometry

Jeffrey P. LeClair¹, Jeffrey L. Collett² and Lynn R. Mazzoleni^{1,3}*

¹Department of Chemistry, Michigan Technological University, 1400 Townsend Drive, Houghton, MI 49931 USA; ²Department of Atmospheric Science, Colorado State University, 1371 Campus Delivery, Fort Collins, CO, 80523 USA; ³Atmospheric Science Program, Michigan Technological University, 1400 Townsend Drive, Houghton, MI 49931 USA

*Corresponding author: Lynn Mazzoleni, Email address: lrmazzol@mtu.edu; Phone: +1-906-487-1853; and Fax: +1-906-487-2061.

2.1 Abstract

Isolated water-soluble analytes extracted from fog water collected during a radiation fog event near Fresno, CA were analyzed using collision induced dissociation and ultrahigh-resolution mass spectrometry. Tandem mass analysis was performed on scan ranges between 100-400 u to characterize the structures of nitrogen and/or sulfur containing species. CHNO, CHOS, and CHNOS compounds were targeted specifically because of the high number of oxygen atoms contained in their molecular formulas. Structural

functional groups were identified by matching fragment ions to precursor ions corresponding to common neutral losses (H_2O , CO_2 , CH_3OH , HNO_3 , CH_3NO_3 , SO_3 , SO_4 and several combinations of these). These polar functional groups are expected to affect the hygroscopic properties of aerosols. In total, 818 precursors were studied with variable structural properties. 22 molecular formulas are consistent with previously characterized monoterpene oxidation products. Five distinct monoterpene derived organonitrates, organosulfates, and nitroxy-organosulfates were observed in this study, including $\text{C}_{10}\text{H}_{16}\text{O}_7\text{S}$, $\text{C}_{10}\text{H}_{17}\text{NO}_7\text{S}$, $\text{C}_{10}\text{H}_{17}\text{NO}_8\text{S}$, $\text{C}_{10}\text{H}_{17}\text{NO}_9\text{S}$, and $\text{C}_{10}\text{H}_{17}\text{NO}_{10}\text{S}$.

KEYWORDS. WSOC, secondary organic aerosol, organonitrates, organosulfates, nitroxy-organosulfates, FT-ICR MS/MS.

2.2 Introduction

Radiation fog events are common during the winter in the California Central Valley (Holets and Swanson 1981; Waldman et al. 1987; Suckling and Mitchell 1988; Underwood et al. 2004). The events form during stagnant and humid conditions. Under a clear sky the moist surface air cools quickly and promotes water vapor condensation onto pre-existing aerosol particles. A variety of emissions from agricultural, industrial, and residential activities in the valley accumulates and undergoes secondary chemical processes. The suspended fog droplets represent an aqueous phase reactor which allows secondary reactions between water-soluble gases, the water-soluble portion of scavenged aerosol particles, and atmospheric oxidants (Waldman and Hoffmann 1987; Fuzzi et al. 1988). In the aqueous phase, compounds undergo further oxidation and subsequent

accretion, likely contributing to enhanced secondary organic aerosol (SOA) production (Blando and Turpin 2000). The oxidation products include organic acids and the poorly characterized higher molecular weight oligomers, multifunctional compounds, organosulfates, and organonitrates (Altieri et al. 2009b; Perri et al. 2009; Tan et al. 2011; Perri et al. 2010; Yasmeen et al. 2010). Secondary aqueous products may form in the absence of photooxidation (Yasmeen et al. 2010). Aqueous accretion reactions may proceed through different mechanisms: hydration, esterification (Altieri et al. 2008), hemiacetal/acetal (Bateman et al. 2008) and aldol condensation (Yasmeen et al. 2010). The aldol condensation mechanism is significant at higher pHs (Yasmeen et al. 2010). The possibilities that exist for reaction products and mechanisms contribute to the complexity and difficulty of the characterization of atmospheric organic matter (AOM). Aqueous phase reactions can contribute to new particle growth and the production of SOA (Blando and Turpin 2000). The compounds observed in polluted fog water are from a variety of emission sources and the secondary reactions that may have occurred before and/or during the sampled fog event. In addition to the effects upon aerosol processes, fog events are of importance because of the effects they can have on environmental health (Waldman and Hoffmann 1987; Waldman et al. 1987; Weathers 1999; Herckes et al. 2007; Collett et al. 2008).

Preliminary studies have shown that AOM is quite complex (Wozniak et al. 2008; Mazzoleni et al. 2010) requiring the use of ultrahigh-resolution mass spectrometry. Molecular formula assignment of its thousands of organic components requires interpretation of well resolved and accurate masses. Electrospray ionization (ESI)

coupled with a Fourier-transform ion cyclotron resonance mass spectrometer (FT-ICR-MS) is ideally suited for analysis of any type of natural organic matter (NOM) (Fievre et al. 1997; Marshall et al. 1998; Kujawinski 2002; Stenson et al. 2002; Sleighter and Hatcher 2007). Although molecular formulas have been identified for water-soluble organic compounds (WSOC) in AOM, investigations of the structure of these compounds are needed. Tandem mass spectrometry (MS/MS) with ultrahigh resolution analysis provides structural characterization of compounds. There have been many studies on the characterization of NOM using high-resolution mass spectrometry (Fievre et al. 1997; Kujawinski 2002; Kujawinski et al. 2002; Tolocka et al. 2004; Reemtsma et al. 2006b; Reinhardt et al. 2007; Sleighter and Hatcher 2007; Gomez-Gonzalez et al. 2008; Walser et al. 2008; Wozniak et al. 2008; Altieri et al. 2009b; Altieri et al. 2009a; Bateman et al. 2009; Laskin et al. 2009; Muller et al. 2009; Witt et al. 2009; Mazzoleni et al. 2010; Bones et al. 2010; Gao et al. 2010; Laskin et al. 2010; Nguyen et al. 2010; Roach et al. 2010), however, far fewer have been done using tandem mass analysis (Tolocka et al. 2004; Reemtsma et al. 2006b; Gomez-Gonzalez et al. 2008; Sadezky et al. 2008; Muller et al. 2009; Witt et al. 2009; Bones et al. 2010; Gao et al. 2010; Laskin et al. 2010).

In previous work to identify the molecular formulas of water-soluble AOM components, measurements were obtained from a hybrid linear quadrupole-ion trap (LTQ)/FT-ICR mass spectrometer (Mazzoleni et al. 2010). Of the 1300+ organic compounds present, nearly 500 of them contained nitrogen (Mazzoleni et al. 2010). From this data, a set of target compounds was selected for further identification. Of particular interest in this study was the use of FT-ICR-MS to obtain tandem mass spectra with ultrahigh-resolution

for isolated organic anions of fog water samples, in order to structurally verify the presence of suspected climate relevant CHNO, CHOS, and CHNOS compounds. Polar functional groups (i.e., hydroxyl, carboxyl, carbonyl, nitrate and sulfate) add a significant amount of oxygen to the total oxygen content which has been shown to be correlated with the hygroscopic properties of the atmospheric aerosols (Zhang et al. 1993; Pang et al. 2006). Additionally, improvement of the structural characterization of atmospheric aerosol components will allow for a better understanding of the aerosol aging process.

In the current study, we focus on the structural characterization of identified water-soluble organic compounds in polluted fog water. Ultrahigh-resolution tandem mass analysis was conducted over various scan ranges between 100 and 400 u to target nitrogen and sulfur containing organic compounds. Identification of the nitrate, methyl-nitrate, sulfate, carboxyl and hydroxyl functional groups associated with AOM is presented. Additionally, several suspected monoterpene derived molecules are presented, some of which have been reported in SOA chamber experiments and/or ambient samples (Gao et al. 2006; Iinuma et al. 2007; Surratt et al. 2007; Surratt et al. 2008; Altieri et al. 2009b; Altieri et al. 2009a).

2.3 Experimental Methods

2.3.1 *Sample Collection and Preparation*

Fog sample collection and preparation were described previously by Mazzoleni et al. (Mazzoleni et al. 2010). Briefly, radiation fog samples were collected in Fresno, CA in January 2006. A large stainless steel Caltech Active Strand Cloudwater Collector (Herckes et al. 2002a; Herckes et al. 2002b) was set up at the California State University experimental farm in an open field. The site represents a polluted urban fog environment, influenced by emissions of residential and industrial activities and transportation. Fog samples were collected over 1-2 hour time intervals and were stored in pre-baked amber glass jars under refrigeration immediately after collection. Strata-X (Phenomenex) solid phase extraction (SPE) was used to isolate fog water analytes. A sample volume of 100 mL (adjusted to pH 4.5, formic acid) was applied to the SPE cartridge. Isolates were extracted with 2 mL of high-purity water (pH adjusted to 10.4 with NH_4OH), methanol, and acetonitrile (10/45/45 vol/vol/vol). A brown color band was observed moving through the SPE material into the sample vial. Grey color was observed on the SPE sorbent, indicating some of the light absorbing compounds were not fully recovered.

2.3.2 Instrumental Parameters

Samples were analyzed with a hybrid 7 T Fourier transform ion cyclotron resonance (FT-ICR) mass spectrometer (LTQ FT Ultra, Thermo Scientific) equipped with electrospray ionization (ESI) source. Negative ions were produced by a source voltage of -3.8 kV. Mass resolving power, was set at 200,000 (at m/z 400) for all spectra. Automatic gain control was used to consistently fill the linear ion trap with the same number of ions ($n = 1 \times 10^6$) for each acquisition and to avoid space charge effects from over-filling the mass analyzer. Target precursor ions were isolated and fragmented with helium collision induced dissociation (CID) in the linear ion trap and then the ions were transferred to the FT-ICR-MS. This tandem mass analysis was done on several selected scan ranges with different isolation widths between 270 and 360 u. A full list of the scan ranges and instrumental parameters are given in Table 5.1. Due to the sample complexity, the isolation of target nominal masses resulted in the fragmentation of several precursor ions simultaneously. Mass spectra with and without CID were collected for each mass range. Individual mass spectra were collected and stored as transients by use of Thermo Xcalibur software. Prior to mass analysis, the instrument was externally calibrated in the negative ion mode with a standard solution of sodium dodecyl sulfate and taurocholic acid; the resulting mass accuracy was better than 2 ppm.

2.3.3 *Data Processing and Assignment of Molecular Compositions*

100+ transients were recorded in the time domain for each scan range and were co-added (Kujawinski et al. 2002; Stenson et al. 2003) with Composer (Sierra Analytics, Modesto, CA). Chemical formulas were assigned to the masses of singly-charged ions $100 < m/z < 400$ with relative abundances (RA) $\geq 0.1\%$ after internal recalibration. A list of the recalibration masses for each mass range is given in Table 5.1. The chemical formula calculator was set to allow up to 30 carbon, 60 hydrogen, 20 oxygen, 3 nitrogen, and 1 sulfur atoms per elemental composition. Data filtering for quality assurance of the assigned formulas was done as described previously in Mazzoleni et al. (2010). Double bond equivalents (DBE) were based on $C_xH_yN_zO_n$ and the equation $DBE = x - (1/2)y + (1/2)z + 1$ (McLafferty and Turecek 1993).

2.4 **Results and Discussion.**

The mass spectra of atmospheric organic matter (AOM) isolated from fog water is very complex, as described by Mazzoleni et al. (2010). The high relative abundance and frequency of the N- and S- containing compounds previously observed in fog water led to the selection of mass ranges for fragmentation analysis. The precursor chemical formulas were grouped by elemental composition i.e. CHO, CHNO, CHOS, and CHNOS. The number and type of precursor compounds studied were as follows: 304 CHNO (37.1%), 173 CHNOS (21.1%), 146 CHOS (18.0%), and 195 CHO (23.8%) compounds. As mentioned, the mass spectra are quite complex, for example there were 8 - 46 individual isobaric masses with $RA > 0.1$ (relative abundance is defined as the abundance of a

particular ion within the scan range it is associated with) identified within a nominal mass. Patterns of mass difference between isobaric masses are evident. A common repeating mass difference of 36 mDa occurs with the exchange of an O for CH₄. This mass difference has been seen in rainwater (Altieriet al. 2009b), aerosol (Reemtsma et al. 2006b; Schmitt-Kopplin et al. 2010), and fulvic acid samples (Stenson et al. 2003; Reemtsma et al. 2006a). Several series of this type can be found within each nominal mass unit. An excerpt of the mass spectra at m/z 343 is shown in Figure 2.1. In the mass range of 343.02 to 343.23, 10 series of 36 mDa mass difference series are present. The series include 2 CHO, 4 CHNO, 2 CHNOS, and 2 CHOS series. Each compound group is denoted with a unique shaped symbol and the series with each group are distinguished by color. Another way to evaluate this trend in the data is to graph the number of carbon atoms vs. m/z (Reemtsma 2010). The circles in Figure 2.1 were scaled to represent the relative abundance of the compounds. The more oxidized compounds are at the lower left of the plot, consistent with the lower numbers of carbon atoms, moving to the right with the exchange of O each for CH₄ (+36 mDa) in the series. There is a decrease of one DBE as the series moves right, corresponding to each exchange. Thus, the highest DBE values for each series are at the lower left of the plot and have the lowest mass defects.

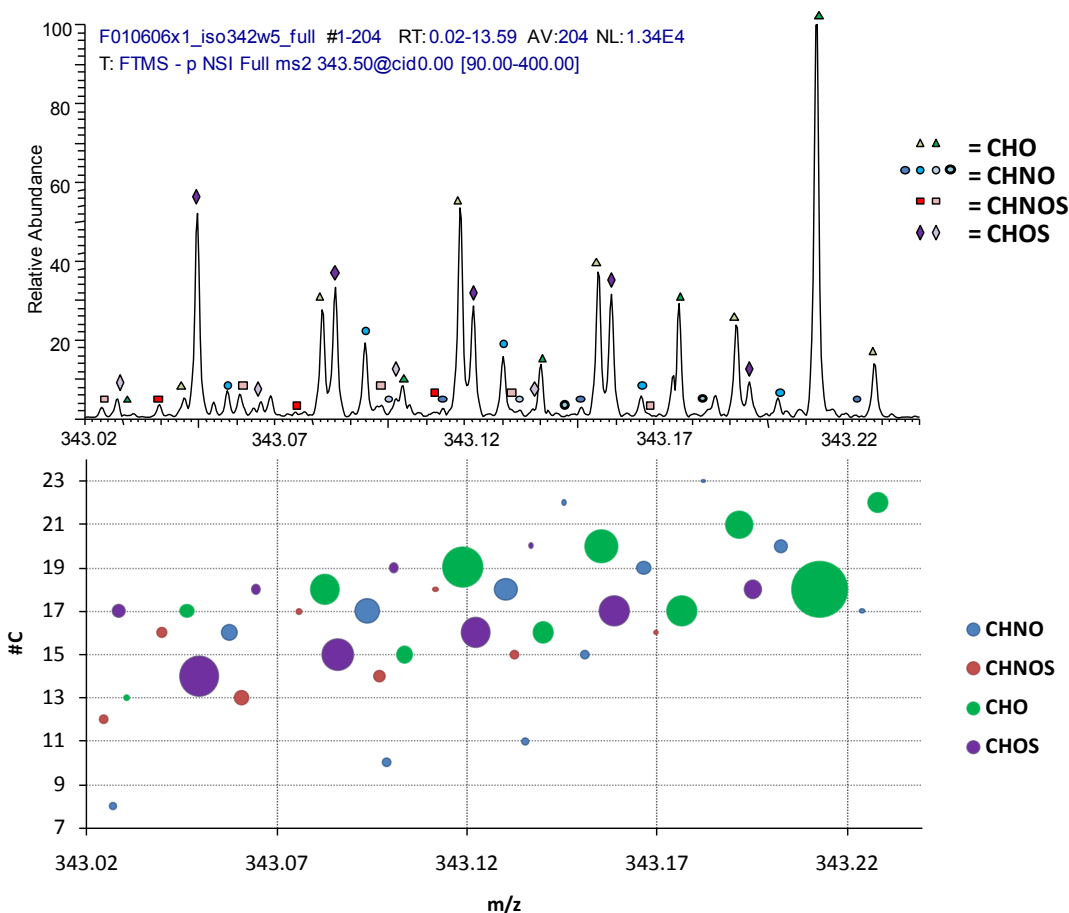


Figure 2.1: An excerpt of the mass spectra from $342.02 < m/z > 343.24$ is shown (top). The compound groups are distinguished by the symbol shape and series with group are distinguished by color. A #C vs. m/z plot of the same mass range $342.02 < m/z > 343$ (bottom). Compound groups are denoted by colored relative abundance scaled symbols and the $-O$, $+CH_4$ series with 36 mDa differences can be seen in diagonal lines with slope of ~ 0.04 .

2.4.1 AOM Fragmentation & Functional Groups

As expected from previous studies of water-soluble organic compounds (WSOC), the five most important neutral losses are CO_2 (44 u), H_2O (18 u), CH_3OH (32 u), HNO_3 (63 u) and/or CH_3NO_3 (77 u), and SO_3 (80 u) and/or SO_4 (96 u). The presence and frequency of these losses indicate the type of functional groups contained in these structures.

Considering the 818 compounds evaluated in this study, 21.9% lost H_2O , 20.4% lost

CH₄O, and 27.6% lost CO₂. The complexity of water soluble AOM precursors makes finding patterns and/or trends in the precursors with and without identified fragment ions very challenging. For this reason, we sorted the data with the Koch and Dittmar (2006) aromaticity index (AI). The use of aromaticity as a metric for structural classification allows for the classification of aliphatic, olefinic, aromatic, and condensed (poly-) aromatic structures. The AI assumes there is a contribution to the molecular DBE from the heteroatoms O, S, and N (e.g. C=O bonds). This contribution is removed by using an alternate DBE equation ($DBE_{AI} = 1 + C - O - S - 0.5H$). The equation from Koch and Dittmar (2006) is given below (Equation 1).

$$AI = DBE_{AI}/C_{AI} = (1 + C - O - S - 0.5H)/(C - O - S - N) \quad (1)$$

If $DBE_{AI} \leq 0$ or $C_{AI} \leq 0$, then $AI = 0$

The AI results in values from 0 to 1.5, where the higher AI values indicate more C-C double bonds, as seen in Table 2.1. Most of the studied compounds were aliphatic and olefinic. 53.1% were defined as aliphatic ($AI = 0$); 33.6% were defined as olefinic ($0 < AI \leq 0.50$); 8.3% were defined as aromatic ($0.5 < AI < 0.67$); and 5.0% were defined as condensed (poly-) aromatics ($AI \geq 0.67$) (see the top of Figure 2.3, located in the Supplemental Information (2.6)). The observed lowest relative abundances

Table 2.1: Statistics of fragmentation losses per compound group and separated into the four aromaticity index (AI) classifications: aliphatic, olefinic, aromatic and condensed aromatic. See also Figure 2.4 in the Supplemental Information.

AI Value	Group	Fragmentation Losses				
		H ₂ O	CH ₄ O	CO ₂	HNO ₃ / CH ₃ NO ₃	SO ₃ /SO ₄
AI = 0 “Aliphatic”	CHO (n = 94)	41	33	43	-	-
	CHNO (n = 120)	22	20	25	59	-
	CHNOS (n = 113)	8	13	7	19	16
	CHOS (n = 107)	17	17	17	-	52
0 < AI < 0.50 “Olefinic”	CHO (n = 84)	44	33	58	-	-
	CHNO (n = 124)	38	44	53	48	-
	CHNOS (n = 39)	1	1	2	0	3
	CHOS (n = 28)	0	0	0	-	13
0.50 < AI < 0.67 “Aromatic”	CHO (n = 16)	0	0	5	-	-
	CHNO (n = 35)	7	6	13	1	-
	CHNOS (n = 11)	1	0	0	0	0
	CHOS (n = 6)	0	0	0	-	0
AI ≥ 0.67 “Condensed Aromatic”	CHO (n = 1)	0	0	0	-	-
	CHNO (n = 25)	0	0	3	0	-
	CHNOS (n = 10)	0	0	0	0	1
	CHOS (n = 5)	0	0	0	-	0

correspond to aromatic ($0.5 < AI < 0.67$) and condensed aromatic compounds ($AI \geq 0.67$). Two van Krevelen plots, with the symbol size scaled to represent the relative abundance and colors to represent the four AI groups, are shown in Figure 2.3. Note the fragment ions have similar AI characteristics as the precursor ions. This is likely because most of the losses considered in this study are functional groups and are not main structural units. However, the density of the fragment ions in this figure may indicate a limitation of AI. Similar van Krevelen plots of the precursors are shown for each compound group in Figure 2.4, which is located in the Supplemental Information section of this chapter (2.6). The CHNO compounds exhibit the most aromatic character, especially with respect to the number of condensed aromatic structures ($AI \geq 0.67$). A total of 25 CHNO compounds with an $AI \geq 0.67$ were observed, representing 61.0% of the total condensed aromatic species. As stated above, the majority of the compounds studied are either aliphatic or olefinic. Aliphatic compounds show the greatest presence representing 48.2% of CHO, 39.5% of CHNO, 77.4% of CHOS, and 61.8% of CHNOS compounds. Compounds with olefinic character are the second most prevalent group, consisting of 43.1% of CHO, 40.8% of CHNO, 22.5% of CHOS, and 16.2% of CHNOS compounds.

The frequencies of the neutral losses by group and AI value are given in Table 2.1. Losses of H_2O come from both hydroxyl and carboxyl functional groups which were prevalent among the CHO compounds at 43.6% and 22.0% CHNO compounds. Molecules that exhibited a water loss were largely (95.5%) olefinic ($0 < AI \leq 0.5$). The neutral loss of methanol was observed from 33.8% of CHO compounds and from 23.0%

of CHNO compounds. The loss of CH₃OH indicates the presence of methoxy groups, likely from hemiacetal/acetal structures which formed between methanol and reactive carbonyl functional groups. Methanol was introduced during the sample handling, but is also expected to be naturally present in fog water (Yasmeen et al. 2010; Leriche et al. 2000). Thus, the observed hemiacetal and acetal structures may be a result of natural or artificial processes (Bateman et al. 2008). However, the fog sample was rendered basic during sample preparation, which could reverse the formation of hemiacetal/acetal that occurred under acidic conditions. 83 of the compounds with methanol losses were aliphatic (AI = 0), as well as 78 compounds having olefinic character ($0 < AI \leq 0.50$). Losses of carboxyl groups were dominant in CHO and CHNO compounds. Similar to the trend with water and methanol losses, 92 of the molecules with CO₂ losses were aliphatic (AI = 0) and 113 had olefinic character ($0 < AI \leq 0.50$).

Nitrate functional groups were of interest in this study because of the numerous and highly abundant CHNO compounds in the sample (Mazzoleni et al. 2010). A total 108 of 304 CHNO compounds, or 35.5%, exhibited a neutral loss of HNO₃ and/or CH₃NO₃. As for CHNOS compounds, 19 of 173 CHNOS compounds, or 11%, exhibited a neutral loss of HNO₃ and/or CH₃NO₃. Comparison of CHNO and CHNOS compounds that lost a nitrate with those that did not indicates that most of the compounds which exhibited the losses (99.2%) (Figure 2.2) were not aromatic. However, there are many

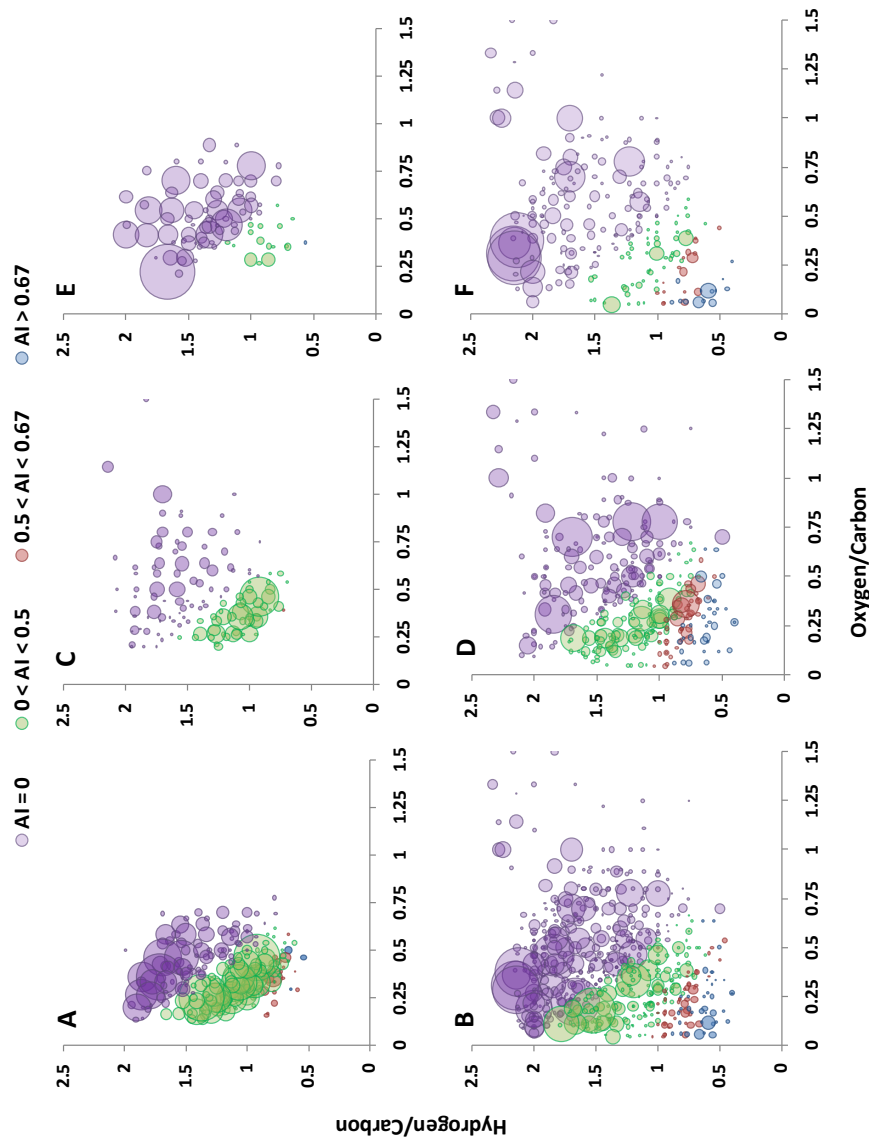


Figure 2.2: van Krevelen diagrams with colored symbols to represent aromaticity index (AI) categories: aliphatic, olefinic, aromatic, and condensed aromatic as described in Table 2.1. Symbols are scaled to represent the relative abundance of analytes with respect to each individual mass spectra. The plots A-F represent precursor losses: A) all compounds with a carboxyl loss; B) all compounds without carboxyl losses; C) CHNO and CHNOS compounds with a nitrate loss; D) CHNO and CHNOS compounds without a nitrate loss; E) CHOS and CHNOS compounds with a sulfate loss; and F) CHOS and CHNOS compounds without a sulfate loss.

aliphatic compounds (AI = 0) of very high relative abundance that did not lose a nitrate group.

The large number (196 of 304 compounds or 64.5%) of CHNO species without a nitrate suggests that there may be other types of nitrogen containing functional groups present in these structures, such as nitro, amine, and imine groups. Nitrophenols and other CHNO compounds with nitro functional groups are expected, however the occurrence of NO and NO₂ were rare and uncertain. NO and NO₂ losses were observed from nitrophenols observed in the range of 138 – 197 u. Similarly Zhang and Anastasio 2001 reported a large amount of inorganic NH₄⁺, as well as the presence of amino acids and amino containing compounds in radiation fog samples from just south of Fresno in the Central Valley (Zhang and Anastasio 2001). The potential for reduced organic nitrogen species in aqueous samples has been well documented (Zhang and Anastasio 2001; 2003; De Haan et al. 2009; Galloway et al. 2009; Laskin et al. 2009; Noziere et al. 2009; Shapiro et al. 2009; Bones et al. 2010; De Haan et al. 2011; Laskin et al. 2010; Noziere et al. 2010). In recent studies (Galloway et al. 2009; Shapiro et al. 2009), the formation of light absorbing products, from glyoxal, in the presence of ammonium sulfate and ammonium nitrate was observed. Ammonium ions have been shown to act as a catalyst for accretion reactions (Noziere et al. 2009; Shapiro et al. 2009; Noziere et al. 2011). Reactions with aldehydes and dicarbonyls (i.e. glyoxal) produce various imidazole compounds (Galloway et al. 2009; Laskin et al. 2010; De Haan et al. 2011) and reactions with polycarbonyls produce imines (Galloway et al. 2009; Bones et al. 2010; Laskin et al. 2010). The reactions of glyoxal and amino acids have shown imidazole and diamine products (De

Haan et al. 2009), while reactions involving methylglyoxal and amino acids/methylamine have shown imidazole and accretion products (De Haan et al. 2011). Similarly, reactions have been shown to occur with monoterpene oxidation products (Bones et al. 2010; Laskin et al. 2010). These reports and our observation of isolated colored fog AOM components, suggests the presence of secondary products from the reaction of NH_4^+ or NH_3 with reactive carbonyls in this sample. The pH of the fog at the time of collection was 6.5. The abundance of agricultural emissions in the California Central Valley and the high partitioning coefficient for NH_3 suggests that it or NH_4^+ were available for reaction potentially forming imidazoles. Two molecular formulas, $\text{C}_{16}\text{H}_{23}\text{NO}_3$ and $\text{C}_{16}\text{H}_{22}\text{N}_2\text{O}_3$, were in common with the laboratory study of limonene/ozonolysis SOA aging in the presence of NH_3 gas by Laskin et al. (2010). The first compound was $\text{C}_{16}\text{H}_{23}\text{NO}_3$ (DBE = 6, RA = 8.47%) at m/z 276.1607, and did not exhibit any common neutral losses. The second compound, $\text{C}_{16}\text{H}_{22}\text{N}_2\text{O}_3$ (DBE = 7, RA = 0.63%), was observed at m/z 289.1560. A loss of CO_2 was observed for this compound. The absence of a nitrate loss, suggests the N may be reduced, as in amine or imine groups, rather than oxidized as in nitrate or nitro groups.

Organosulfates are of interest because of their prominence in the mass spectra of the sample. As with nitrate functional groups, sulfates are also important because they indicate the location of oxygen atoms in the structures. Analysis of the fragment ions resulted in finding losses representing sulfate for 44% of 146 CHOS. It may be possible that some of these CHOS compounds without identified sulfate losses contain non-terminal sulfate groups (Iinuma et al. 2007). Losses of sulfate were identified for 11% of

173 CHNOS compounds within the study. A comparison of compounds that lost a sulfate moiety and those that did not is shown in Figure 2.2. As illustrated, the loss of sulfate was found most often in CHOS and CHNOS aliphatic ($AI = 0$) compounds. Comparatively, only a few losses of sulfate were observed for the olefins ($0 < AI \leq 0.50$) and no losses of sulfate were observed for the aromatic molecules ($0.50 < AI < 0.67$). Several aliphatic CHOS compounds of very high relative abundances were observed without matching fragment ions representing $[M-SO_4]^-$. Over all of the CHNOS compounds ($n = 173$), 22.5% of them lost either a sulfate or nitrate. Only two CHNOS compounds showed a loss of both a sulfate and a nitrate.

2.4.2 Fragmentation of Selected SOA Components

Recent chamber studies of monoterpene derived organosulfates and nitroxy-organosulfates have been done and formation mechanisms of the probable structures were presented (Schmitt-Kopplin et al. 2010; Gao et al. 2006; Iinuma et al. 2007; Surratt et al. 2007; Surratt et al. 2008). Several investigators (Iinuma et al. 2007; Surratt et al. 2007; Gomez-Gonzalez et al 2008; Surratt et al. 2008; Altieri et al. 2009b) have reported observations of organosulfates and nitroxy-organosulfates in ambient samples. Here, the similarities between our observational data and those studies and a few new formulas unique to this study are presented. Due to the mild average temperature of 55 °F in Fresno, emissions of terpenes were very likely present.

The presence of organosulfates (CHOS), nitroxy-organosulfates (CHNOS), and organonitrates (CHNO) in aqueous atmospheric samples have been reported in several studies (Gao et al. 2006; Iinuma et al. 2007; Surratt et al. 2007; Gomez-Gonzalez et al. 2008; Surratt et al. 2008; Altieri et al. 2009b; Altieri et al. 2009a; Mazzoleni et al. 2010; Schmitt-Kopplin et al. 2010). Several of the same molecular formulas were observed in this targeted fragmentation study. The first is an organosulfate at m/z 279.0546 with a molecular formula of $C_{10}H_{16}O_7S$ (DBE = 3) and relative abundance of 25%. It was previously observed in ambient and laboratory samples (Surratt et al. 2007; Surratt et al. 2008; Altieri et al. 2009b) and the probable structures were proposed by Surratt and colleagues (Surratt et al. 2007; Surratt et al. 2008). Several fragment ions corresponding to the neutral losses of two water molecules (36 u), SO_3 , and SO_4 were observed. Similar fragment ions are expected for other monoterpene oxidation products. Interestingly, the fragment ion that represents a loss of SO_4 from this precursor is m/z 183.1027 ($C_{10}H_{16}O_3$), likely corresponding to pinonic acid. Similar to m/z 279, another compound $C_{11}H_{18}O_7S$ with DBE = 3 at m/z 293.0703 with a relative abundance of 4.26% and related to $C_{10}H_{16}O_7S$ by a difference of CH_2 was observed with both losses of SO_4 and SO_3 . Additional possible organosulfates were identified, but all of which had lower relative abundances. One was identified as $C_{10}H_{16}O_8S$ at m/z 295.0496 with a DBE = 3 and with a relative abundance of 0.7%. Fragment ions representing losses of H_2O , SO_3 , and SO_4 were identified. This is identical to what was observed for the compound at m/z 279.0546. Another possible organosulfate was identified as $C_{10}H_{16}O_9S$ at m/z 311.0444 with a DBE = 3 and with a relative abundance of 0.2%. It is very similar to the others

with respect to DBE and the number of carbon atoms, but no fragment ions matching the neutral losses were identified. Possibly, this is because of the low abundance of the precursor ion which would result in fragment ions below the method detection limit. Another similar compound, $C_{11}H_{18}O_8S$ (DBE = 3), was identified at m/z 309.0652 with a relative abundance of 0.83%. Two CHOS compounds that may represent monoterpene “dimers” were found. The precursor $C_{17}H_{26}O_5S$ (DBE = 5), was identified at m/z 341.1431 (9.97% RA). Fragment ions corresponding to losses of H_2O , CH_4O , CO_2 , and SO_3 were identified for this compound. Another compound differs from the last by CH_2 . This organosulfate, $C_{18}H_{28}O_5S$ with DBE = 5, was present at m/z 355.1588 with a relative abundance of 2.26%. The only fragment ion observed was a loss of SO_3 . Two other possible organosulfates were identified at m/z 279.1637 as $C_{13}H_{28}O_4S$ (DBE = 0 and RA = 100%) and at m/z 353.2007 as $C_{16}H_{34}O_6S$ (DBE = 0 and RA = 100%). None of the typical neutral losses were observed for either compound.

A possible nitrooxy-organosulfate was observed at m/z 294.0655 was identified as $C_{10}H_{17}NO_7S$ (DBE = 3) with a relative abundance of 33%. A loss of a HNO_3 group corresponded to it, which is consistent with previous studies (Schmitt-Kopplin et al. 2010; Gao et al. 2006; Surratt et al. 2007; Surratt et al. 2008). The same molecular formula has been reported in a few studies (Gao et al. 2006; Surratt et al. 2007; Surratt et al. 2008; Altieri et al. 2009b; Schmitt-Kopplin et al. 2010). Chamber studies indicate that it was formed from alpha-pinene oxidation (Gao et al. 2006; Surratt et al. 2007; Surratt et al. 2008; Schmitt-Kopplin et al. 2010). However, the same molecular formula could result from the oxidation of other monoterpene precursors (Inuma et al. 2007). Several

different structures have been proposed for this molecule, but Iinuma et al. (2007) and Surratt et al. (2008) both proposed nighttime NO_3 radical oxidation of monoterpenes. Similar reaction pathways might have occurred before or during the fog event sampled. Another two compounds included in this fragmentation analysis were observed in both ambient and chamber samples (Surratt et al. 2007; Surratt et al. 2008; Schmitt-Kopplin et al. 2010). The first was $\text{C}_{10}\text{H}_{17}\text{NO}_8\text{S}$, DBE = 3, at m/z 310.0604 with a relative abundance of 7.5%. A fragment ion representing the loss of HNO_3 was observed. The second, $\text{C}_{10}\text{H}_{17}\text{NO}_9\text{S}$ (DBE = 3), at m/z 326.0555 was observed with a relative abundance of 2.6%. Consistent with the other possible nitrooxy-organosulfate structures, a neutral loss of HNO_3 was determined from the fragment ions. This compound was seen in both Schmitt-Kopplin et al. (2010) and Surratt et al. (2007). The specific structures of these compounds depend on the structure of the precursor monoterpene and the possible oxidation mechanism. Another CHNOS compound that remains largely uncharacterized, but observed previously (Iinuma et al. 2007; Surratt et al. 2008) is $\text{C}_{10}\text{H}_{17}\text{NO}_{10}\text{S}$ (DBE = 3) with a relative abundance of 22% at m/z 342.0503. Neither of the previous studies proposed a structure for it. Iinuma et al. (2007) observed a loss of HNO_3 , which is consistent with our finding. In addition to the HNO_3 loss, a CH_3NO_3 loss was also observed. This loss suggests that the nitrate is present as a methyl-nitrate substituent on the molecule. Another molecule, $\text{C}_{10}\text{H}_{17}\text{NO}_6\text{S}$ (DBE = 3) at m/z 278.0706 was present with a relative abundance of 4.7%. However, neither a nitrate or sulfate loss was observed. In any case, this compound cannot contain both nitrate and sulfate functional groups because it contains only six oxygen atoms. Another compound in the

same CH₂ homologous series, C₁₁H₁₉NO₆S (DBE = 3) with 0.72% relative abundance was identified at m/z 292.0862. Despite its lower relative abundance, fragment ions corresponding to the losses of CH₄O, CO₂, and SO₃ were observed.

There are similarities to monoterpene structures with respect to the #C and #H (C₁₀-C₁₁ and H₁₅-H₁₉) in several of the CHNO compounds. This may suggest they are derived from monoterpenes. Five NO₇ and NO₈ compounds with DBE = 3 or 4 and C# = 10 or 11 were identified: m/z 274.0934 C₁₁H₁₇NO₇ (DBE = 4, RA = 13.82%), m/z 276.1091 C₁₁H₁₉NO₇ (DBE = 3, RA = 7.29%), m/z 276.0727 C₁₀H₁₅NO₈ (DBE = 4, RA = 6.58%), m/z 290.0884 C₁₁H₁₇NO₈ (DBE = 4, RA = 4.02%), and m/z 292.1040 C₁₁H₁₉NO₈ (DBE = 3, RA = 2.58%). Fragment ions representing losses of HNO₃ and CH₃NO₃ were found for all five analytes, thus these molecules have methyl-nitrate functional groups. Methyl-nitrate functional groups have been proposed (Surratt et al. 2007; Surratt et al. 2008); however, none of the previous studies reported a neutral loss of CH₃NO₃. The two NO₇ compounds differ by only 2 hydrogen atoms which equates to one DBE. Losses of CO₂, and CO₂+H₂O (62 u) were observed for C₁₁H₁₇NO₇ and a loss of two water molecules (36 u) were observed for C₁₁H₁₉NO₇. This indicates that the double bond in the CO₂ functional group is likely responsible for the difference in DBE values. Two of the three NO₈ compounds, C₁₀H₁₅NO₈ and C₁₁H₁₇NO₈, differ by a CH₂ unit and C₁₁H₁₉NO₈ differs by two hydrogen atoms from C₁₁H₁₇NO₈. In addition to their nitrate losses, C₁₀H₁₅NO₈ lost a CO₂+H₂O (62 u) and C₁₁H₁₉NO₈ lost two water molecules (36 u). CHNO compounds with two nitrogen atoms were also observed. N₂O₇ and N₂O₈ compounds may be the result of monoterpene oxidation products with two nitrate groups. At m/z

275.0886, $C_{10}H_{16}N_2O_7$ (DBE = 4) was identified with a relative abundance of 1.51%. A fragment ion corresponding to the loss of HNO_3 was observed. A compound with similar characteristics was identified at m/z 289.1046, $C_{11}H_{18}N_2O_7$ (DBE = 4) with 0.63% relative abundance, however, no fragment ions were observed. Two low abundance (< 1%) N_2O_8 compounds were identified as $C_9H_{14}N_2O_8$ (DBE = 4) and $C_{10}H_{16}N_2O_8$ (DBE = 4) at m/z 277.0674 and m/z 291.0838. Fragment ions indicating the loss of HNO_3 were found for $C_9H_{14}N_2O_8$, but not for $C_{10}H_{16}N_2O_8$. The low relative abundance of these compounds is a probable reason for not finding any relevant fragment ions.

Three possible CHNO monoterpene SOA “dimers” were observed. The first was observed at m/z 352.1770 and identified as $C_{18}H_{27}NO_6$ (DBE = 6, RA = 0.87%). The second, m/z 354.1926 was identified as $C_{18}H_{29}NO_6$ (DBE = 5, RA = 0.73%). The third, m/z 354.1562 was identified as $C_{17}H_{25}NO_7$ (DBE = 6) with relative abundance of 0.91%. Fragment ions corresponding to losses of CO_2 , CO_2+H_2O , HNO_3 , and CH_3NO_3 were observed for each of these compounds. The loss of a methyl-nitrate for each of these three possible “dimers” suggests that they have a methyl-nitrate functional group. Additional fragment ions, such as a loss of CH_3OH+CO_2 for $C_{18}H_{27}NO_6$, losses of H_2O and CH_3OH for $C_{18}H_{29}NO_6$, and losses of H_2O , CH_3OH , and CH_3OH+CO_2 for $C_{17}H_{25}NO_7$ were observed. As stated previously, the losses of CH_3OH indicate the presence of acetal/hemiacetal containing structures.

Fifteen common molecular formulas between this study and recent ultrahigh resolution MS analysis of alpha-pinene/ozonolysis SOA (Putman et al. 2011) were found in a mass

range of 292-356 u. Although the molecular formulas are identical, they may represent different isomeric structures. The first, identified as $C_{17}H_{26}O_7$ (DBE = 5) at m/z 341.1609 with 13.39% relative abundance. The second was observed at m/z 355.1767 and was identified as $C_{18}H_{28}O_7$ (DBE = 5) with a relative abundance of 1.61%. Neutral losses corresponding to H_2O , CH_3OH , CO_2 , CO_2+H_2O (62 u), CH_3OH+CO_2 (76 u), and double CO_2 (88 u) were observed. The two compounds may have similar structures because the same losses were observed for each of them and they differ by CH_2 . The third compound observed at m/z 353.1611 and identified as $C_{18}H_{26}O_7$ (DBE = 6) with 1.80% relative abundance appears to be similar to the first and second compounds, suggesting that they are structurally related. This molecule differs from $C_{18}H_{28}O_7$ by two hydrogen atoms and from $C_{17}H_{26}O_7$ by a carbon atom. Fragment ions corresponding to losses of H_2O , CO_2 , and CO_2+H_2O (62 u) were observed for this compound. These losses were also seen for the first and second compounds. The fourth, $C_{17}H_{26}O_6$ (DBE = 5) with a relative abundance of 0.45% was observed at m/z 325.1662. Losses of CO_2 and CO_2+H_2O (62 u) were identified for it. Several additional common compounds were found with low relative abundance (eight with RA < 4%). Eight C_{16} compounds were in common with the Putman et al. 2011 alpha-pinene/ozonolysis SOA (Putman et al. 2011). They may also represent monoterpene SOA components. These C_{16} compounds range from $O_5 - O_8$ with DBE = 5 - 6, with two compounds per oxygen number, each differing by two hydrogen atoms or one DBE. Fragment ions were observed for 6 of the 8 C_{16} compounds corresponding to neutral losses including H_2O , CH_3OH , double H_2O , CO_2 ,

CO₂+H₂O, and CH₃OH+CO₂. These CHO compounds may also be present as the core of more functionalized compounds.

2.4.3 Atmospheric Implications and Oxidation State

Recently, Kroll et al. (2011) proposed the use of the average carbon oxidation state (OS_c) to describe the oxidative aging of atmospheric organic aerosols. Due to the complex nature of atmospheric water-soluble organic compounds, the OS_c is estimated solely from the total O:C and H:C ratios. In this way the oxygen is assumed to be bonded to carbon. Further there is a great deal of uncertainty in the effect of N on the OS_c because both oxidized N (in the form of nitro and nitrate functional groups) and reduced N (in the form of amines, imines, and imidazoles) are expected in aerosol organic compounds. Kroll et al. (2011) suggested that nitrogen containing functional groups represent only a small part of total WSOC and thus they would have a small effect on the OS_c estimate. However, in this fog sample, a substantial fraction of the total number of identified AOM species is organic nitrogen containing compounds (Mazzoleni et al. 2010). Thus, the presence of various nitrogen and sulfur containing functional groups may have a significant effect on the estimate of the OS_c. For example, both nitrogen and sulfur in the form of ONO₂ and OSO₃ were observed in this study. These functional groups contain 2-3 non-carbon associated oxygen atoms.

Less than half of all of the CHNO and CHNOS compounds present in this sample exhibited a loss of a nitrate functional group, there might be other nitrogen containing

functional groups present, such as amines, imines, and nitros (as described above). As with the CHNO and CHNOS compounds, less than half of the CHOS and CHNOS compounds showed a neutral sulfate loss. This suggests a presence of other types of sulfur functional groups. It is possible there may be molecules with an internal sulfate bridge (Iinuma et al. 2007) or a sulfonate functional group. Both of these contain oxygen atoms which are not directly bonded to carbon. Further work is needed to identify additional functional groups and to overcome some of the detection limit issues observed in this study.

To gain a more concrete understanding of the chemical composition and the type and frequency of various N- and S-containing functional groups, the use of both (-) and (+) mode ultrahigh-resolution MS on the same sample is necessary. In fact, a recent ultrahigh-resolution MS study on rainwater showed that (-) mode MS only accounted for 25% of the total N-containing species, while (+) mode accounted for the other 75% (Altieri et al. 2009a). Also, the presence of reduced S-containing functional groups in the (+) mode is likely. However, mass spectrometry cannot provide all of the information regarding the nature of the all of the functional groups present. Other analytical techniques, in addition to ultrahigh-resolution mass spectrometry, are required in order to determine the presence of the various types of nitrogen and sulfur containing molecules.

2.5 Acknowledgements

We thank Drs. Melissa Soule & Elizabeth Kujawinski of the Woods Hole Oceanographic Institution (WHOI) Mass Spectrometry Facility for instrument time and assistance with data acquisition (NSF OCE-0619608 and Gordon and Betty Moore Foundation). The authors acknowledge the NSF Division of Atmospheric Chemistry (ATM-0222607) for support to collect fog samples. JPL thanks WHOI for a travel grant. The authors gratefully acknowledge the Michigan Tech Research Excellence Fund for a seed grant which provided support for this research.

2.6 Supplemental Information

Additional figures for data visualization are also provided in the following pages.

Supplemental Information

Fragmentation Analysis of Water-Soluble Atmospheric Organic Matter using Ultrahigh- Resolution Mass Spectrometry

Jeffrey P. LeClair¹, Jeffrey L. Collett² and Lynn R. Mazzoleni^{1,3}*

¹Department of Chemistry, Michigan Technological University, 1400 Townsend Drive,
Houghton, MI 49931 USA

²Department of Atmospheric Science, Colorado State University, 1371 Campus Delivery,
Fort Collins, CO, 80523 USA

³Atmospheric Science Program, Michigan Technological University, 1400 Townsend
Drive, Houghton, MI 49931 USA

*Corresponding author: Dr. Lynn Mazzoleni, Email address: irmazzol@mtu.edu; Phone
+1-906-487-1853; and Fax 906-487-2061

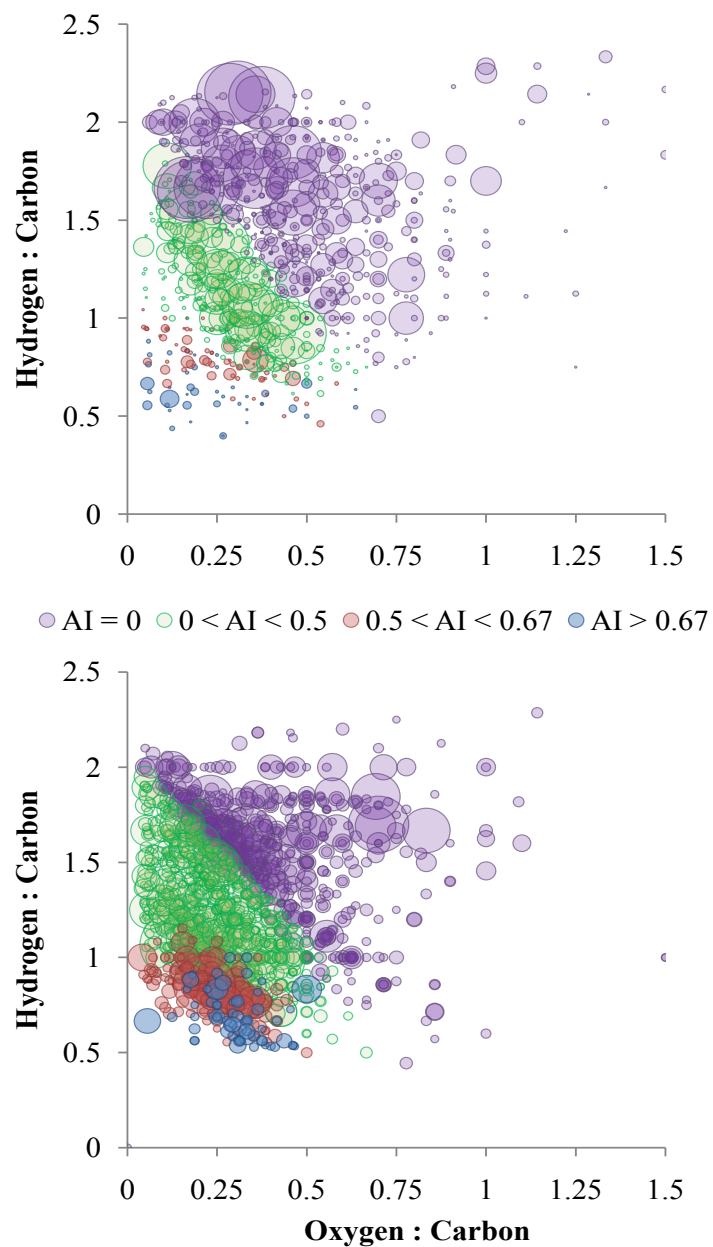


Figure 2.3: A comparison of all identified precursor compounds (top) and fragment ions (bottom) is shown here. A calculation of aromaticity index (AI) based on Koch et al.(Koch and Dittmar 2006) was performed and is reflected by the color coding of the points on these Van Krevelen diagrams. An explanation of the color coding can be seen in Table 2.1. The size of the points is dependent on the percent relative abundance for each. In both the top and bottom of the diagram, a few points of low relative abundance lie beyond the O:C = 1.5 cutoff.

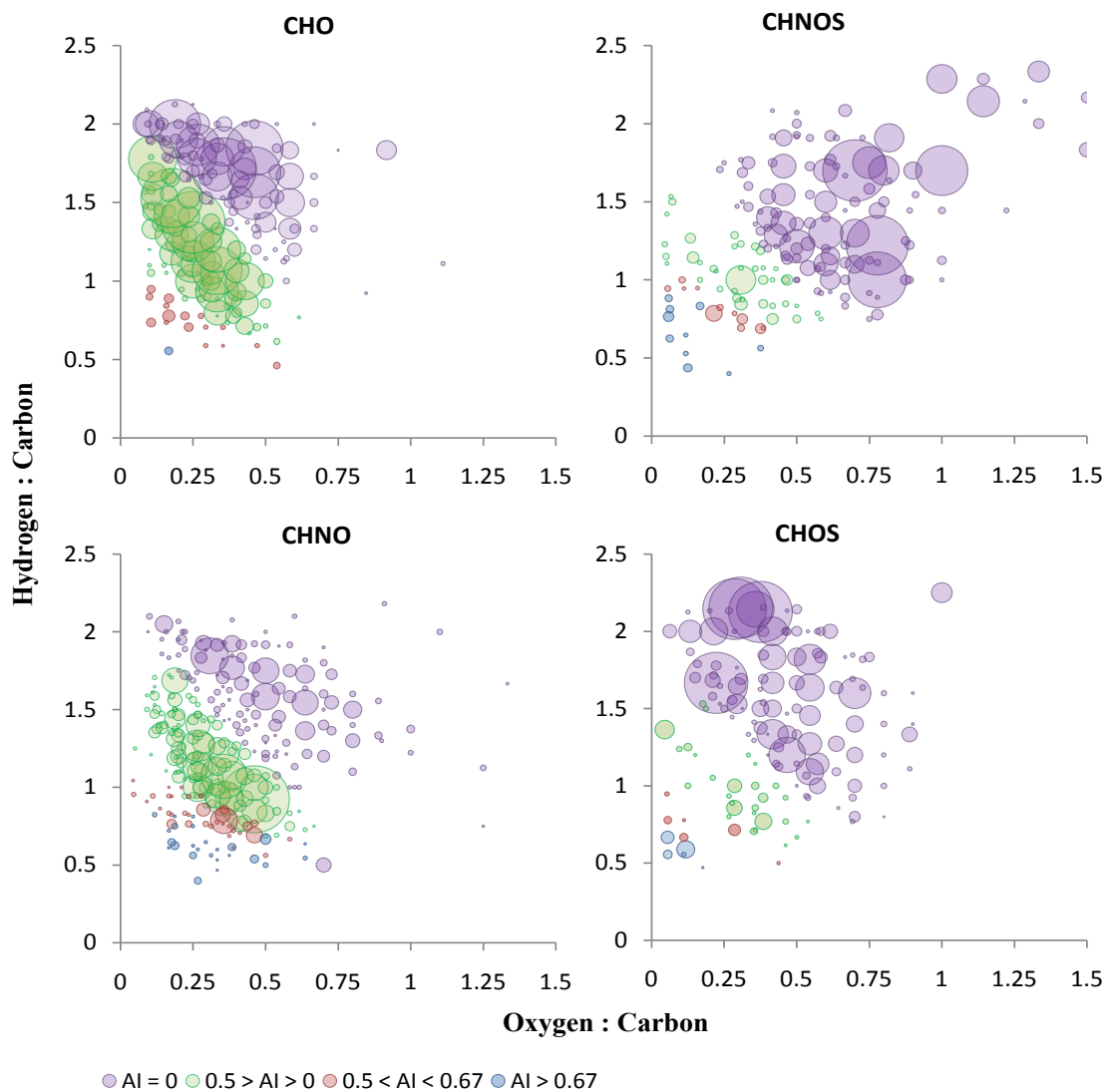


Figure 2.4: A comparison of precursor compounds from each compound class is shown here. A calculation of aromaticity index (AI) based on Koch and Dittmar (2006) was performed and is reflected by the color coding of the points on these Van Krevelen diagrams. An explanation of the color coding can be seen in Table 2.1. The size of the points is dependent on the percent relative abundance for each. In the CHNOS and CHNO sections of the figure, a few points of low relative abundance lie beyond the O:C = 1.5 cutoff.

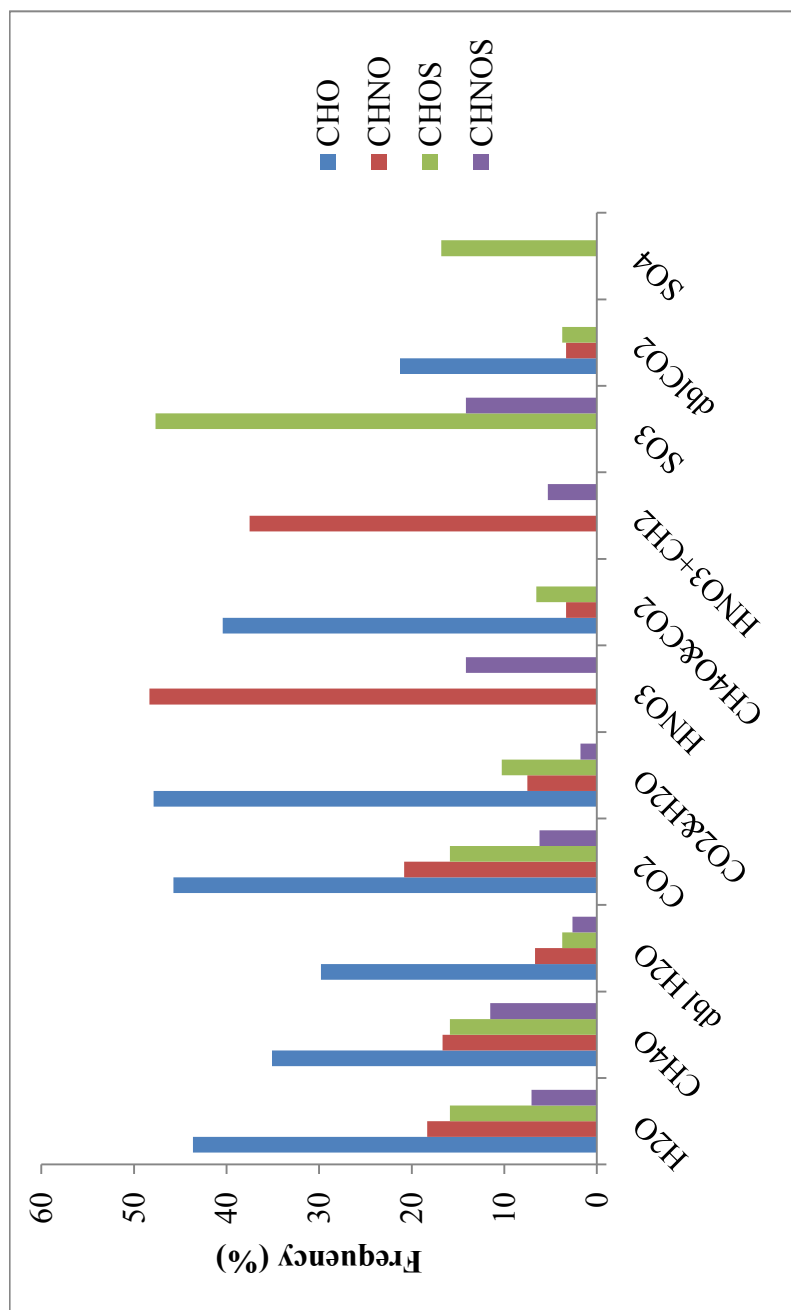


Figure 2.5: The frequency of neutral losses separated by chemical group. These compounds are all “aliphatic” species (AI = 0)(Koch and Dittmar 2006).

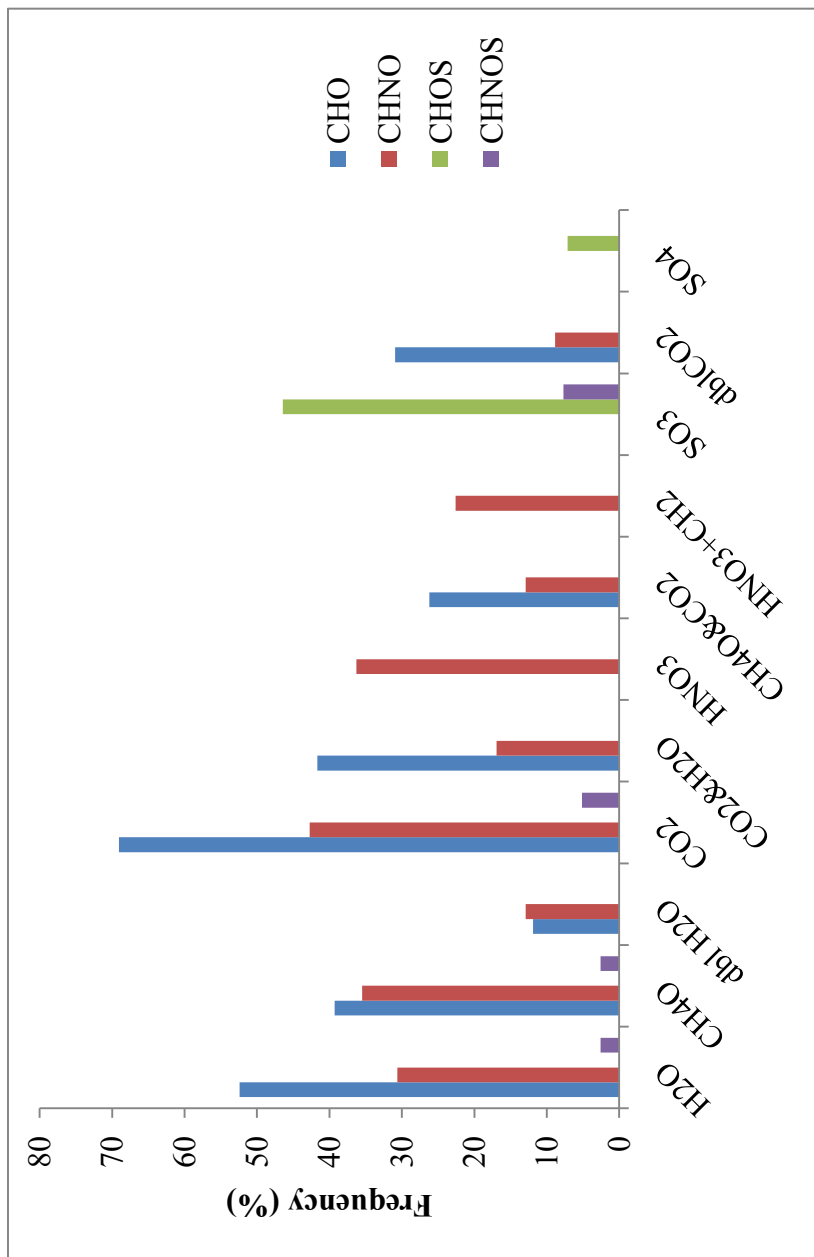


Figure 2.6: The frequency of neutral losses separated by chemical group. These compounds are all “olefinic” species ($0 < AI < 0.50$) (Koch and Dittmar 2006).

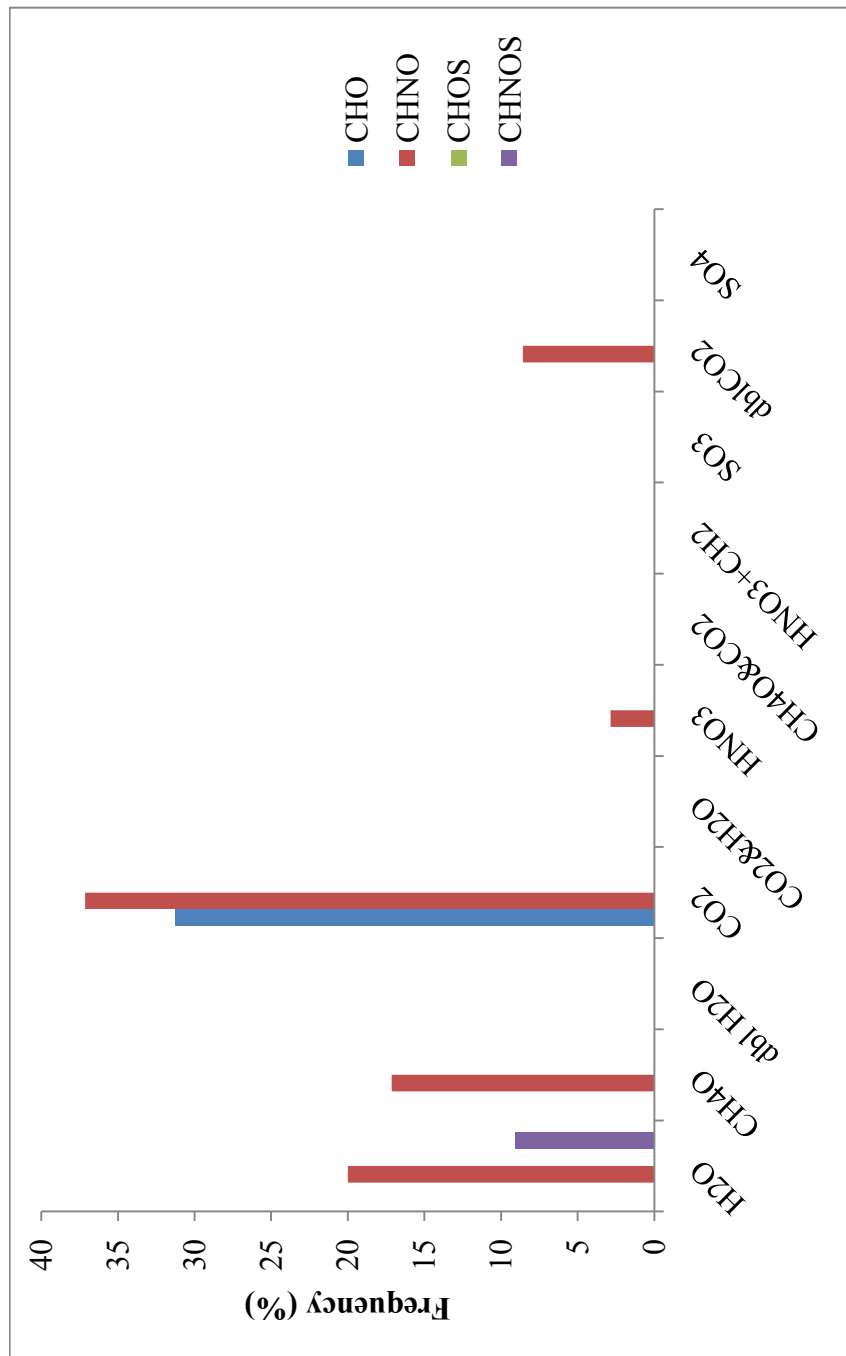


Figure 2.7: The frequency of neutral losses separated by chemical group. These compounds are all “aromatic” species ($0.50 < AI < 0.67$) (Koch and Dittmar 2006)..

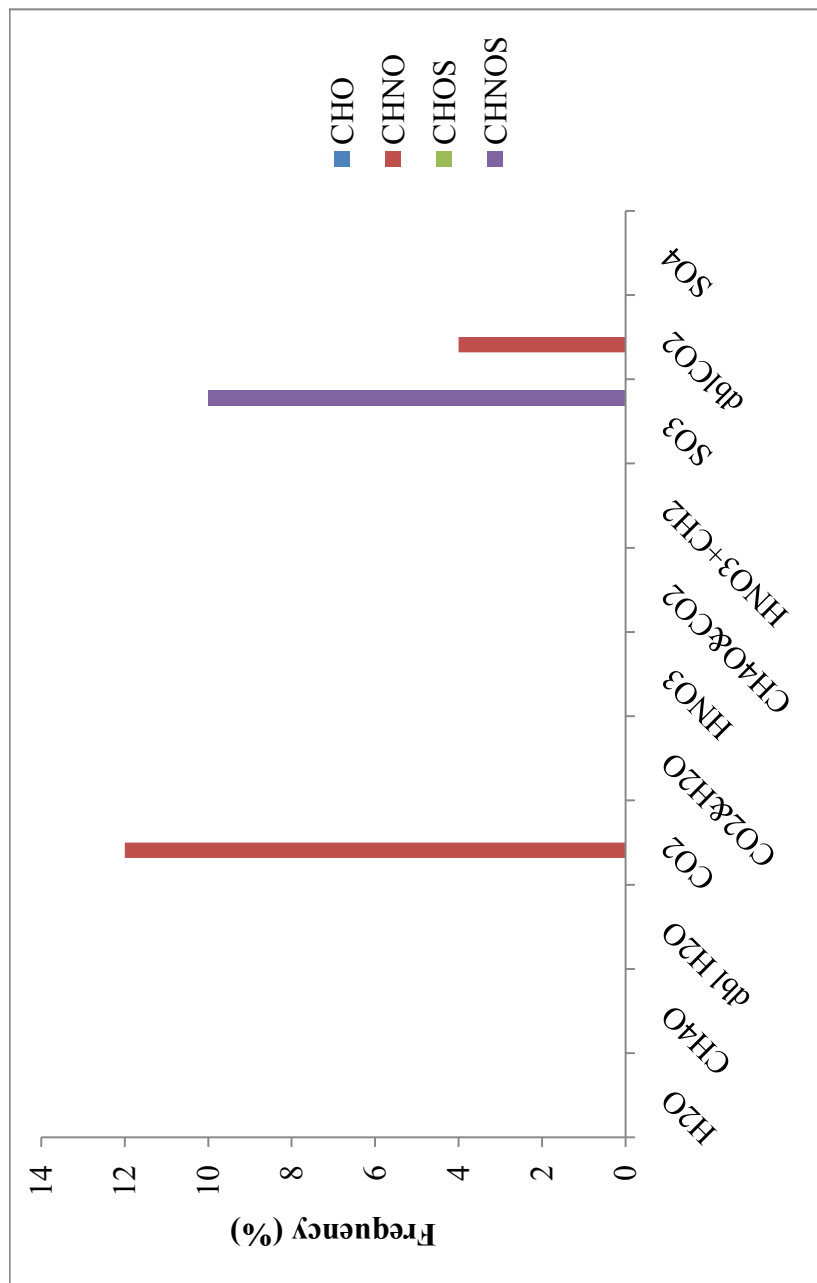


Figure 2.8: frequency of neutral losses separated by chemical group. These compounds are all “condensed aromatic” species ($AI > 0.67$) (Koch and Dittmar 2006).

2.7 Additional Fragmentation Studies

This section was not included with the rest of Chapter 2 for submission to Environmental Science and Technology (ACS journal).

A total of 22 neutral losses were evaluated in order to describe the occurrence of the fragmentation patterns observed in the CID spectra of the various scan ranges. The losses were divided into 2 categories: priority and additional losses. The fragmentation results presented in Chapter 2 were of higher priority because they involved neutral losses from specific functional groups or moieties (e.g., H₂O, CH₃OH, CO₂, nitrate, and sulfate). These losses are collectively referred to as the priority losses. The additional losses which are not directly related to functional groups (e.g., C₃H₈, CO, CH₂O, etc.) are collectively referred to as additional losses. Consistent with Chapter 2, the results are discussed in terms of the calculated Aromaticity Index (AI) (Koch and Dittmar 2006) which was discussed in Chapter 2. The results in both Chapter 2 and this section of Chapter 3 involve the same precursors, the majority of which appear to be aliphatic (AI = 0) or olefinic ($0 < AI < 0.50$) in structure. This section will briefly summarize the losses presented in Chapter 2 (see Chapter 2 for all additional information on these losses), while using them as a context to help describe the additional losses.

As presented in Figure 2.9, a majority of the priority losses for CHO compounds were associated with AI defined aliphatic or olefinic groups. Approximately 30% of the AI defined aromatic CHO compounds were associated with a loss of a CO₂ group. Over all

of the CHO compounds, the highest frequency of losses was of CO₂ from olefinic compounds. Also important are the combination losses of CO₂+H₂O, CH₄O+CO₂, and double CO₂. Their presence here confirms the polyacidic nature of AOM (Saxena and Hildemann 1996; Decesari et al. 2000; Cappiello et al. 2003).

Losses of secondary priority for CHO compounds are presented in Figure 2.10. From this figure it can be seen that the olefinic compounds had a higher frequency of losses for most of the neutral losses than any other AI class.

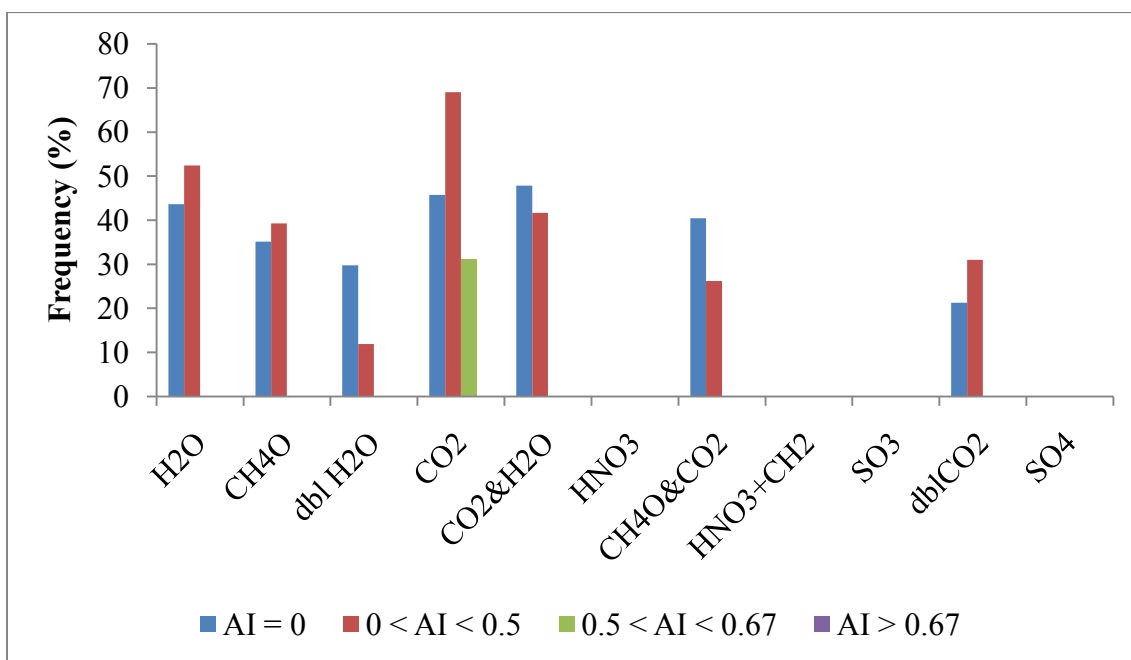


Figure 2.9: Priority Losses for CHO Compounds. The frequency of neutral losses for CHO separated by aromaticity index (AI)(Koch and Dittmar 2006).

This was not the case with the losses corresponding to CH₂O₂ and C₂H₂O₄ from aliphatic precursors. The only loss seen from aromatic precursors was CH₂O₂, which was only seen ~12% of the time. There were no losses from condensed aromatic species. This is

not a surprise as AOM is typically aliphatic. The highest frequency of losses was observed for aliphatic compounds that lost CH_2O_2 and olefinic compounds that lost C_3H_8 . Comparison of Figures 2.9 and 2.10 indicates that the neutral loss of CO_2 from olefinic precursors is the most important loss for the CHO compounds. However, the loss of CH_2O_2 has a higher frequency for aliphatic compounds than CO_2 . The loss of CH_2O_2 is suspected to be from a carboxyl group as well. Its origin is likely due to a nonionized carboxyl group on a polyacidic molecule which experienced a rearrangement upon fragmentation.

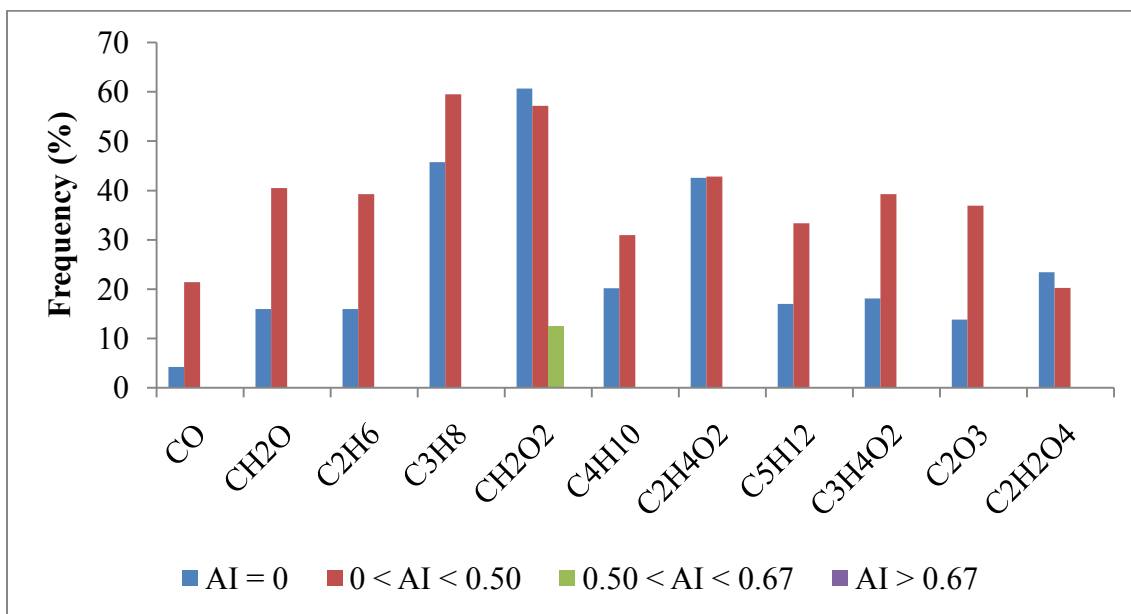


Figure 2.10: Additional Losses for CHO Compounds. The frequency of neutral losses for CHO separated by aromaticity index (AI)(Koch and Dittmar 2006).

Next, the losses from the CHNO compounds are presented in Figures 2.11 and 2.12. A summary of the priority losses described in Chapter 2 are presented in Figure 2.11. HNO_3 is the most important loss is from aliphatic CHNO compounds and was observed

for 48 % of the compounds. This loss is also important for the olefinic compounds, which exhibited this loss about 37% of the time. The loss of CO₂ was observed for 43% of the olefinic CHNO compounds and for 37% of aromatic compounds. This is the loss of the highest frequency for aromatic CHNO compounds and is attributed to the polyacidic nature of AOM (Saxena and Hildemann 1996; Decesari et al. 2000; Cappiello et al. 2003). Interestingly, the olefinic CHNO compounds have the highest frequency of losses for nearly every additional loss presented in Figure 2.12. The highest frequency of a type of loss is CH₂O₂ followed by C₃H₈ for olefinic compounds. All of the losses associated with the other AI categories were observed less than 20% of the time. The only loss seen from the condensed aromatic CHNO structures was CO and was only seen about 4% of the time.

The comparison of Figures 2.11 and 2.12 indicates that the loss of CH₂O₂ from olefinic CHNO compounds is just as important as the loss of HNO₃ from aliphatic CHNO compounds. It is also worth mentioning that the loss of CO₂ is as important as the loss of C₃H₈ for olefinic CHNO compounds. This may indicate the presence of alkyl chains.

CHOS priority losses are presented below in Figure 2.13. None of the AI defined aromatic or condensed aromatic CHOS compounds exhibited any of the priority losses. The most important loss was that of SO₃ from both aliphatic and olefinic compounds. All other losses were observed to be less than 20% and the only losses from olefinic compounds are SO₃ and SO₄. It is interesting to compare the loss of SO₃ with the loss of SO₄.

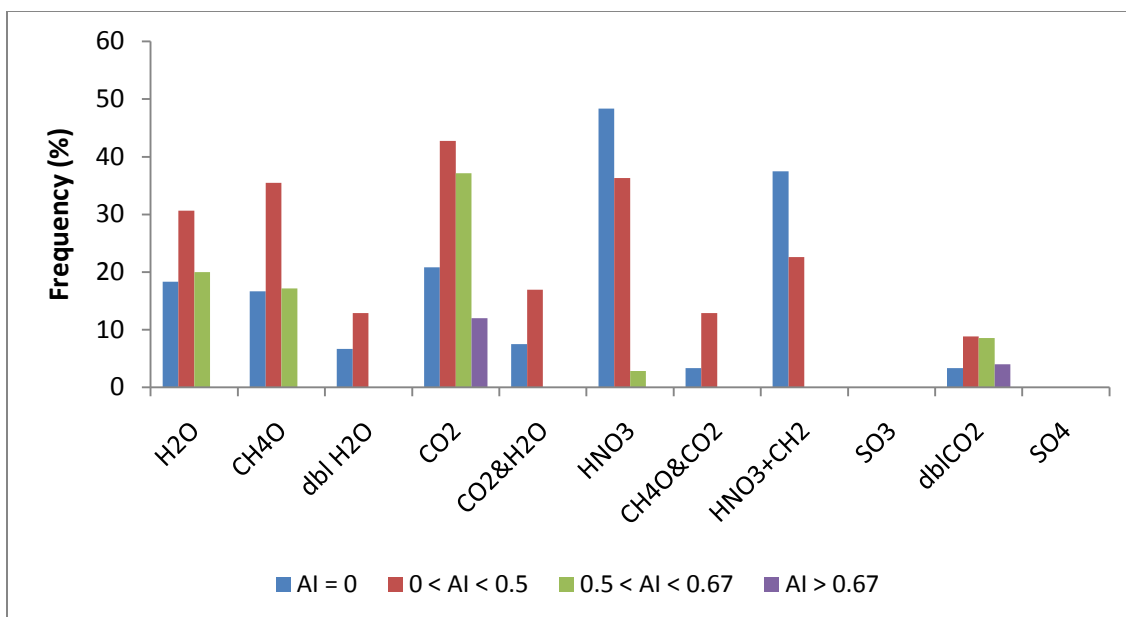


Figure 2.11: Priority Losses for CHNO Compounds. The frequency of neutral losses for CHNO separated by aromaticity index (AI)'(Koch and Dittmar 2006).

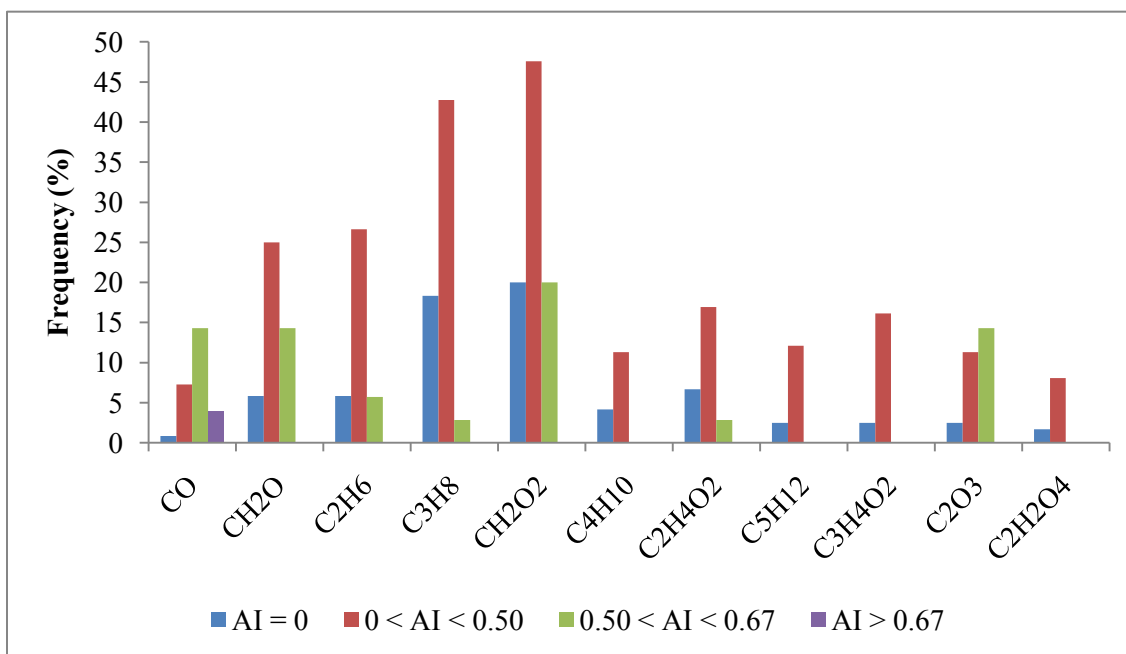


Figure 2.12: Additional Losses for CHNO Compounds. The frequency of neutral losses for CHNO separated by aromaticity index (AI)'(Koch and Dittmar 2006).

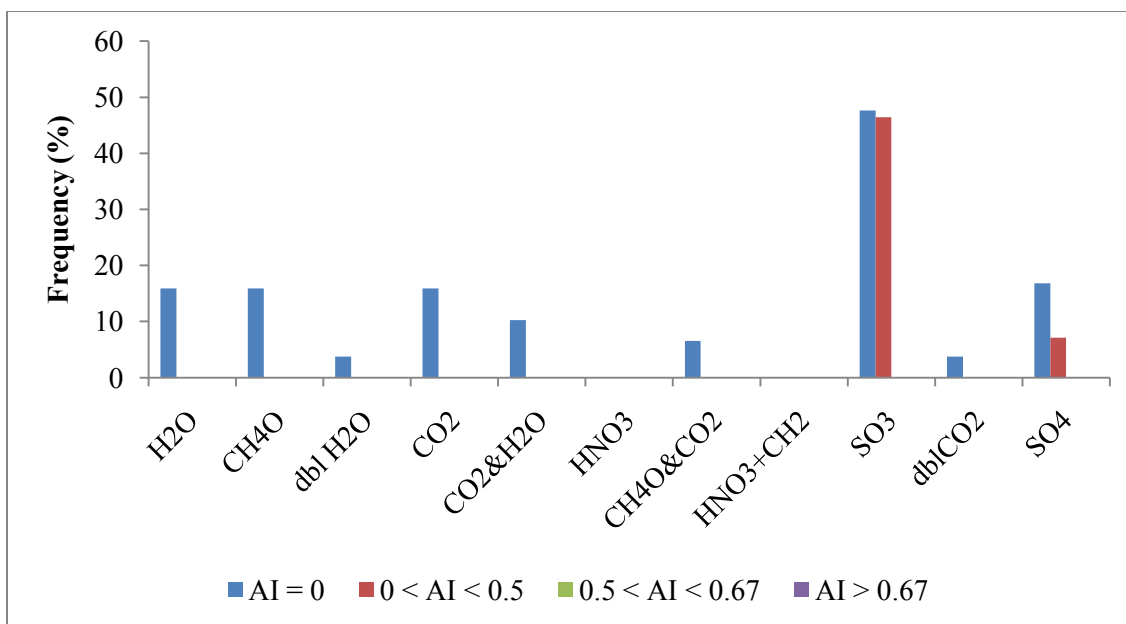


Figure 2.13: Priority Losses for CHOS Compounds. The frequency of neutral losses for CHOS separated by aromaticity index (AI)'(Koch and Dittmar 2006)

The discrepancy suggests that the sulfate groups more often fragment to leave an oxygen atom on the main structure of the molecule during fragmentation rather than cleave the whole sulfate group.

All of the losses associated with the CHOS compounds shown in Figure 2.14 are from aliphatic precursors. However, the frequencies of all of the losses were less than 20%, and most of them were less than 12%. The two most prevalent losses were C_3H_8 followed by CH_2O_2 . A comparison between Figures 2.13 and 2.14 indicates that the loss of SO_3 was by far the most important loss for both aliphatic and olefinic compounds. In fact, it is over twice as frequent as any other loss.

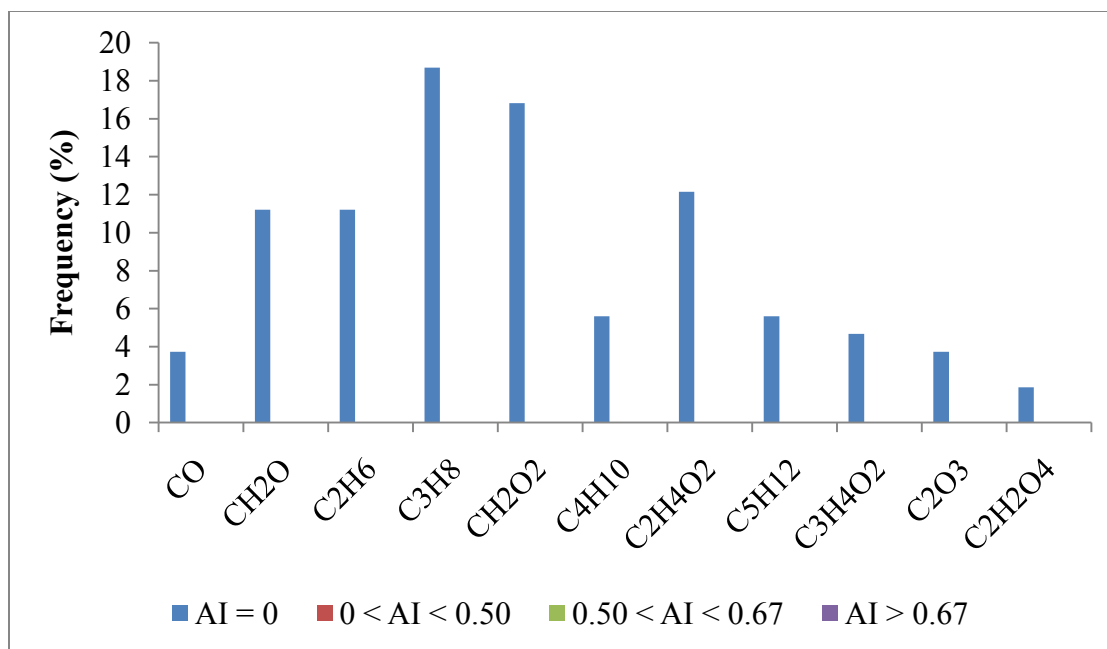


Figure 2.14: Additional Losses for CHOS Compounds. The frequency of neutral losses for CHOS separated by aromaticity index (AI) (Koch and Dittmar 2006)

CHNOS compounds were matched with neutral losses with a low frequency (Figure 2.15). All of the priority losses were less than 15%. Losses from aliphatic compounds appeared to be the most common. HNO₃ and SO₃ losses from aliphatic precursors were the most frequent over all. The only aromatic loss was that of H₂O, seen 9% of the time and the only condensed aromatic loss was SO₃, which was seen 10% of the time. The low frequency of the SO₃ losses is likely an explanation for the lack of any SO₄ losses because the presence of SO₄ losses is consistently at a much lower frequency than that of SO₃. Additional losses from CHNOS compounds were even less frequent (Figure 2.16) than the priority losses shown in Figure 2.15. All losses in Figure 2.16 were seen less than 8% of the time. The most frequent losses were CH₂O₂ at 7.9% from aliphatic compounds and CH₂O at 7.7% from the olefinic compounds.

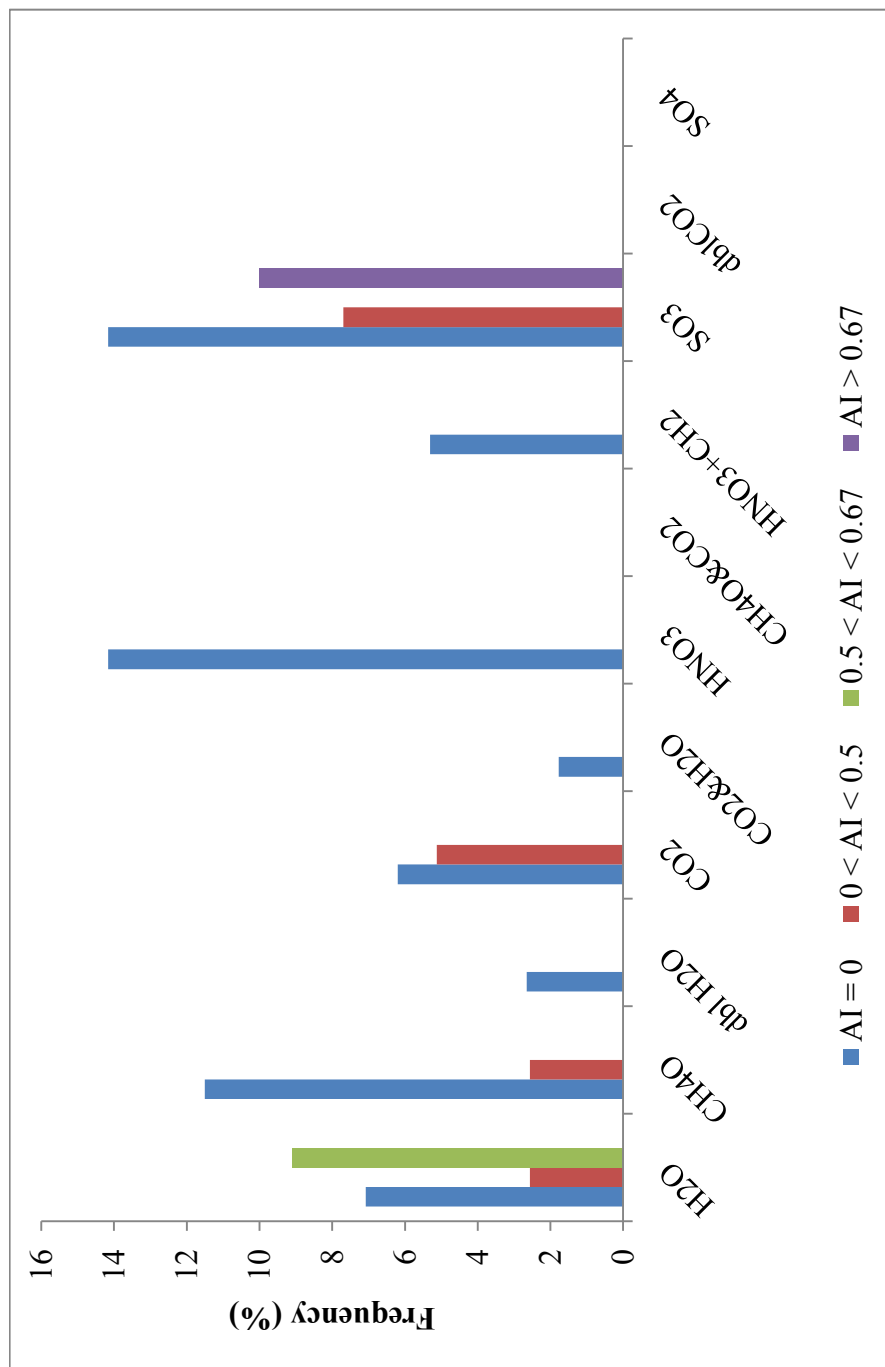


Figure 2.15: Losses for CHNOS Compounds. The frequency of neutral losses for CHNOS separated by aromaticity index (AI) (Koch and Dittmar 2006).

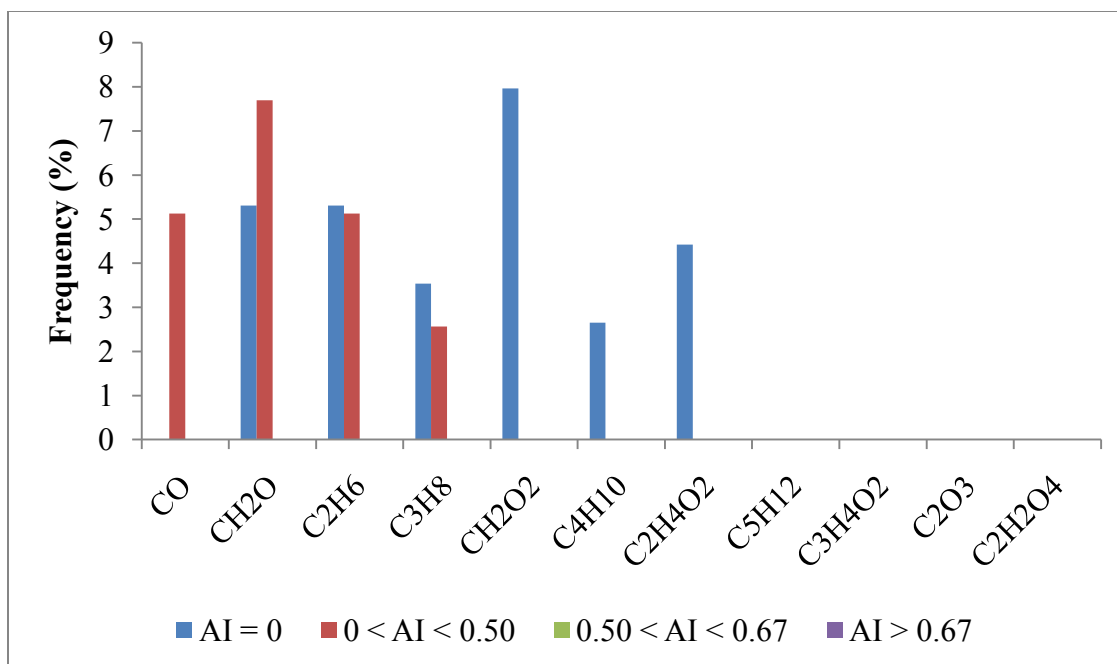


Figure 2.16: Additional Losses for CHNOS Compounds. The frequency of neutral losses for CHNOS separated by aromaticity index (AI) (Koch and Dittmar 2006).

In all, between Figures 2.15 and 2.16, it can be seen that the only loss associated with the AI defined aromatic compounds is H₂O and the only loss associated with the AI defined condensed aromatic compound is SO₃.

Earlier in Chapter 2, the monoterpene derived compounds were presented. These compounds are defined as non-volatile atmospheric oxidation products. The compounds of particular interest are the monoterpene derived organosulfates and nitroxy-organosulfates and have been reported previously in the literature (Inuma et al. 2007; Surratt et al. 2007; Gomez-Gonzalez et al. 2008; Surratt et al. 2008; Schmitt-Kopplin et al. 2010). The only compound of this type with additional neutral losses was C₁₀H₁₇NO₁₀S at m/z 342.0503. This compound exhibited a loss of C₂H₄O₂ in addition to

the losses of HNO_3 and CH_3NO_3 which were mentioned earlier in Chapter 2. To expand our analysis of the monoterpene derived compounds, the common molecular formulas in the mass range of 292-356 u between this study and a recent study of alpha-pinene/ozonolysis SOA (Putman et al. 2011) are presented. Several observations were also discussed earlier in Chapter 2. Although the molecular formulas of these compounds are identical, they may represent different isomeric structures. These compounds had a carbon atom range of C_{16} - C_{18} and oxygen atom range of O_4 - O_8 . The frequency of the priority losses for these CHO compounds can be seen in Figure 2.17. All of these CHO precursors fell into the aliphatic AI defined category. The losses with the highest frequencies were CO_2 which were detected for 84% of the compounds and the combination loss of $\text{CO}_2+\text{H}_2\text{O}$ which was detected for 78% of the compounds. All of the other losses were detected less than 55% of the time, however, losses of H_2O , $\text{CH}_4\text{O}+\text{CO}_2$, double CO_2 , and CH_4O were also important losses from these compounds. The neutral losses seen in Figure 2.18 were less frequent than those presented in Figure 2.17. From this group, the most notable losses were CH_2O_2 and $\text{C}_2\text{H}_4\text{O}_2$ which occurred 53% of the time. A comparison of the two figures (2.17 and 2.18) indicates that the frequency of these two losses were similar with the loss of H_2O ; however, the losses of CO_2 and the combination loss of $\text{CO}_2+\text{H}_2\text{O}$ remain the most important losses for these suspected CHO monoterpene derivatives.

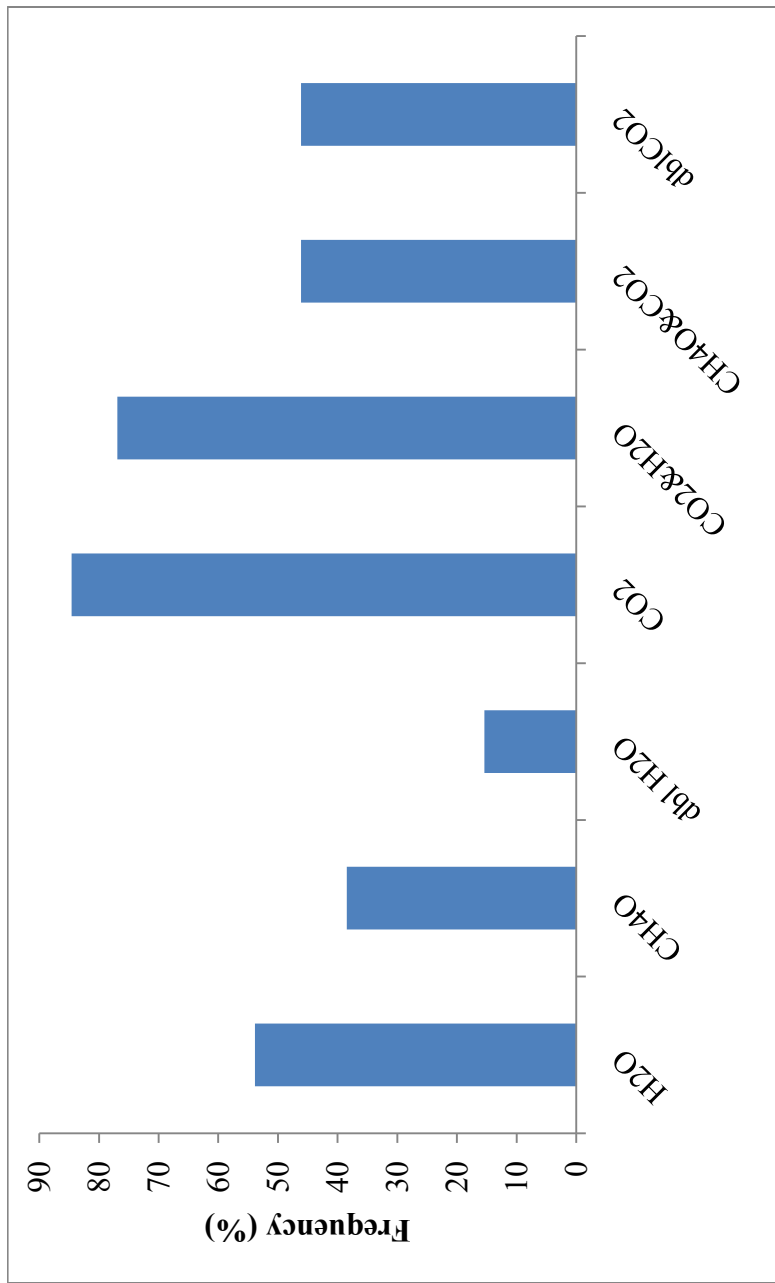


Figure 2.17: Frequency of priority losses for previously reported CHO monoterpene derivatives.

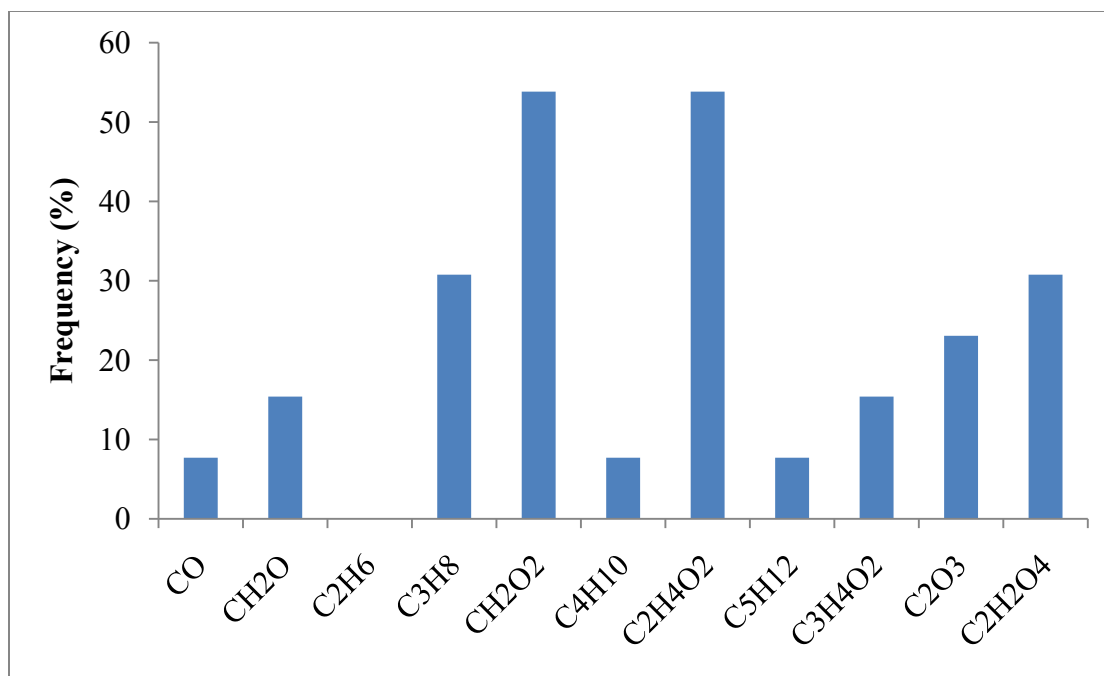


Figure 2.18: Frequency of additional losses for previously reported CHO monoterpene derivatives.

A comparison of selected neutral fragmentation losses by compound group and AI are presented below in Table 2.2. The losses associated with CHNOS and CHOS compounds were almost entirely the AI defined aliphatic compounds (AI = 0). The losses are presented with comparison to CO₂ for relative significance.

The process of matching fragment ions to precursors involved first generating a list of likely neutral losses. If a precursor ion were to exhibit a certain neutral loss, it would result in a certain fragment ion formula. Possible fragment ion formulas were generated for every precursor ion corresponding to each neutral loss. The list of actual fragment ion formulas was then matched to a list of possible fragment ion formulas on a per scan basis.

Table 2.2: Comparison of Additional Neutral Losses.

AI Value	Group	Fragmentation Losses					
		CH ₂ O	C ₂ H ₆	C ₃ H ₈	CO ₂	C ₅ H ₁₂	C ₃ H ₄ O ₂
AI = 0 "Aliphatic"	CHO (n = 94)	15	15	43	43	16	17
	CHNO (n = 120)	7	7	22	25	3	3
	CHNOS (n = 113)	6	6	4	7	0	0
	CHOS (n = 107)	12	12	20	17	6	5
0 < AI < 0.50 "Olefinic"	CHO (n = 84)	34	33	50	58	28	33
	CHNO (n = 124)	31	33	53	53	15	20
	CHNOS (n = 39)	3	2	1	2	0	0
	CHOS (n = 28)	0	0	0	0	0	0
0.50 < AI < 0.67 "Aromatic"	CHO (n = 16)	0	0	0	5	0	0
	CHNO (n = 35)	5	2	1	13	0	0
	CHNOS (n = 11)	0	0	0	0	0	0
	CHOS (n = 6)	0	0	0	0	0	0
AI ≥ 0.67 "Condensed Aromatic"	CHO (n = 1)	0	0	0	0	0	0
	CHNO (n = 25)	0	0	0	3	0	0
	CHNOS (n = 10)	0	0	0	0	0	0
	CHOS (n = 5)	0	0	0	0	0	0

In general, the low molecular weight neutral losses result in matches between fragment and precursor ions with good certainty. However when higher mass differences are observed between fragment and precursor ions, they may represent more than 1 expected neutral loss and thus more than one match between the ions is possible. In other words, a fragment ion of a certain formula and m/z could result from more than one precursor being fragmented, due to different neutral losses. Also, a precursor could be assigned two fragment ions of the same nominal mass. Examples of the neutral losses with the same nominal mass, but different exact masses include: CH₂O and C₂H₆, CO₂ and C₃H₈, and C₃H₄O₂ and C₅H₁₂. The values shown in Table 2.2 for each of these sets are very similar, with the exception of the CO₂ losses from aromatic compounds (0.50 < AI < 0.67). There is no way to verify that one or the other, or both losses occurred. In the case

of CO_2 and C_3H_8 , for example, CO_2 may be more likely because of the polyacidic nature of water-soluble atmospheric organic matter. However, van Krevelen diagrams can be used to see the overall differences between the different groups of precursors. Figure 2.19 represents a comparison of the precursors affiliated with each of the neutral losses with the same nominal masses. For CH_2O and C_2H_6 , there are 59 precursors that share these two losses, while 54 precursors have only CH_2O and 51 have only C_2H_6 . CO_2 and C_3H_8 share 99 precursors. CO_2 is lost from 127 unique precursors and C_3H_8 is lost from 95. $\text{C}_3\text{H}_4\text{O}_2$ and C_5H_{12} are shown to be lost from 17 of the same precursors, while $\text{C}_3\text{H}_4\text{O}_2$ is lost from 61 unique precursors and C_5H_{12} is lost from 51 unique precursors.

In each of these three cases, the comparison is between an alkyl loss and an oxygen containing loss. It can be seen that some of the precursors corresponding to the alkyl losses have a larger H:C and a smaller O:C, however, it is important to note that there are many precursors that occupy the same region of both parts of the diagram. When this is the case, it is hard to say which loss actually happened. The fact that some of the precursors showing alkyl losses occupy a different region of the diagrams would make sense, as compounds exhibiting alkyl losses should have less oxygen and more hydrogen than compounds exhibiting oxygenated losses. This would suggest that in some cases, both losses may have occurred. In addition, all of the precursors corresponding to the alkyl losses analyzed have similar H:C and O:C ratios.

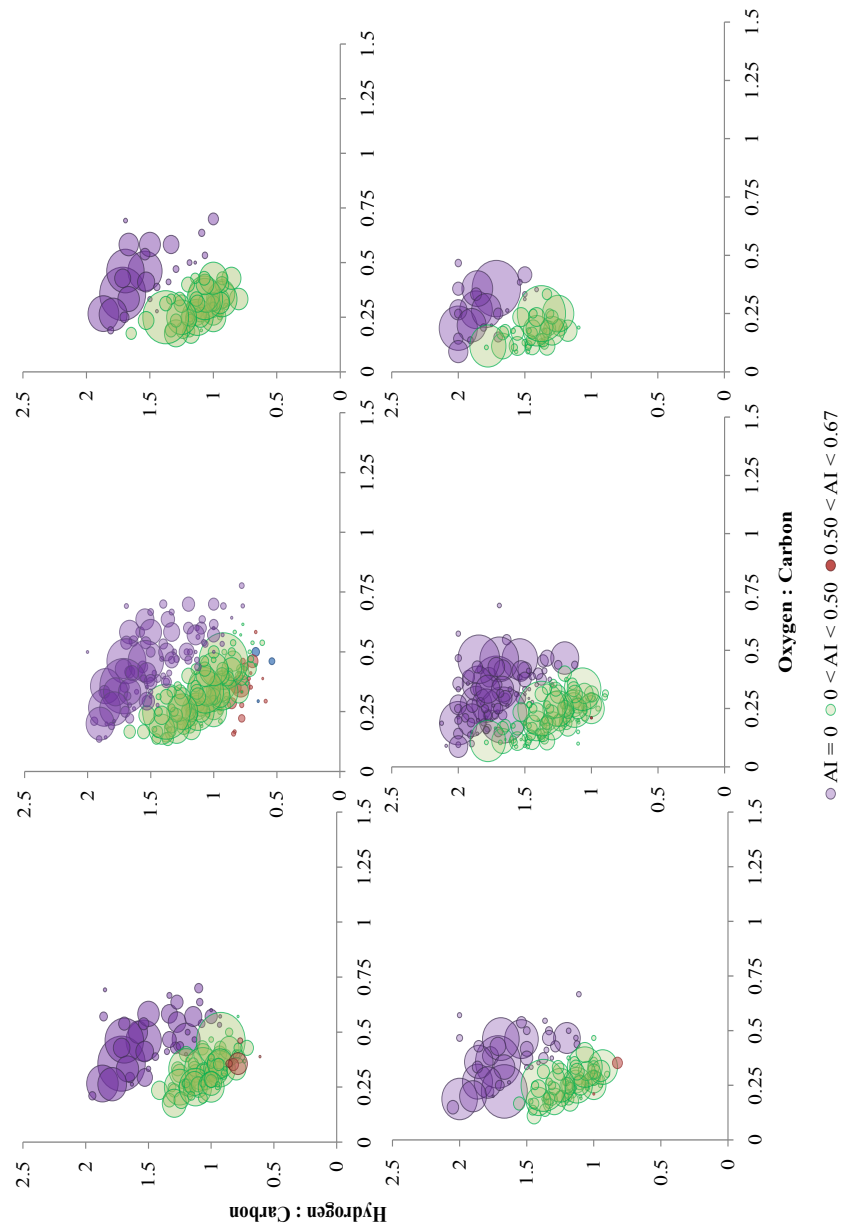


Figure 2.19: Left Side: CH_2O (Top) vs. C_2H_6 (Bottom); Middle: CO_2 (Top) vs. C_3H_8 (Bottom); and Right Side: $\text{C}_3\text{H}_4\text{O}_2$ (Top) vs. C_5H_{12} (Bottom). The squares indicate the precursors that show both losses.

To better characterize the precursors from which the alkyl losses originated, it was necessary to look for multiple alkyl losses from the same compound (Table 2.2). This represents the presence of alkyl chains of varying length. Again, AI was used to better understand the structure of the precursors. The majority of CHO and CHNO compounds to exhibit multiple alkyl losses have olefinic ($0 < \text{AI} < 0.50$) character, however, there are some aliphatic ($\text{AI} = 0$) compounds, especially with regard to the CHO compounds (Table 2.3). Interestingly, all of the CHOS compounds to exhibit multiple alkyl losses are aliphatic. Very few multiple alkyl losses were observed for CHNOS compounds, suggesting that alkyl chains are unimportant for this compound class. Also, as expected the alkyl losses appear to be unimportant when considering aromatic compounds ($0.50 < \text{AI} < 0.67$).

Table 2.3: Table of compounds that lost multiple alkyl groups, categorized by aromaticity index (AI).

Multiple Neutral Alkyl Losses	AI = 0						0 < AI < 0.50						0.50 < AI < 0.67							
	"Aliphatic"						"Olefinic"						"Aromatic"							
	CHO	CHNO	CHNOS	CHOS	CHOS	CHOS	CHO	CHNO	CHNOS	CHOS	CHOS	CHOS	CHO	CHNO	CHNOS	CHOS	CHO	CHNO	CHNOS	CHOS
C ₂ H ₆ , C ₃ H ₈	4	1	1	5	5	5	9	16	1	-	-	-	-	1	-	-	-	-	-	-
C ₂ H ₆ , C ₃ H ₈ , C ₄ H ₁₀	2	1	-	2	2	2	5	5	-	-	-	-	-	-	-	-	-	-	-	-
C ₂ H ₆ , C ₃ H ₈ , C ₄ H ₁₀ , C ₅ H ₁₂	8	3	-	2	2	2	15	7	-	-	-	-	-	-	-	-	-	-	-	-
C ₃ H ₈ , C ₄ H ₁₀	3	1	-	1	1	1	-	-	-	-	-	-	-	-	-	-	-	-	-	-
C ₃ H ₈ , C ₄ H ₁₀ , C ₅ H ₁₂	6	-	-	-	-	-	6	2	-	-	-	-	-	-	-	-	-	-	-	-
C ₄ H ₁₀ , C ₅ H ₁₂	-	-	-	1	1	1	-	-	-	-	-	-	-	-	-	-	-	-	-	-
C ₃ H ₈ , C ₅ H ₁₂	2	-	-	2	2	2	7	5	-	-	-	-	-	-	-	-	-	-	-	-
C ₂ H ₆ , C ₃ H ₈ , C ₅ H ₁₂	-	-	-	1	1	1	-	1	-	-	-	-	-	-	-	-	-	-	-	-
C ₂ H ₆ , C ₄ H ₁₀	-	-	1	-	-	-	-	-	-	-	-	-	-	-	-	-	-	-	-	-

3 Analysis of Nitrophenols and Other Selected Compounds

3.1 LC/MS Methodology

Many nitrophenol compounds were present in high relative abundance in the fog water sample. CID mass spectra were collected at m/z 138, 152, 166, 183, and 197. The goal of developing LC/MS methodology was to use chromatography to remove isobaric interferences from the nominal masses representing the nitrophenols. This would isolate the nitrophenols in the time domain, making interpretation of the fragmentation data more reliable.

3.1.1 Nitrophenol Quantitation

Calibration levels for the four nitrophenol standards (4-nitrophenol, 3-methyl-4-nitrophenol, 2,4-dinitrophenol, and 2-methyl-4,6-dinitrophenol) were made in a 50:50 ACN:H₂O solvent mix. The calibration levels for each ranged from 0.5-20.0 ng/ μ L.

Table 3.1: Nitrophenol standard calibration level concentrations

Compound	Calibration Levels (ng/ μ L)							
	0.05	0.20	1.0	2.5	5.0	10.0	15.0	20.0
4-nitrophenol	0.063	0.250	1.250	3.125	6.250	12.500	18.750	25.000
3-methyl-4-nitrophenol	0.065	0.258	1.290	3.225	6.450	12.900	19.350	25.800
2,4-dinitrophenol	0.056	0.222	1.110	2.775	5.550	11.100	16.650	22.200
2-methyl-4,6-dinitrophenol	0.054	0.216	1.080	2.700	5.400	10.800	16.200	21.600

An LC pump solvent gradient program was designed for the fog water sample matrix in order to prevent the nitrophenols from coeluting, while allowing the more aliphatic organic matter to elute off the PFP column before the nitrophenols and the more aromatic organic matter to elute after the nitrophenols. This is all with the main goal of having the nitrophenols fairly isolated while they elute. The LC solvents used were ACN with 0.1% formic acid and H₂O with 0.1% formic acid. Formic acid concentrations of 0.2% and 0.3% were also tried, however 0.1% formic acid yielded the best results. The solvent gradient was created to never exceed 65% ACN in order to keep the PFP column properties constant. The nitrophenols were found to elute from the column at a solvent ratio of about 70/30 H₂O/ACN.

Table 3.2: LCQ Solvent Gradient Program

Time (min)	% ACN	% H₂O
0 - 2.0	0.0	100.0
6.5 - 8.5	30.0	70.0
18.5	45.0	55.0
20.0 - 25.0	60.0	40.0
25.1 - 29.0	0.0	100.0

The gradient program was created and tested using the prepared standard solutions as well as fog water samples. Standards were run first, to identify retention times of the four compounds. Due to the complexity of the sample matrix, these retention times would change slightly when running the sample. After the sample matrix showed the presence of each of the nitrophenols, a nitrophenol spiked sample (80/20 sample/10 ng/μL nitrophenol standard solution) was run to confirm their presence.

Due to the fog water sample complexity it was necessary to use the most abundant fragment ion from each nitrophenol for quantitative purposes. Otherwise, there would be no way of knowing if the parent ion peak abundance was caused by only one compound. In the case of these nitrophenols, the most abundant fragment ion for each was due to the loss of a NO radical [M-30]. In order to get the best results, it was necessary to optimize both the isolation widths and the collision energies for each of the nitrophenol compounds. The optimized settings can be seen in the table below.

Table 3.3: MS method parameters

Compound	m/z	RT (min)	Collision Energy	Iso. Width (m/z)	Fragment Ion (m/z)
4-nitrophenol	138	7.19	22.0	1.0	108
3-methyl-4-nitrophenol	152	8.12	22.0	1.0	122
2,4-dinitrophenol	183	8.00	22.0	1.0	153
2-methyl-4,6-dinitrophenol	197	10.20	26.0	1.0	167

Now that all of the LC method settings were optimized, it was necessary to re-tune the LCQ to ensure the best instrument settings. The objective of re-tuning was to optimize the front end ion optics of the mass spectrometer as well as the electrospray ionization parameters. This was done by direct infusion into the ESI via the syringe pump using the 10 ng/ μ L nitrophenol calibration standard. The instrument was tuned using a 30/70 ACN/H₂O solvent mixture from the LC pump because this was the approximate solvent concentration that causes the nitrophenols to elute from the column. After re-tuning, all

of the method settings were confirmed first with standards and second with the sample matrix.

All standards were then run in triplicate for the creation of a calibration curve for each nitrophenol standard. The spray voltage was -3.5 kV. Using Xcalibur: Quan Browser, calibration curves were created by selecting the peaks manually for integration. Fog water samples were then run and treated as unknowns in Quan Browser. The nitrophenol peaks were again selected manually for integration, allowing for quantitation.

3.1.2 Exploration of Higher Molecular Weight Compounds

Included in the instrument method used to quantitate the nitrophenols present were many larger molecular weight compounds (m/z 200-400). These compounds eluted from the column after the nitrophenols and were of interest because they had the highest relative abundance in the last half of the run. The goal was to perform an estimated quantitation of these compounds, using the calibration curve created for 4-nitrophenol. Other than that, the quantitation was to be done in the same manner as the nitrophenols, by using the fragment with the highest relative abundance. The first group of compounds was identified to be linear alkylbenzene sulfonates (LAS), while the rest remain unknown. Due to the presence of multiple peaks for each LAS compound and the co-elution of the other unknowns over a span of three minutes, quantitation was not possible. To resolve this issue, more work must be done on the solvent gradient program.

Table 3.4: Higher molecular weight compounds

Compound	m/z	RT (min)	Collision Energy	Iso. Width (m/z)	Fragment Ion (m/z)
LAS - 1	297	17.40 - 18.20	27.0	1.0	183
LAS - 2	311	19.00 - 20.10	27.0	1.0	183
LAS - 3	325	20.33 - 21.00	27.0	1.0	183
LAS - 4	339	21.07 - 21.57	27.0	1.0	183
Unknown - 1	289	23.20 - 26.50	25.0	1.0	175
Unknown - 2	305	23.20 - 26.50	25.0	1.0	175
Unknown - 3	357	23.20 - 26.50	25.0	1.0	289
Unknown - 4	373	23.20 - 26.50	25.0	1.0	305

3.2 FT-ICR-MS Analysis of Nitrophenols Found Between 100-200 u

3.2.1 Nitrophenol Analysis

As mentioned above many nitrophenol compounds were present in high relative abundance in the fog water sample. CID mass spectra were collected at m/z 138, 152, 166, 183, and 197. These areas were selected because they contained high relative abundance nitrophenols. Any fragment ions not mentioned are most likely from precursors other than those mentioned here. The simplest was identified to be the mono-substituted nitrophenol, C₆H₅NO₃, with DBE = 5 at m/z 138.0197. No fragmentation was observed. This was probably due to low collision energy in the linear ion trap. Figure 3.1 gives a possible structure to this nitrophenol, however, the exact substitution of the nitro group cannot be confirmed. Based on previous studies, it is likely that this is either 2- or 4-nitrophenol.

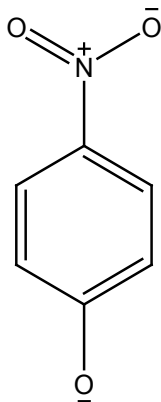


Figure 3.1: Possible nitrophenol structure of m/z 138

The next nitrophenol was identified to be $C_7H_7NO_3$ at m/z 152.0353 with DBE = 5 and 100% RA. The fragment peak at m/z 122.0373 [M-29.998] was identified as $C_7H_7O_2$ (DBE = 5) and was suspected to be a loss of NO radical. Bagglio et al. observes similar behavior from nitrophenols (1999). Another fragment ion was identified at m/z 137.0118 [M-15.0235] to be $C_6H_4NO_3$ (DBE = 6) and is likely the result of a CH_3 radical loss. Formula assignment for these fragment peaks was only possible by allowing radical losses. This is the case for the rest of the nitrophenols presented here that exhibit radical losses. The CID spectra for m/z 152 can be seen in Figure 3.2.

F010606x1_iso152w1_cid32 #1-104 RT: 0.02-6.99 AV: 104 NL: 2.28E4
T: FTMS - c NSI Full ms2 152.00@cid32.00 [50.00-175.00]
x10

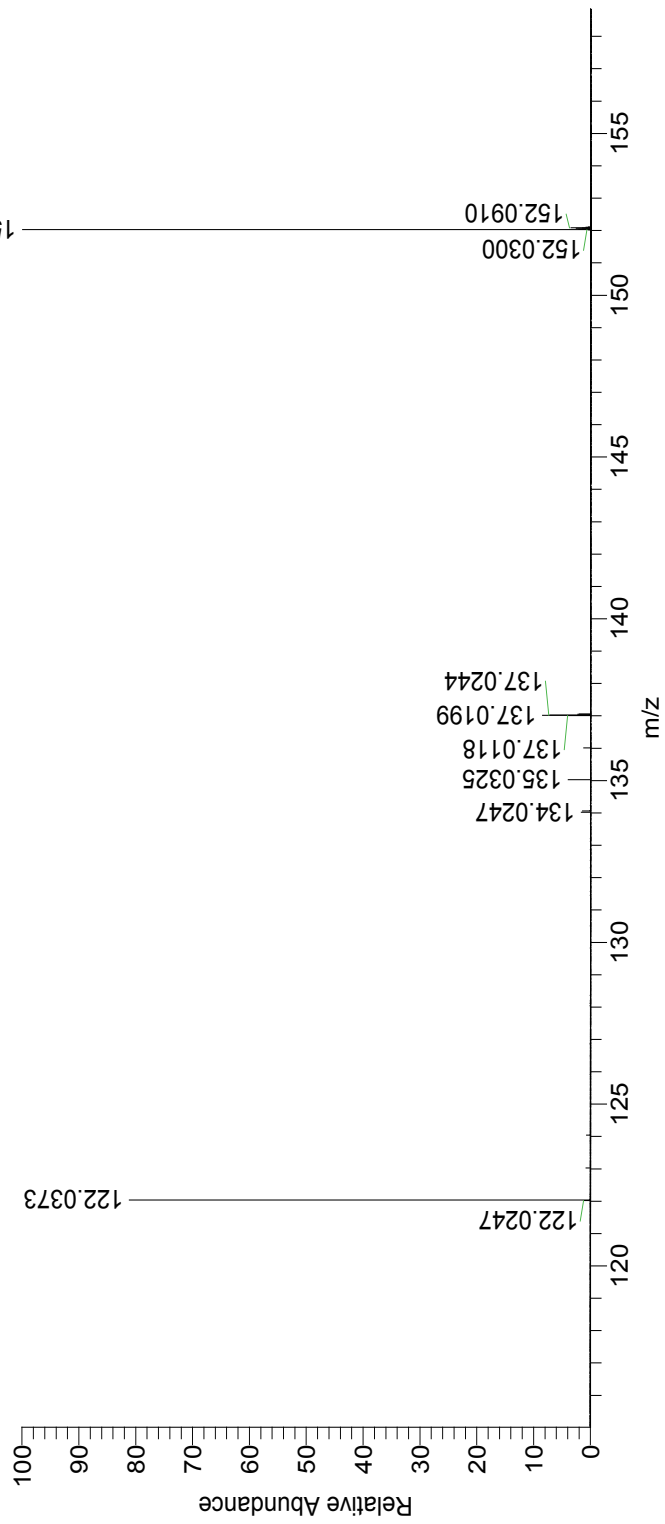


Figure 3.2: CID spectra of the nitrophenol at m/z 152.

From this data, an exact substitution pattern for the structure of this nitrophenol cannot be confirmed. A structure with a possible substitution pattern was given in Sancho et al. (2002) (Figure 3.3).

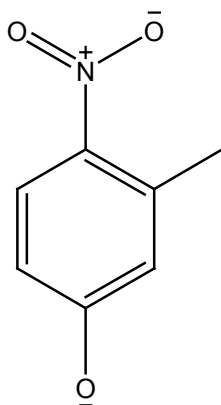


Figure 3.3: Possible structure of 3-methyl-4-nitrophenol

Another nitrophenol at m/z 166.0510, $C_8H_9NO_3$, was identified with $DBE = 5$ and relative abundance of 100%. The CID spectra can be seen in Figure 3.4. The fragment ion peak present at m/z 136.0530 [M-29.998] was identified as $C_8H_9O_2$ and is likely a loss of NO radical. The fragment peak at m/z 151.0275 [M-15.0235] was identified as $C_7H_6NO_3$ ($DBE = 6$) and is probably the result of a loss of a CH_3 radical. The fragment ion identified as $C_8H_8NO_2$ ($DBE = 6$) at m/z 149.0482 [M-17.002736] could be a loss of an OH radical, however, the mechanism is not known. The fragment peak at m/z 138.0197 [M-28.0313], $C_6H_5NO_3$ ($DBE = 5$), was identified to be a loss of an ethyl group (C_2H_4), providing enough insight to propose a structure (Figure 3.5). As with the other structures, the exact substitution pattern could not be confirmed.

F010606x1_iso166w1_cid27 #1-104 RT: 0.00-7.19 AV: 104 NL: 2.77E3
T: FTMS - p NSI Full ms2 166.00@cid27.00 [50.00-200.00]

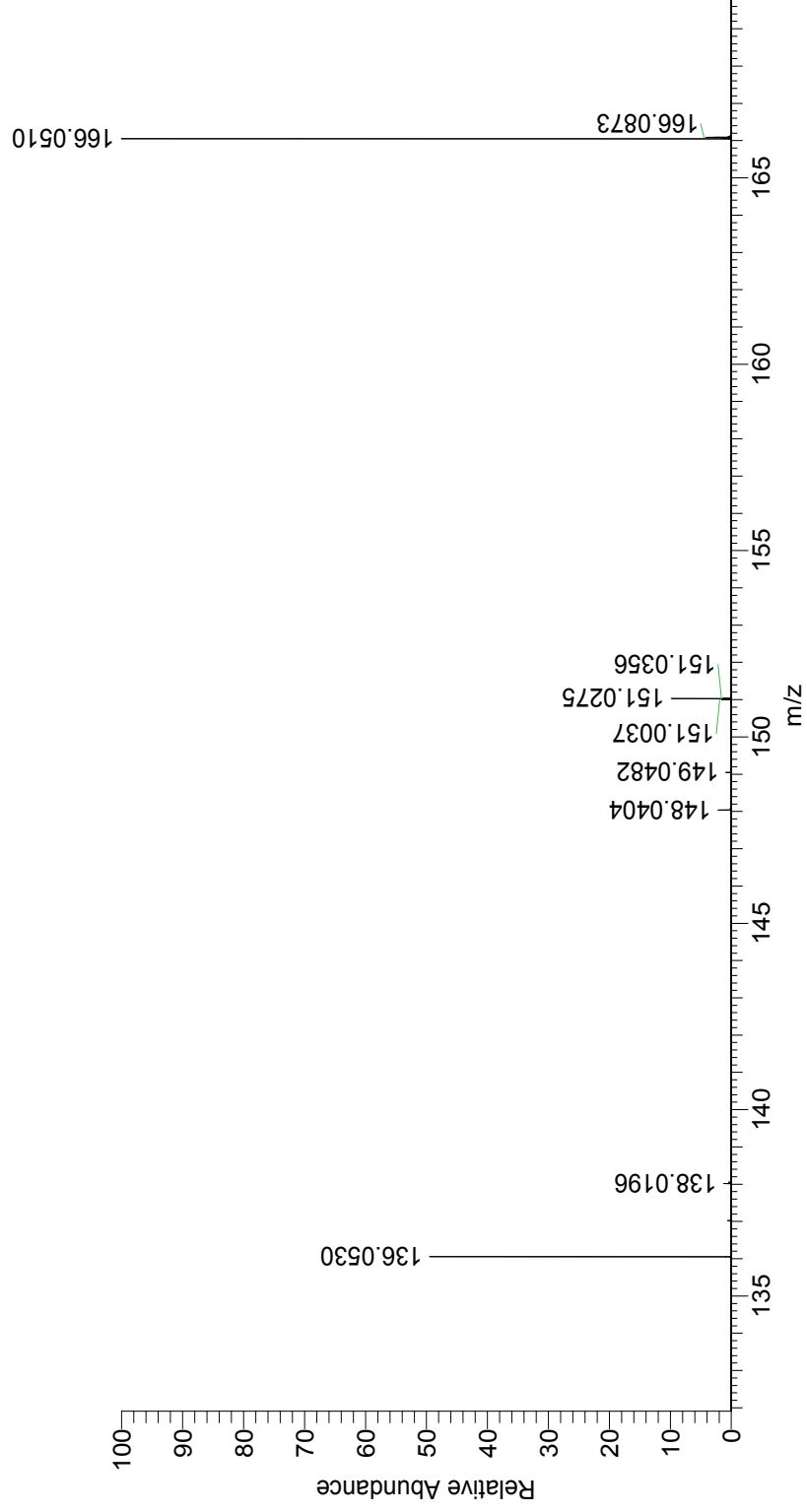


Figure 3.4: CID spectra containing the nitrophenol at m/z 166

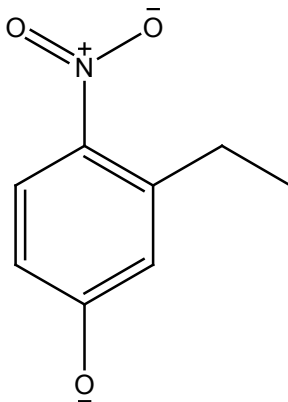


Figure 3.5: Possible structure of the nitrophenol at m/z 166

All three of the nitrophenols presented above differ by only a CH_2 group, putting them all in the same homologous series. The next homologous series of interest was a group of dinitrophenols. The peak at m/z 183.0047 was identified to be $\text{C}_6\text{H}_4\text{N}_2\text{O}_5$ with a DBE = 6 and a relative abundance of 36.9%. This is the first of the dinitrophenol compounds identified. The CID spectra can be seen in Figure 3.6. A close up of the m/z 183 precursor ions can be seen in Figure 3.7.

The fragment peak at m/z 153.0067 [M-29.998] was identified to be $\text{C}_6\text{H}_4\text{NO}_4$ (DBE = 6), the suspected characteristic loss of a NO radical. A double loss of NO radicals was identified at m/z 123.0088 [M-59.996] to be $\text{C}_6\text{H}_4\text{O}_3$ with DBE = 5. Another fragment ion peak was identified at m/z 137.0118 [M-45.9929] to be $\text{C}_6\text{H}_3\text{NO}_3$ (DBE = 6). This fragment is likely the result of a loss of a NO_2 radical. The possible structure of this dinitrophenol can be seen in Figure 3.8.

F010606x1_iso183w1_cid25 #1-104 RT: 0.02-7.35 AV: 104 NL: 9.09E4
T: FTMS - p NSI Full ms2 183.00@cid25.00 [50.00-200.00]

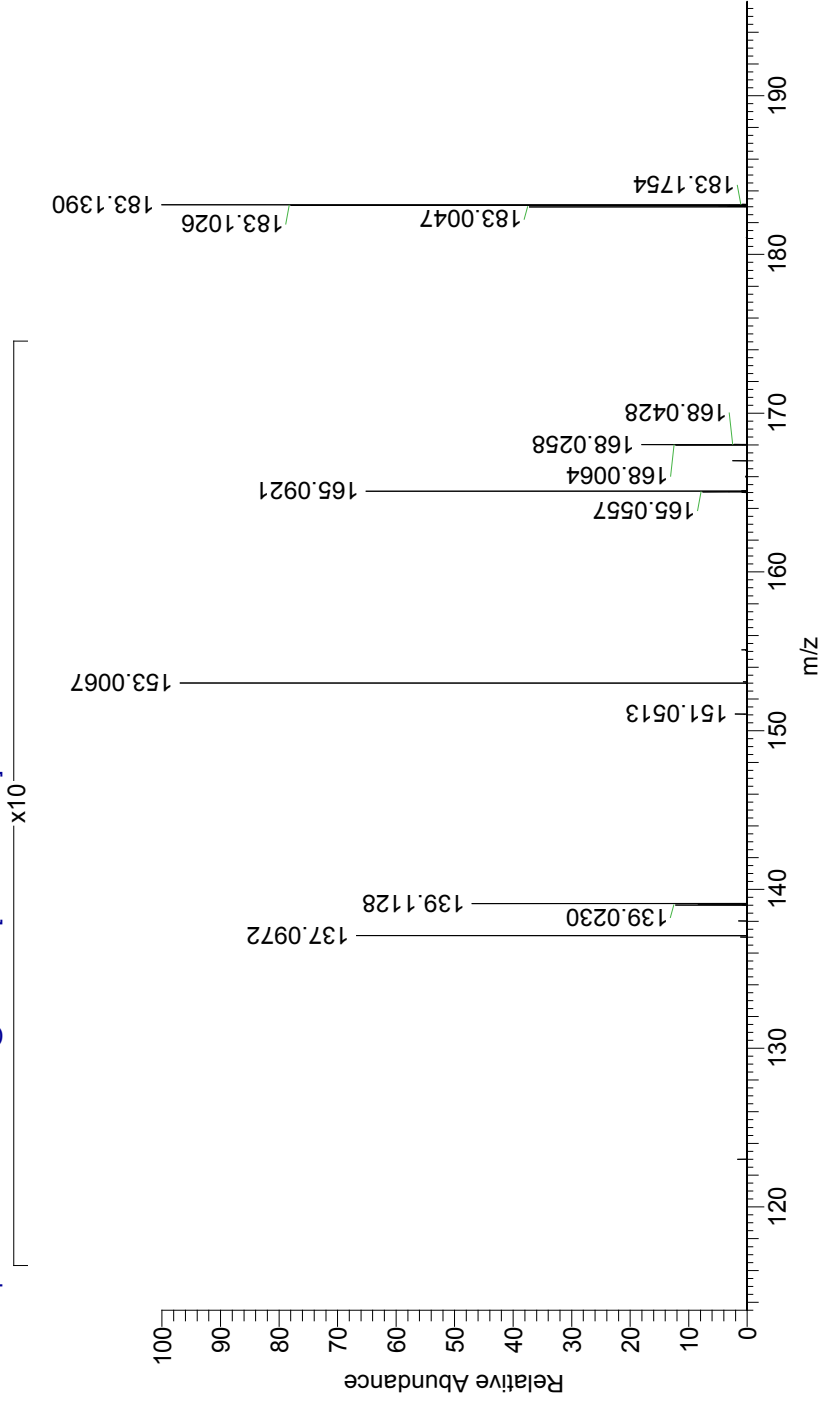


Figure 3.6: CID spectra of the nitrophenol at m/z 183

F010606x1_iso183w1_cid25 #1-104 RT: 0.02-7.35 AV: 104 NL: 9.09E4
T: FTMS - p NSI Full ms2 183.00@cid25.00 [50.00-200.00]

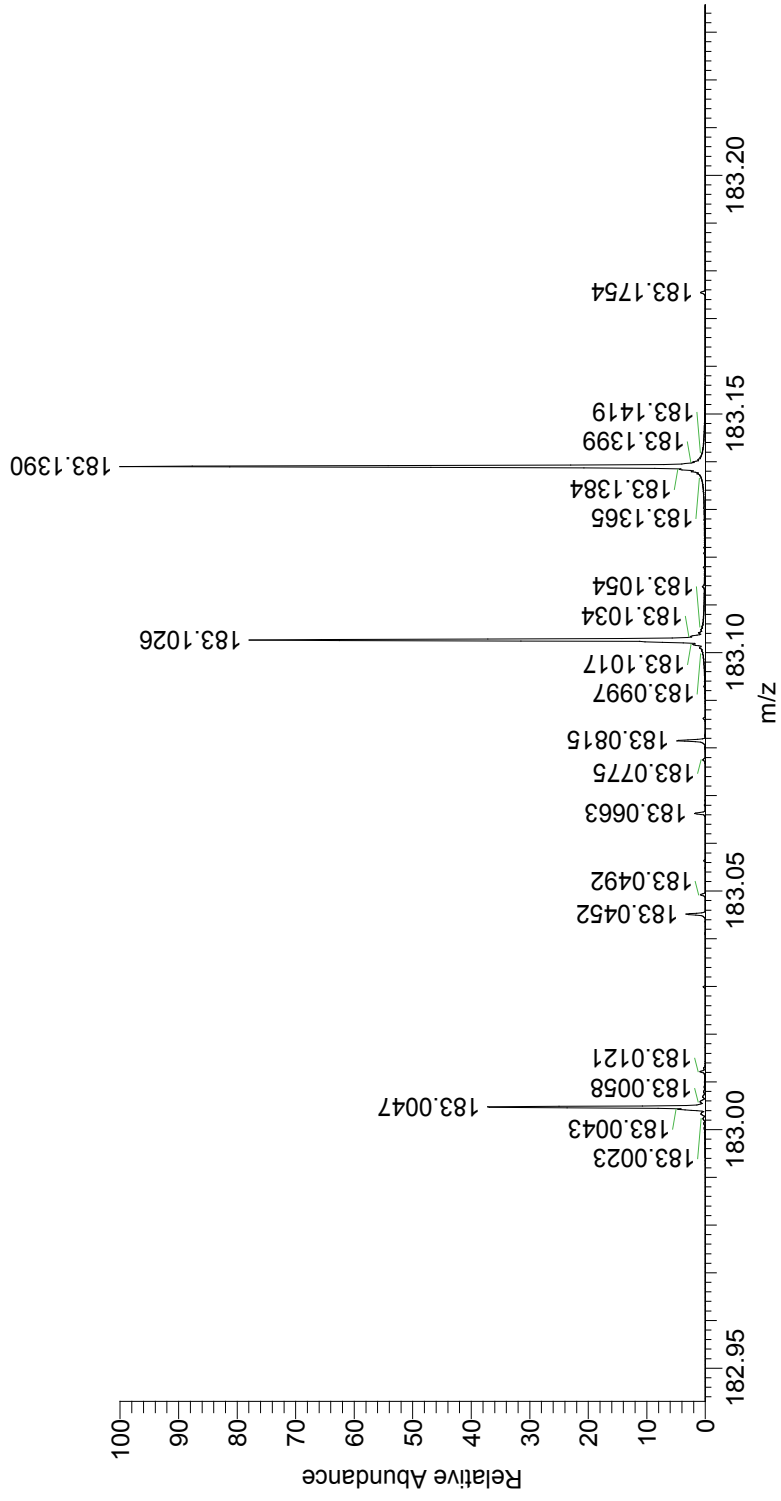


Figure 3.7: Close up of the precursors present in the scan containing the nitrophenol at m/z 183

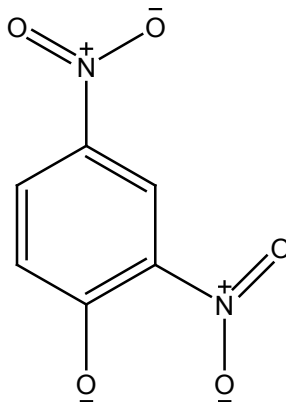


Figure 3.8: Possible structure of the dinitrophenol at m/z 183.0047

The next dinitrophenol in the homologous series was identified as $C_7H_6N_2O_5$ at m/z 197.0204 with a DBE = 6 and a relative abundance of 70.9%. The CID spectrum is presented in Figure 3.9. A zoomed in view of m/z 197 shows the different precursor ions (Figure 3.10).

A loss of [M-29.998] was identified at m/z 167.0224 as $C_7H_6NO_4$ (DBE = 6) and is the result of the suspected characteristic NO radical loss, consistent with the other nitrophenols identified. The proposed structure of this dinitrophenol is presented below (Figure 3.11) and as with all the other nitrophenol structures, the exact substitution cannot be confirmed. A fragment peak at m/z 137.0244 [M-59.996] was identified as $C_7H_6O_3$ with DBE = 5, which is likely to be the result of a loss of two NO radical groups. The fragment peak at m/z 180.0177, [M-17.0027], could be a loss of an OH radical from the dinitrophenol at m/z 197.0204. However, if it is an OH radical loss from the dinitrophenol, the mechanism remains unknown.

F010606x1_iso197w1_cid30 #1-104 RT: 0.02-7.23 AV: 104 NL: 8.28E3
T: FTMS - c NSI Full ms2 197.00@cid30.00 [50.00-225.00]

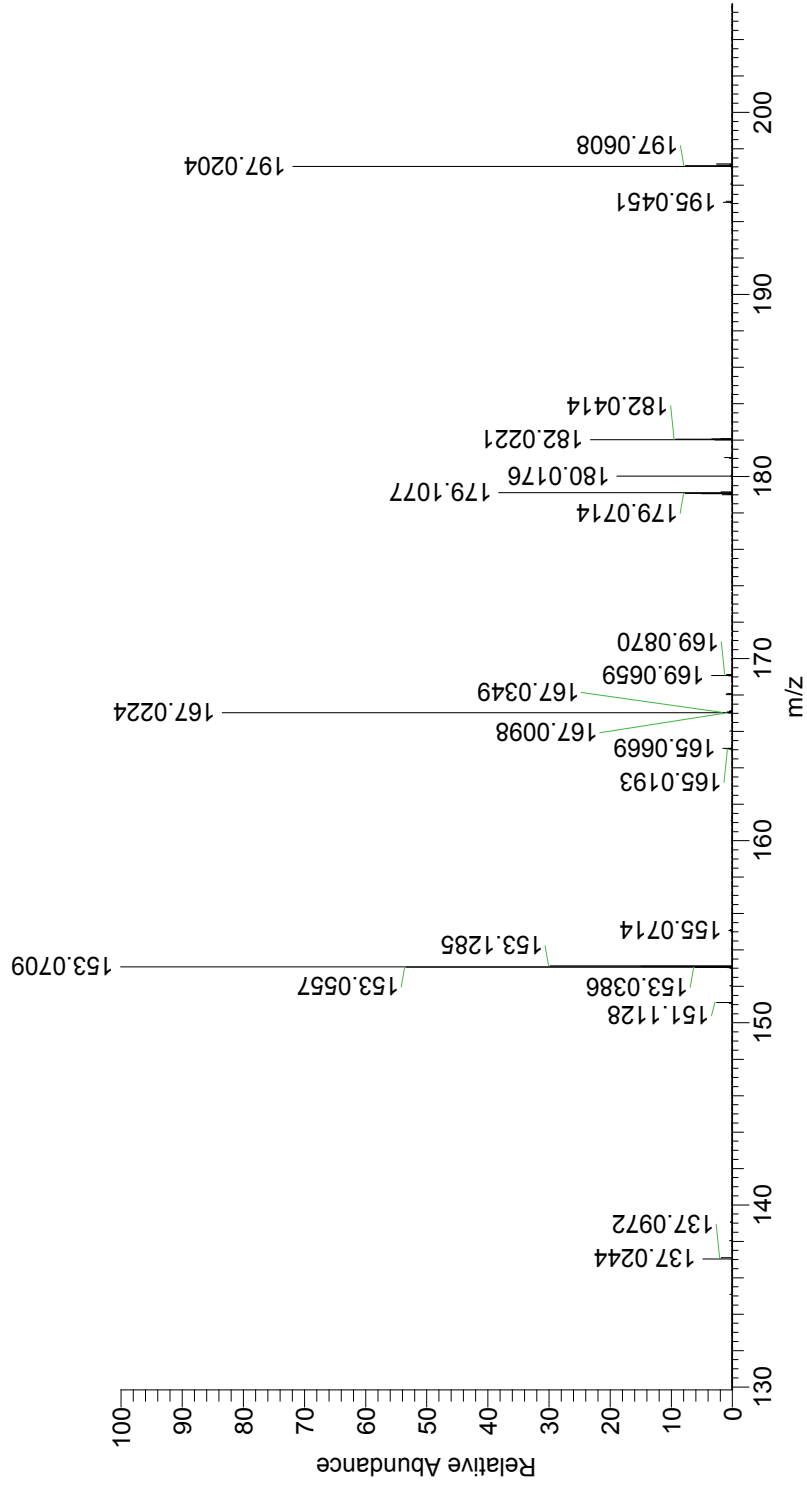


Figure 3.9: CID spectra of the scan containing the nitrophenol at m/z 197.

F010606x1_iso197w1_cid30 #1-104 RT: 0.02-7.23 AV: 104 NL: 5.95E3
T: FTMS - c NSI Full ms2 197.00@cid30.00 [50.00-225.00]

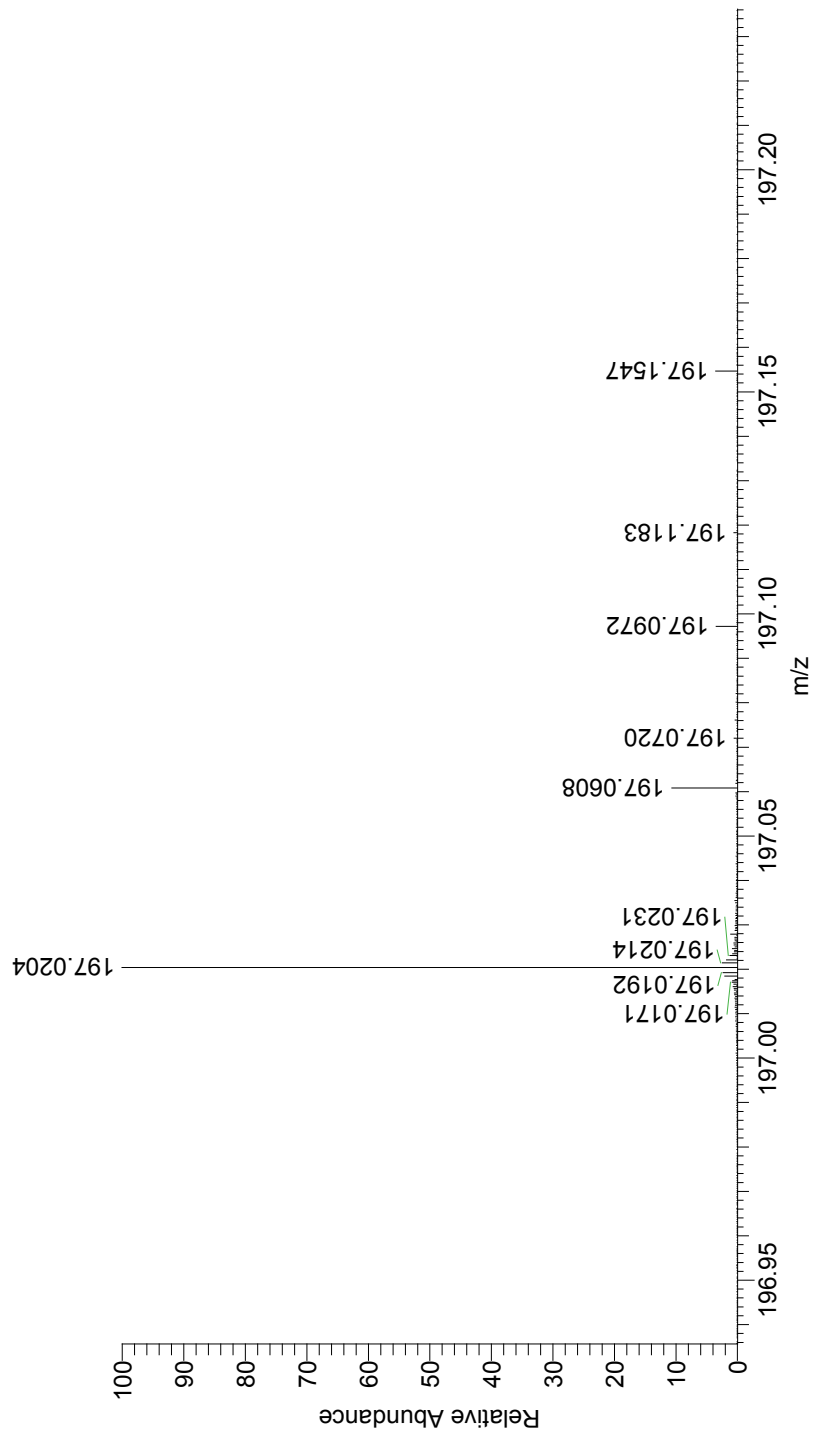


Figure 3.10: Close up of the precursors present in the scan containing the nitrophenol at m/z 197

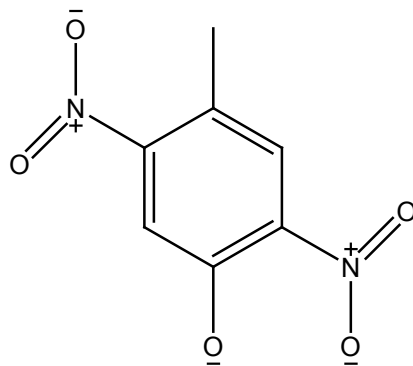


Figure 3.11: Possible structure of the dinitrophenol at m/z 197

3.2.2 NO Loss Mechanism

All of the nitrophenols studied up to this point have exhibited an apparent NO radical loss [M-29.998] and all of the alkyl substituted nitrophenols showed a suspected methyl radical loss [M- 15.0235]. It is also suspected that there is an OH radical loss from the dinitrophenol at m/z 197. In order for these losses to occur, there must be some sort of rearrangement and radical loss upon fragmentation. Based on Baglio et al. (1999), a mechanism was proposed for the loss of NO radical (Figure 3.12).

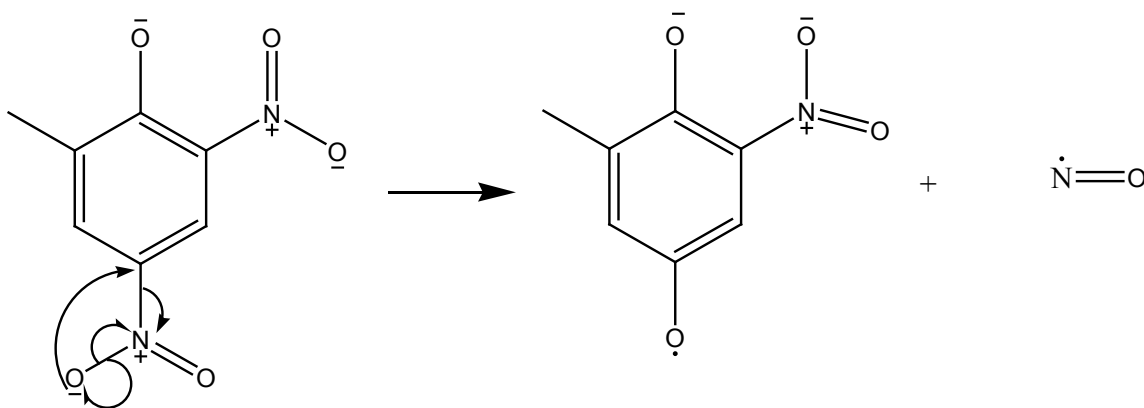


Figure 3.12: Proposed NO radical loss mechanism

An odd-electron loss from an even electron ion is rare when using electrospray ionization (ESI) and goes against the even electron rule. So, in order to confirm this there was a need to look into the literature to find some more cases of this observed behavior.

Levsen et al. (2007) describes the fragmentation patterns of nitroaromatic compounds using ESI-MS. They describe that the major fragmentation pathways for nitroaromatic compounds is by a loss of NO and/or NO₂ radicals. This is because the odd-electron ions produced are more stable than if even-electron ions were produced. Using ESI-MS, Schmidt et al. (2006) also talks about the fragmentation behavior of nitroaromatic compounds. Their work gives specific nitrophenol examples (3,5-dinitrophenol, 2,4-dinitrophenol, and 2-methyl-3-nitrophenol). They also show a loss of NO and/or NO₂ radicals which result in a distonic product ion. The possible mechanism is not as clearly stated as in Baglio et al. (1999). However the resulting product ion appears to be same.

The Schmidt et al. (2006) paper gives the fragmentation pattern up through MS⁴ analysis. This allows them to distinguish between the different substitutions of 3,5-DNP and 2,4-DNP (m/z 183). This is only possible by MS³ and beyond, as the MS² ions that result from both parents are the same (m/z 137 and 153). Since our analysis only involves MS² fragmentation, we cannot say that we have one or the other present and we cannot rule out that we do or do not have a mixture of the two, as we see fragments at both m/z 137 [M-NO₂] and 153 [M-NO].

The suspected loss of CH₃ with alkyl substituted nitrophenols is still under investigation. However, some work was found on the possible loss of an OH radical. Baglio et al (1999) describes this when an alkyl group has an ortho- substitution with respect to the hydroxyl group (ortho effect) which is now just a negatively charged oxygen atom after ionization (negative mode). Levsen et al (2007) also mentions a possible loss of an OH radical, however, the mechanism is different and they do not give much detail with regard to nitrophenols. So far, there has been no further information on this loss.

3.2.3 *Other High Abundance Low Mass Range Compounds (100-200 u)*

Two compounds of high relative abundance, other than the dinitrophenol, were identified in the m/z 183 isolation width. The first was identified to be C₁₀H₁₆O₃ (DBE = 3) at m/z 183.1026 with a relative abundance of 77.0%. This compound has the same formula as pinonic acid. A fragment ion at m/z 165.0921 [M-18.0105] was identified to be C₁₀H₁₄O₂ with DBE = 4 and is the result of a neutral loss of H₂O. Another fragment ion indicating the neutral loss of CO₂ was identified as C₉H₁₆O (DBE = 2) at m/z 139.1128 [M-43.9898]. The neutral loss of CO was also identified to be the result of fragmentation producing the fragment ion at m/z 155.1077 [M-27.9949], which is C₉H₁₆O₂ with DBE = 2. These neutral losses are consistent with the conclusion that this compound is pinonic acid. The second compound of high abundance identified was C₁₁H₂₀O₂ at m/z 183.1390 with DBE = 2 and relative abundance of 100%. Fragmentation analysis identified two fragment ions corresponding to two neutral losses from C₁₁H₂₀O₂. These are m/z

165.1285 [M-18.0105] identified as a loss of H₂O to create C₁₁H₁₈O (DBE = 3) and m/z 153.0921 [M-30.0469] identified as C₉H₁₄O₂ (DBE = 3) corresponding to a loss of C₂H₆.

3.3 Fragmentation Analysis of Nitrophenol Standards by LC/MS

The next step was to confirm the observed behavior from the fragmentation studies performed previously by using the LCQ Fleet to perform MS² fragmentation analysis on a series of standard nitrophenol compounds. However, being that this is a nominal mass instrument, exact masses were not obtainable. The standards used for this analysis were: 2-nitrophenol (m/z 138), 4-nitrophenol (m/z 138), 3-methyl-4-nitrophenol (m/z 152), 2,4-dinitrophenol (m/z 183), and 2-methyl-4,6-dinitrophenol (m/z 197). The main goal of this MS² fragmentation analysis was to investigate both alkyl and radical losses.

All of the nitrophenols that were fragmented exhibited a loss of approximately [M-30], which is consistent with the loss of a NO radical from nitrophenol compounds that had been suspected. The only fragmentation observed for the 2- and 4-nitrophenols resulted from a NO radical loss, [M-30], at m/z 108. A loss of approximately [M-60], resulting in a fragment peak at m/z 123, was observed from 2,4-dinitrophenol, resulting from what could be a loss of two NO groups, which is consistent with the FT-ICR-MS analysis. While fragmenting 3-methyl-4-nitrophenol a small fragment peak at m/z 106 was observed, resulting from loss of approximately [M-46], which could be the result of a loss of a NO₂ radical group. This loss was not seen in the ultrahigh-resolution mass spectra. These results help to confirm the identity of the nitrophenol compounds.

3.4 Quantification of Nitrophenols in Fog Water by LC/MS

The fog water sample being investigated was not meant to be used for quantification; therefore, the results presented here are not an atmospheric representation. The goal of quantifying the nitrophenols was to develop an LC/MS method for quantification of compounds within a complex matrix. The methods employed are described in detail in the LC/MS Methods section. The method produced reproducible results. Different but very similar calibration curves were used to quantify the four nitrophenols in the fog water sample and average concentrations were obtained (Table 3.5). A duplicate sample was also tested in twice and the average concentrations (using the same calibration curve) of the nitrophenols can also be seen in Table 3.5.

Table 3.5: Average Concentration of Nitrophenols in Fog Water

	4-nitrophenol	3-methyl-4-nitrophenol	2,4-dinitrophenol	2-methyl-4,6-dinitrophenol
m/z	138	152	183	197
Fog water	1.444 mg/L	0.303 mg/L	0.628 mg/L	0.200 mg/L
Fog water duplicate	3.1485 mg/L	0.698 mg/L	1.818 mg/L	0.540 mg/L

The most striking aspect of Table 3.5 is the difference in concentrations between the sample and its duplicate. This may be due to a couple sources of error, such as sample handling and evaporation of sample. The fog water sample used had been opened and sampled from many times since it was collected which may have led to higher concentrations due to evaporation as compared to the duplicate sample, which had not undergone the same procedures.

3.5 Linear Alkylbenzene sulfonate (LAS) Analysis

There were many suspected linear alkylbenzene sulfonate (LAS) compounds of high abundance in this fog water sample (Mazzoleni et al. 2010). LAS have also been observed previously in a rainwater sample (Altieri et al. 2009b). These studies are the first to observe this class of compounds in atmospheric samples. LAS compounds are of interest because of their high abundance and their harmful behavior in the environment (Debelius et al. 2008). They are a commonly used surfactant that is found in detergents and personal-care products (Debelius et al. 2008).

LAS compounds were identified at: m/z 297.1532 to be $C_{16}H_{26}O_3S$ (DBE = 4, RA = 100%), m/z 311.1689 to be $C_{17}H_{28}O_3S$ (DBE = 4, RA = 100%), m/z 325.1846 to be $C_{18}H_{30}O_3S$ (DBE = 4, RA = 100%), and m/z 353.2157 to be $C_{20}H_{34}O_3S$ (DBE = 4, RA = 3.0%). The first three of these have been previously reported (Altieri et al. 2009b; Mazzoleni et al. 2010). All of the LAS compounds identified here lie in the same CH_2 homologous series. Another suspected LAS compound was identified at m/z 341.1794 to be $C_{18}H_{30}O_4S$ with DBE = 4 and a relative abundance of 100%. This compound is not in the same homologous series as the others; however, its fragment ions are consistent with the fragment ions of the other LAS compounds. Fragment ions and their corresponding LAS precursor ions can be seen in Table 3.6. All of the fragment ions shown in Table 6 are in the same CH_2 homologous series.

Table 3.6: Fragmentation behavior of LAS compounds

Fragment Ions			Corresponding LAS Compounds (m/z)
m/z	Formula	DBE	
183.0122	C8H8O3S	5	297, 311, 325, 341, 353
197.0278	C9H10O3S	5	297, 311, 325, 353
211.0435	C10H12O3S	5	311, 325, 353
225.0591	C11H14O3S	5	311, 325, 341, 353
239.0748	C12H16O3S	5	311, 325, 341, 353
253.0905	C13H18O3S	5	311, 325, 341, 353
267.1062	C14H20O3S	5	311, 325, 341, 353
281.1218	C15H22O3S	5	325, 341, 353
295.1374	C16H24O3S	5	341
323.1688	C18H28O3S	5	341

LAS compounds can be identified by their characteristic alkyl chain, the length of which determines their surfactant behavior. Based on the presence of the main fragment ion at m/z 183 and a structural template for LAS compounds previously reported (Lara-Martin et al. 2006), structures are proposed here for three of the LAS precursors (Figure 3.13). From these structures, it can be seen that they only differ in the length of their alkyl chain.

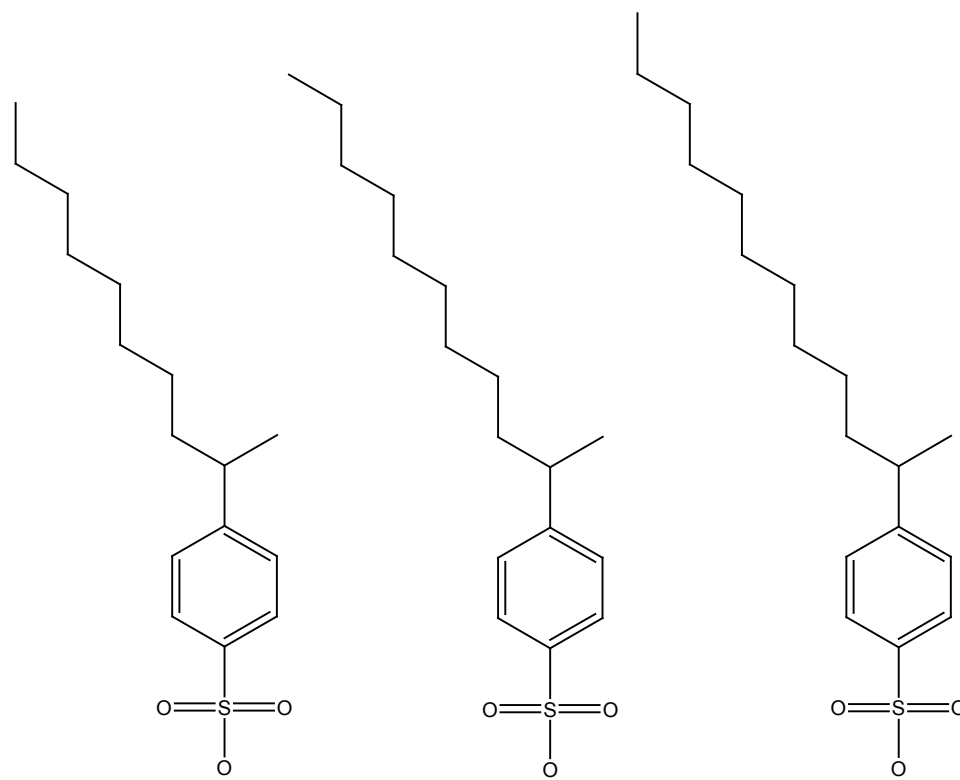


Figure 3.13: Proposed LAS Structures for m/z 297, 311, and 325

Each of the fragment ions shown in Table 3.6 is the result of a loss a different number of CH_2 units from the characteristic alkyl chain. Lara-Martin et al. (2007) proposes structures of the key fragment ions that were observed in this study (Figure 3.14). Of these fragment ions, m/z 183 is the most common and is seen for all of the LAS compounds presented here.

The LAS compound found at m/z 341, $\text{C}_{18}\text{H}_{30}\text{O}_4\text{S}$, contains an extra oxygen atom when compared to the other LAS compounds. Fragmentation analysis yielded a neutral loss of H_2O from this molecule, giving the fragment ion at m/z 323.1688 (Table 3.6). This indicates that the molecule must contain a hydroxyl group, but based on this analysis its

location cannot be determined. Differing from the rest of the LAS compounds, this may suggest that the LAS at m/z 341 is a degradation product of a more characteristic LAS compound. A loss of SO_3 was also observed for m/z 341. This loss was not observed for any of the other LAS compounds.

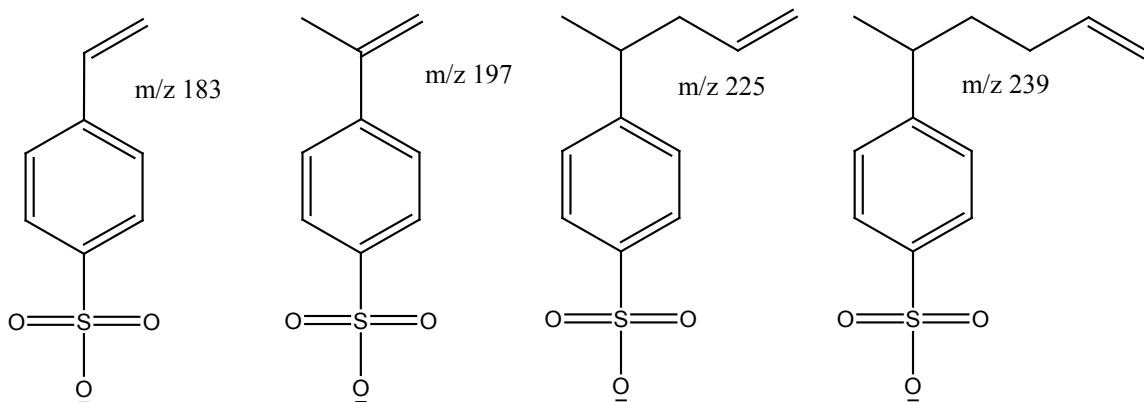


Figure 3.14: Neutral structures of key LAS fragment ions.

So far, there has been no conclusive evidence to explain the presence of LAS in the atmosphere. If they are present in the atmosphere, how do they get there? It is possible that the presence of LAS in the sample could be explained by the fact that they are widely used in detergents (Debelius et al. 2008). They may be present on the surface of glassware/equipment used in the sampling and storage process or on the surface of the glass of solvent containers. If this is the case, they are sample contaminants. In fact, preliminary studies have indicated that these LAS compounds are present in multiple brands of high purity methanol.

4 References

- Agency CEP. 2000. Establishment of Numeric Criteria for Priority Toxic Pollutants for the State of California. Water Quality Standards.
- Allen SK, Allen CW. 1997. Phenol concentrations in air and rain water samples collected near a wood preserving facility. *Bulletin of Environmental Contamination and Toxicology* 59(5):702-707.
- Altieri KE, Seitzinger SP, Carlton AG, Turpin BJ, Klein GC, Marshall AG. 2008. Oligomers formed through in-cloud methylglyoxal reactions: Chemical composition, properties, and mechanisms investigated by ultra-high resolution FT-ICR mass spectrometry. *Atmospheric Environment* 42(7):1476-1490.
- Altieri KE, Turpin BJ, Seitzinger SP. 2009a. Composition of dissolved organic nitrogen in continental precipitation investigated by ultra-high resolution FT-ICR mass spectrometry. *Environmental Science and Technology* 43(18):6950-5.
- Altieri KE, Turpin BJ, Seitzinger SP. 2009b. Oligomers, organosulfates, and nitrooxy organosulfates in rainwater identified by ultra-high resolution electrospray ionization FT-ICR mass spectrometry. *Atmospheric Chemistry and Physics* 9(7):2533-2542.
- Andreae MO, Jones CD, Cox PM. 2005. Strong present-day aerosol cooling implies a hot future. *Nature* 435(7046):1187-1190.
- Baglio D, Kotzias D, Larsen BR. 1999. Atmospheric pressure ionisation multiple mass spectrometric analysis of pesticides. *Journal of Chromatography A* 854(1-2):207-220.
- Bateman AP, Walser ML, Desyaterik Y, Laskin J, Laskin A, Nizkorodov SA. 2008. The effect of solvent on the analysis of secondary organic aerosol using electrospray ionization mass spectrometry. *Environmental Science & Technology* 42(19):7341-7346.
- Bateman AP, Nizkorodov SA, Laskin J, Laskin A. 2009. Time-resolved molecular characterization of limonene/ozone aerosol using high-resolution electrospray ionization mass spectrometry. *Physical Chemistry Chemical Physics* 11(36):7931-42.
- Blando JD, Turpin BJ. 2000. Secondary organic aerosol formation in cloud and fog droplets: a literature evaluation of plausibility. *Atmospheric Environment* 34(10):1623-1632.
- Bolzacchini E, Bruschi M, Hjorth J, Meinardi S, Orlandi M, Rindone B, Rosenbohm E. 2001. Gas-phase reaction of phenol with NO₃. *Environmental Science & Technology* 35(9):1791-1797.

- Bones DL, Henricksen DK, Mang SA, Gonsior M, Bateman AP, Nguyen TB, Cooper WJ, Nizkorodov SA. 2010. Appearance of strong absorbers and fluorophores in limonene-O₃ secondary organic aerosol due to NH₄⁺-mediated chemical aging over long time scales. *Journal of Geophysical Research-Atmospheres* 115:14.
- Cappiello A, De Simoni E, Fiorucci C, Mangani F, Palma P, Truffelli H, Decesari S, Facchini MC, Fuzzi S. 2003. Molecular characterization of the water-soluble organic compounds in fogwater by ESIMS/MS. *Environmental Science & Technology* 37(7):1229-1240.
- Collett JL, Herckes P, Youngster S, Lee T. 2008. Processing of atmospheric organic matter by California radiation fogs. Elsevier Science Inc. p. 232-241.
- De Haan DO, Hawkins LN, Kononenko JA, Turley JJ, Corrigan AL, Tolbert MA, Jimenez JL. 2011. Formation of nitrogen-containing oligomers by methylglyoxal and amines in simulated evaporating cloud droplets. *Environmental Science & Technology* 45(3):984-991.
- De Haan DO, Corrigan AL, Smith KW, Stroik DR, Turley JJ, Lee FE, Tolbert MA, Jimenez JL, Cordova KE, Ferrell GR. 2009. Secondary organic aerosol-forming reactions of glyoxal with amino acids. *Environmental Science & Technology* 43(8):2818-2824.
- Debelius B, Forja JM, Del Valls A, Lubian LM. 2008. Effect of linear alkylbenzene sulfonate (LAS) and atrazine on marine microalgae. *Marine Pollution Bulletin* 57(6-12):559-568.
- Decesari S, Facchini MC, Fuzzi S, Tagliavini E. 2000. Characterization of water-soluble organic compounds in atmospheric aerosol: A new approach. *Journal of Geophysical Research-Atmospheres* 105(D1):1481-1489.
- Fievre A, Solouki T, Marshall AG, Cooper WT. 1997. High-resolution Fourier transform ion cyclotron resonance mass spectrometry of humic and fulvic acids by laser desorption/ionization and electrospray ionization. *Energy & Fuels* 11(3):554-560.
- Fuzzi S, Orsi G, Nardini G, Facchini MC, McLaren S, McLaren E, Mariotti M. 1988. Heterogeneous processes in the Po Valley radiation fog. *Journal of Geophysical Research-Atmospheres* 93(D9):11141-11151.
- Fuzzi S, Andreae MO, Huebert BJ, Kulmala M, Bond TC, Boy M, Doherty SJ, Guenther A, Kanakidou M, Kawamura K, et al. 2006. Critical assessment of the current state of scientific knowledge, terminology, and research needs concerning the role of organic aerosols in the atmosphere, climate, and global change. *Atmospheric Chemistry and Physics* 6:2017-2038.
- Galloway MM, Chhabra PS, Chan AWH, Surratt JD, Flagan RC, Seinfeld JH, Keutsch FN. 2009. Glyoxal uptake on ammonium sulphate seed aerosol: reaction products and reversibility of uptake under dark and irradiated conditions. *Atmospheric Chemistry and Physics* 9(10):3331-3345.

- Gao S, Surratt JD, Knipping EM, Edgerton ES, Shahgholi M, Seinfeld JH. 2006. Characterization of polar organic components in fine aerosols in the southeastern United States: Identity, origin, and evolution. *Journal of Geophysical Research-Atmospheres* 111(D14):27.
- Gao YQ, Hall WA, Johnston MV. 2010. Molecular composition of monoterpene secondary organic aerosol at low mass loading. *Environmental Science & Technology* 44(20):7897-7902.
- Gelencser A, May B, Simpson D, Sanchez-Ochoa A, Kasper-Giebl A, Puxbaum H, Caseiro A, Pio C, Legrand M. 2007. Source apportionment of PM_{2.5} organic aerosol over Europe: Primary/secondary, natural/anthropogenic, and fossil/biogenic origin. *Journal of Geophysical Research-Atmospheres* 112(D23).
- Gomez-Gonzalez Y, Surratt JD, Cuyckens F, Szmigielski R, Vermeylen R, Jaoui M, Lewandowski M, Offenberg JH, Kleindienst TE, Edney EO et al. . 2008. Characterization of organosulfates from the photooxidation of isoprene and unsaturated fatty acids in ambient aerosol using liquid chromatography/(-) electrospray ionization mass spectrometry. *Journal of Mass Spectrometry* 43(3):371-382.
- Harrison MAJ, Barra S, Borghesi D, Vione D, Arsene C, Olariu RL. 2005a. Nitrated phenols in the atmosphere: a review. *Atmospheric Environment* 39(2):231-248.
- Harrison MAJ, Heal MR, Cape JN. 2005b. Evaluation of the pathways of tropospheric nitrophenol formation from benzene and phenol using a multiphase model. *Atmospheric Chemistry and Physics* 5:1679-1695.
- Herckes P, Hannigan MP, Trenary L, Lee T, Collett JL, Jr. 2002a. Organic compounds in radiation fogs in Davis (California). *Atmospheric Research* 64(1-4):99-108.
- Herckes P, Lee T, Trenary L, Kang GG, Chang H, Collett JL. 2002b. Organic matter in Central California radiation fogs. *Environmental Science & Technology* 36(22):4777-4782.
- Herckes P, Chang H, Lee T, Collett JL. 2007. Air pollution processing by radiation fogs. *Water Air and Soil Pollution* 181(1-4):65-75.
- Herterich R. 1991. Gas-chromatographic determination of nitrophenols in atmospheric liquid water and airborne-particulates. *Journal of Chromatography* 549(1-2):313-324.
- Hinkel M, Reischl A, Schramm KW, Trautner F, Reissinger M, Hutzinger O. 1989. Concentration levels of nitrated phenols in conifer needles. *Chemosphere* 18(11-12):2433-2439.
- Holets S, Swanson RN. 1981. High-inversion fog episodes in central California. *Journal of Applied Meteorology* 20(8):890-899.

- Iinuma Y, Muller C, Berndt T, Boge O, Claeys M, Herrmann H. 2007. Evidence for the existence of organosulfates from beta-pinene ozonolysis in ambient secondary organic aerosol. *Environmental Science & Technology* 41(19):6678-6683.
- IPCC. 2007. *Climate change 2007: Synthesis Report*. Geneva, Switzerland: IPCC.
- Koch BP, Dittmar T. 2006. From mass to structure: an aromaticity index for high-resolution mass data of natural organic matter. *Rapid Communications in Mass Spectrometry* 20(5):926-932.
- Kohler M, Heeb NV. 2003. Determination of nitrated phenolic compounds in rain by liquid chromatography/atmospheric pressure chemical ionization mass spectrometry. *Analytical Chemistry* 75(13):3115-3121.
- Kroll JH, Donahue NM, Jimenez JL, Kessler SH, Canagaratna MR, Wilson KR, Altieri KE, Mazzoleni LR, Wozniak AS, Bluhm H et al. 2011. Carbon oxidation state as a metric for describing the chemistry of atmospheric organic aerosol. *Nature Chemistry* 3(2):133-139.
- Kujawinski EB. 2002. Electrospray ionization Fourier transform ion cyclotron resonance mass spectrometry (ESI FT-ICR MS): characterization of complex environmental mixtures. *Environmental Forensics* 3(3-4):207-216.
- Kujawinski EB, Hatcher PG, Freitas MA. 2002. High-resolution Fourier transform ion cyclotron resonance mass spectrometry of humic and fulvic acids: Improvements and comparisons. *Analytical Chemistry* 74(2):413-419.
- Lara-Martin PA, Gomez-Parra A, Gonzalez-Mazo E. 2006. Development of a method for the simultaneous analysis of anionic and non-ionic surfactants and their carboxylated metabolites in environmental samples by mixed-mode liquid chromatography-mass spectrometry. *Journal of Chromatography A* 1137(2):188-197.
- Lara-Martin PA, Gomez-Parra A, Kochling T, Sanz JL, Gonzalez-Mazo E. 2007. Monitoring the primary biodegradation of linear alkylbenzene sulfonates and their coproducts in anoxic sediments using liquid chromatography-mass spectrometry. *Environmental Science & Technology* 41(10):3580-3586.
- Laskin A, Smith JS, Laskin J. 2009. Molecular characterization of nitrogen-containing organic compounds in biomass burning aerosols using high-resolution mass spectrometry. *Environmental Science & Technology* 43(10):3764-3771.
- Laskin J, Laskin A, Roach PJ, Slysz GW, Anderson GA, Nizkorodov SA, Bones DL, Nguyen LQ. 2010. High-resolution desorption electrospray ionization mass spectrometry for chemical characterization of organic aerosols. *Analytical Chemistry* 82(5):2048-2058.
- Leriche M, Voisin D, Chaumerliac N, Monod A, Aumont B. 2000. A model for tropospheric multiphase chemistry: Application to one cloudy event during the CIME experiment. *Atmospheric Environment* 34(29-30):5015-5036.

- Leuenberger C, Czuczwa J, Tremp J, Giger W. 1988. Nitrated phenols in rain- Atmospheric occurrence of phytotoxic pollutants. *Chemosphere* 17(3):511-515.
- Levsen K, Schiebel HM, Terlouw JK, Jobst KJ, Elend M, Preib A, Thiele H, Ingendoh A. 2007. Even-electron ions: a systematic study of the neutral species lost in the dissociation of quasi-molecular ions. *Journal of Mass Spectrometry* 42(8):1024-1044.
- Luttke J, Scheer V, Levsen K, Wunsch G, Cape JN, Hargreaves KJ, StoretonWest RL, Acker K, Wieprecht W, Jones B. 1997. Occurrence and formation of nitrated phenols in and out of cloud. *Atmospheric Environment* 31(16):2637-2648.
- Marshall AG, Hendrickson CL, Jackson GS. 1998. Fourier transform ion cyclotron resonance mass spectrometry: A primer. *Mass Spectrometry Reviews* 17(1):1-35.
- Marshall AG, Sunghwan K, Rodgers RP. 2006. Truly "exact" mass: Elemental composition can be determined uniquely from molecular mass measurement at ~0.1 mDa accuracy for molecules up to ~500 Da. *International Journal of Mass Spectrometry* 251(2-3):260-265.
- Mazzoleni LR, Ehrmann BM, Shen X, Marshall AG, Collett JL. 2010. Water-soluble atmospheric organic matter in fog: exact masses and chemical formula identification by ultrahigh-resolution Fourier transform ion cyclotron resonance mass spectrometry. *Environmental Science and Technology* 44(10):3690-7.
- McLafferty FW, Turecek F. 1993. Interpretation of mass spectra. Fourth Edition. University Science Books, Sausalito, CA. 370.
- Morville S, Scheyer A, Mirabel P, Millet M. Spatial and geographical variations of urban, suburban and rural atmospheric concentrations of phenols and nitrophenols. 2006: Ecomed Publishers. p. 83-89.
- Muller L, Reinnig MC, Hayen H, Hoffmann T. 2009. Characterization of oligomeric compounds in secondary organic aerosol using liquid chromatography coupled to electrospray ionization Fourier transform ion cyclotron resonance mass spectrometry. *Rapid Communications in Mass Spectrometry* 23(7):971-979.
- Natangelo M, Mangiapan S, Bagnati R, Benfenati E, Fanelli R. 1999. Increased concentrations of nitrophenols in leaves from a damaged forestal site. *Chemosphere* 38(7):1495-1503.
- Nguyen TB, Bateman AP, Bones DL, Nizkorodov SA, Laskin J, Laskin A. 2010. High-resolution mass spectrometry analysis of secondary organic aerosol generated by ozonolysis of isoprene. *Atmospheric Environment* 44(8):1032-1042.
- Nojima. 1975. Studies on photochemistry of aromatic hydrocarbons II: The formation of nitrophenols and nitrobenzene by the photochemical reaction of benzene in the presence of nitrogen monoxide *Chemosphere* 4(2):77-82.

- Noziere B, Dziedzic P, Cordova A. 2010. Inorganic ammonium salts and carbonate salts are efficient catalysts for aldol condensation in atmospheric aerosols. *Physical Chemistry Chemical Physics* 12(15):3864-3872.
- Noziere B, Dziedzic P, Cordova A. 2009. Products and kinetics of the liquid-phase reaction of glyoxal catalyzed by ammonium ions (NH_4^+). *Journal of Physical Chemistry A* 113(1):231-237.
- Pang Y, Turpin BJ, Gundel LA. 2006. On the importance of organic oxygen for understanding organic aerosol particles. *Aerosol Science and Technology* 40(2):128-133.
- Perri MJ, Lim YB, Seitzinger SP, Turpin BJ. 2010. Organosulfates from glycolaldehyde in aqueous aerosols and clouds: Laboratory studies. *Atmospheric Environment* 44(21-22):2658-2664.
- Perri MJ, Seitzinger S, Turpin BJ. 2009. Secondary organic aerosol production from aqueous photooxidation of glycolaldehyde: Laboratory experiments. *Atmospheric Environment* 43(8):1487-1497.
- Poschl U. 2005. Atmospheric aerosols: Composition, transformation, climate and health effects. *Angewandte Chemie-International Edition* 44(46):7520-7540.
- Putman AL, Offenberg JH, Fisseha R, Kundu S, Rahn TA, Mazzoleni LR. 2011. Ultrahigh-Resolution FT-ICR Mass Spectrometry Characterization of Alpha-Pinene Ozonolysis SOA. *Atmospheric Environment*. (In review).
- Ramanathan V, Crutzen PJ, Kiehl JT, Rosenfeld D. 2001. Atmosphere - Aerosols, climate, and the hydrological cycle. *Science* 294(5549):2119-2124.
- Reemtsma T. 2010. The carbon versus mass diagram to visualize and exploit FTICR-MS data of natural organic matter. *Journal of Mass Spectrometry* 45(4):382-390.
- Reemtsma T, These A, Springer A, Linscheid M. 2006a. Fulvic acids as transition state of organic matter: Indications from high resolution mass spectrometry. *Environmental Science & Technology* 40(19):5839-5845.
- Reemtsma T, These A, Venkatachari P, Xia XY, Hopke PK, Springer A, Linscheid M. 2006b. Identification of fulvic acids and sulfated and nitrated analogues in atmospheric aerosol by electrospray ionization Fourier transform ion cyclotron resonance mass spectrometry. *Analytical Chemistry* 78(24):8299-8304.
- Reinhardt A, Emmenegger C, Gerrits B, Panse C, Dommen J, Baltensperger U, Zenobi R, Kalberer M. 2007. Ultrahigh mass resolution and accurate mass measurements as a tool to characterize oligomers in secondary organic aerosols. *Analytical Chemistry* 79(11):4074-4082.
- Richartz H, Reischl A, Trautner F, Hutzinger O. 1990. Nitrated phenols in fog. *Atmospheric Environment Part A-General Topics* 24(12):3067-3071.
- Rippen G, Zietz E, Frank R, Knacker T, Klopffer W. 1987. Do airborne nitrophenols contribute to forest decline. *Environmental Technology Letters* 8(10):475-482.

- Roach PJ, Laskin J, Laskin A. 2010. Molecular characterization of organic aerosols using nanospray-desorption/electrospray ionization-mass spectrometry. *Analytical Chemistry* 82(19):7979-7986.
- Rudich Y, Donahue NM, Mentel TF. 2007. Aging of organic aerosol: Bridging the gap between laboratory and field studies. *Annual Review of Physical Chemistry* 58:321-352.
- Sadezky A, Winterhalter R, Kanawati B, Rompp A, Spengler B, Mellouki A, Le Bras G, Chaimbault P, Moortgat GK. 2008. Oligomer formation during gas-phase ozonolysis of small alkenes and enol ethers: new evidence for the central role of the Criegee Intermediate as oligomer chain unit. *Atmospheric Chemistry and Physics* 8(10):2667-2699.
- Sancho JV, Pozo OJ, Lopez FJ, Hernandez F. 2002. Different quantitation approaches for xenobiotics in human urine samples by liquid chromatography/electrospray tandem mass spectrometry. *Rapid Communications in Mass Spectrometry* 16(7):639-645.
- Saxena P, Hildemann LM. 1996. Water-soluble organics in atmospheric particles: A critical review of the literature and application of thermodynamics to identify candidate compounds. *Journal of Atmospheric Chemistry* 24(1):57-109.
- Schmidt AC, Herzsuh R, Matysik FM, Engewald W. 2006. Investigation of the ionisation and fragmentation behaviour of different nitroaromatic compounds occurring as polar metabolites of explosives using electrospray ionisation tandem mass spectrometry. *Rapid Communications in Mass Spectrometry* 20(15):2293-2302.
- Schmitt-Kopplin P, Gelencser A, Dabek-Zlotorzynska E, Kiss G, Hertkorn N, Harir M, Hong Y, Gebefugi I. 2010. Analysis of the unresolved organic fraction in atmospheric aerosols with ultrahigh-resolution mass spectrometry and nuclear magnetic resonance spectroscopy: Organosulfates as photochemical smog constituents. *Analytical Chemistry* 82(19):8017-8026.
- Shafer WE, Schonherr J. 1985. Accumulation and transport of phenol, 2-nitrophenol, and 4-nitrophenol in plant cuticles. *Ecotoxicology and Environmental Safety* 10(2):239-252.
- Shapiro EL, Szprengiel J, Sareen N, Jen CN, Giordano MR, McNeill VF. 2009. Light-absorbing secondary organic material formed by glyoxal in aqueous aerosol mimics. *Atmospheric Chemistry and Physics* 9(7):2289-2300.
- Shea PJ, Weber JB, Overcash MR. 1983. Biological activities of 2,4-dinitrophenol in plant-soil systems. *Residue Reviews* 87:1-41.
- Sleighter RL, Hatcher PG. 2007. The application of electrospray ionization coupled to ultrahigh resolution mass spectrometry for the molecular characterization of natural organic matter. *Journal of Mass Spectrometry* 42(5):559-574.

- Stenson AC, Landing WM, Marshall AG, Cooper WT. 2002. Ionization and fragmentation of humic substances in electrospray ionization Fourier transform-ion cyclotron resonance mass spectrometry. *Analytical Chemistry* 74(17):4397-4409.
- Stenson AC, Marshall AG, Cooper WT. 2003. Exact masses and chemical formulas of individual Suwannee River fulvic acids from ultrahigh resolution electrospray ionization Fourier transform ion cyclotron resonance mass spectra. *Analytical Chemistry* 75(6):1275-1284.
- Suckling PW, Mitchell MD. 1988. Fog climatology of the Sacramento urban area. *Professional Geographer* 40(2):186-194.
- Surratt JD, Kroll JH, Kleindienst TE, Edney EO, Claeys M, Sorooshian A, Ng NL, Offenberg JH, Lewandowski M, Jaoui M, et al. 2007. Evidence for organosulfates in secondary organic aerosol. *Environmental Science & Technology* 41(2):517-527.
- Surratt JD, Gomez-Gonzalez Y, Chan AWH, Vermeylen R, Shahgholi M, Kleindienst TE, Edney EO, Offenberg JH, Lewandowski M, Jaoui M, et al. 2008. Organosulfate formation in biogenic secondary organic aerosol. *Journal of Physical Chemistry A* 112(36):8345-8378.
- Tan Y., Lim Y., Altieri KE, Seitzinger SP, Turpin BJ. 2011. Mechanisms leading to oligomers and SOA through aqueous photooxidation: Insights from OH radical oxidation of acetic acid. *Atmospheric Chemistry and Physics Discussion*.
- Tolocka MP, Jang M, Ginter JM, Cox FJ, Kamens RM, Johnston MV. 2004. Formation of oligomers in secondary organic aerosol. *Environmental Science & Technology* 38(5):1428-1434.
- Underwood SJ, Ellrod GP, Kuhnert AL. 2004. A multiple-case analysis of nocturnal radiation-fog development in the Central Valley of California utilizing the GOES nighttime fog product. *Journal of Applied Meteorology* 43(2):297-311.
- Vione D, Maurino V, Minero C, Pelizzetti E. 2005. Aqueous atmospheric chemistry: Formation of 2,4-dinitrophenol upon nitration of 2-nitrophenol and 4-nitrophenol in solution. *Environmental Science & Technology* 39(20):7921-7931.
- Waldman JM, Hoffmann MR. 1987. Depositional aspects of pollutant behavior in fog and intercepted clouds. *Advances in Chemistry Series*(216):79-129.
- Waldman JM, Jacob DJ, Munger JW, Hoffmann MR. 1987. Pollutant deposition in radiation fog. *ACS Symposium Series* 349:250-257.
- Walser ML, Desyaterik Y, Laskin J, Laskin A, Nizkorodov SA. 2008. High-resolution mass spectrometric analysis of secondary organic aerosol produced by ozonation of limonene. *Physical Chemistry Chemical Physics* 10(7):1009-1022.
- Weathers KC. 1999. The importance of cloud and fog in the maintenance of ecosystems. *Trends in Ecology & Evolution* 14(6):214-215.

- Witt M, Fuchser J, Koch BP. 2009. Fragmentation studies of fulvic acids using collision induced dissociation Fourier transform ion cyclotron resonance mass spectrometry. *Analytical Chemistry* 81(7):2688-2694.
- Wozniak AS, Bauer JE, Sleighter RL, Dickhut RM, Hatcher PG. 2008. Technical Note: Molecular characterization of aerosol-derived water soluble organic carbon using ultrahigh resolution electrospray ionization Fourier transform ion cyclotron resonance mass spectrometry. *Atmospheric Chemistry and Physics* 8(17):5099-5111.
- Yasmeen F, Sauret N, Gal JF, Maria PC, Massi L, Maenhaut W, Claeys M. 2010. Characterization of oligomers from methylglyoxal under dark conditions: a pathway to produce secondary organic aerosol through cloud processing during nighttime. *Atmospheric Chemistry and Physics* 10(8):3803-3812.
- Zhang Q, Anastasio C. 2001. Chemistry of fog waters in California's Central Valley - Part 3: Concentrations and speciation of organic and inorganic nitrogen. *Atmospheric Environment* 35(32):5629-5643.
- Zhang Q, Anastasio C. 2003. Free and combined amino compounds in atmospheric fine particles (PM_{2.5}) and fog waters from Northern California. *Atmospheric Environment* 37(16):2247-2258.
- Zhang XQ, McMurry PH, Hering SV, Casuccio GS. 1993. Mixing characteristics and water-content of submicron aerosols measured in Los-Angeles and at the Grand-Canyon. *Atmospheric Environment Part A-General Topics* 27(10):1593-1607.

5 Appendix

Table 5.1: A complete list of the mass spectrometry scan parameters is listed. Also, recalibration and composition parameters used in Composer for formula assignments are listed. This table is provided on the included CD-R via a Microsoft Excel 2007 workbook named “5_Appendix Tables_LeClair_2011.xlsx” on the “Table 5.1_MS2 Method Parameters” tab.

Table 5.2: A complete list of all formula assigned precursor ions involved in this study is provided on the included CD-R via a Microsoft Excel 2007 workbook named “5_Appendix Tables_LeClair_2011.xlsx” on the “Table 5.2_Priority Losses” tab. Neutral losses of interest are listed corresponding to precursor ions. A “1” is used to denote that a neutral loss was observed for that particular precursor. Under the scan column for the scan 311_1 means that it had an isolation width of 1.8 and 311_2 means that it had an isolation width of 6. A description of the provided data is as follows: column “A” lists the relative abundance for each m/z; column “B” lists the negative ion mass-to-charge ratio (m/z) measured and internally recalibrated; column “C” lists the absolute error of the formula assignment in ppm; column “D” lists the calculated double bond equivalents (DBE) of the neutral molecule; column “E” lists the assigned neutral mass molecular formula; column “F” lists the scan in which the corresponding precursor ion was observed; column “G” lists the precursor ions that had a neutral loss of H₂O; column “H” lists the precursor ions that had a neutral loss of CH₄O; column “I” lists the

precursor ions that had a neutral loss of two H₂O molecules; column “J” lists the precursor ions that had a neutral loss of CO₂; column “K” lists the precursor ions that had a neutral loss of CO₂ + H₂O; column “L” lists the precursor ions that had a neutral loss of HNO₃; column “M” lists the precursor ions that had a neutral loss of CH₄O + CO₂; column “N” lists the precursor ions that had a neutral loss of CH₃NO₃; column “O” lists the precursor ions that had a neutral loss of SO₃; column “P” lists the precursor ions that had a neutral loss of two CO₂ molecules; column “Q” lists the precursor ions that had a neutral loss of SO₄.

Table 5.3: A complete list of all formula assigned precursor ions involved in this study is provided on the included CD-R via a Microsoft Excel 2007 workbook named “5_Appendix Tables_LeClair_2011.xlsx” on the “Table 5.3_Additional Losses” tab. Neutral losses of interest are listed corresponding to precursor ions. A “1” is used to denote that a neutral loss was observed for that particular precursor. Under the scan column for the scan 311_1 means that it had an isolation width of 1.8 and 311_2 means that it had an isolation width of 6. A description of the provided data is as follows: column “A” lists the relative abundance for each m/z; column “B” lists the negative ion mass-to-charge ratio (m/z) measured and internally recalibrated; column “C” lists the absolute error of the formula assignment in ppm; column “D” lists the calculated double bond equivalents (DBE) of the neutral molecule; column “E” lists the assigned neutral mass molecular formula; column “F” lists the scan in which the corresponding precursor ion was observed; column “G” lists the precursor ions that had a neutral loss of CO; column “H” lists the precursor ions that had a neutral loss of CH₂O; column “I” lists the

precursor ions that had a neutral loss of C_2H_6 ; column “J” lists the precursor ions that had a neutral loss of C_3H_8 ; column “K” lists the precursor ions that had a neutral loss of CH_2O_2 ; column “L” lists the precursor ions that had a neutral loss of C_4H_{10} ; column “M” lists the precursor ions that had a neutral loss of $C_2H_4O_2$; column “N” lists the precursor ions that had a neutral loss of C_5H_{12} ; column “O” lists the precursor ions that had a neutral loss of $C_3H_4O_2$; column “P” lists the precursor ions that had a neutral loss of CO + CO_2 molecules; column “Q” lists the precursor ions that had a neutral loss of $C_2H_2O_4$.

Table 5.4: A complete list of all formula assigned fragment ions produced during tandem mass analysis by collision induced dissociation for the scans included in this study is provided on the included CD-R via a Microsoft Excel 2007 workbook named “5_Appendix Tables_LeClair_2011.xlsx” on the “Table 5.4_Fragment Ions” tab. All fragment ions are listed first by scan and second by m/z. The letter “R” at the end of the Scan name denotes the allowance of radical ions. A description of the provided data is as follows: column “A” lists the relative abundance for each m/z; column “B” lists the negative ion mass-to-charge ratio (m/z) measured and internally recalibrated; column “C” lists the absolute error of the formula assignment in ppm; column “D” lists the calculated double bond equivalents (DBE) of the neutral molecule; column “E” lists the assigned neutral mass molecular formula; column “F” lists the scan in which the corresponding fragment ion was observed.